HZDR-036

MICROBIAL DIVERSITY IN OPALINUS CLAY AND INTERACTION OF DOMINANT MICROBIAL STRAINS WITH ACTINIDES

Henry Moll, Laura Lütke, Velina Bachvarova,
Robin Steudner, Andrea Geißler, Evelyn Krawczyk-Bärsch,
Sonja Selenska-Pobell, Gert Bernhardt

Wissenschaftlich-Technische Berichte
HZDR-036 · ISSN 2191-8708

WISSENSCHAFTLICH-
TECHNISCHE BERICHTE

HZDR
HELMHOLTZ
ZENTRUM DRESDEN
ROSSENDORF

Wissenschaftlich-Technische Berichte
HZDR-036
Juni 2013

Henry Moll, Laura Lütke, Velina Bachvarova,
Robin Steudtner, Andrea Geißler, Evelyn Krawczyk-Bärsch,
Sonja Selenska-Pobell, Gert Bernhard

MICROBIAL DIVERSITY IN OPALINUS CLAY AND INTERACTION OF DOMINANT MICROBIAL STRAINS WITH ACTINIDES

HZDR

HELMHOLTZ
ZENTRUM DRESDEN
ROSSENDORF

Druckausgabe: ISSN 2191-8708

Elektronische Ausgabe: ISSN 2191-8716

Qucosa: http://fzd.qucosa.de/startseite/

Das diesem Bericht zugrunde liegende Vorhaben wurde mit Mitteln des Bundesministeriums für Wirtschaft und Technologie unter dem Förderkennzeichen 02E10618 gefördert. Die Verantwortung für den Inhalt dieser Veröffentlichung liegt bei den Autoren.

Vorhaben:

MIKROBIELLE DIVERSITÄT IM TONGESTEIN (OPALINUS-TON) UND WECHSELWIRKUNG DOMINANTER MIKROORGANISMEN MIT ACTINIDEN

2013

Herausgegeben vom

Helmholtz-Zentrum Dresden - Rossendorf

Bautzner Landstr. 400

01328 Dresden

Germany

Abstract

For the first time microbial tDNA could be isolated from 50 g unperturbed Mont Terri Opalinus Clay. Based on the analysis of the tDNA the bacterial diversity of the unperturbed clay is dominated by representatives of *Firmicutes*, *Betaproteobacteria*, and *Bacteriodetes*. *Firmicutes* also dominate after treatment of the clay with R2A medium. Bacteria isolated from Mont Terri Opalinus Clay on R2A medium were related to *Sporomusa* spp., *Paenibacillus* spp., and *Clostridium* spp.. All further investigations are concentrated on the unique isolates *Sporomusa* sp. MT-2 and *Paenibacillus* sp. MT-2. Cells of the type *Sporomusa* sp. MT-2 and *Paenibacillus* sp. MT-2 were comprehensively analyzed in terms of growing, morphology, functional groups of the cell envelope, and cell membrane structure.
Strong actinide(An)/lanthanide(Ln)-interactions with the Opalinus Clay isolates and the Äspö-strain *Pseudomonas fluorescens* (CCUG 32456) could be determined within a broad pH range (2-8). The metals bind as a function of pH on protonated phosphoryl, carboxyl and deprotonated phosphoryl sites of the respective cell membrane. The thermodynamic surface complexation constants of bacterial An/Ln-species were determined and can be used in modeling programs. Depending on the used An different interaction mechanisms were found (U(VI): biosorption, partly biomineralisation; Cm(III): biosorption, indications for embedded Cm(III); Pu: biosorption, bioreduction and indications for embedded Pu). Different strategies of coping with U(VI) were observed comparing *P. fluorescens* planktonic cells and biofilms under the chosen experimental conditions. An enhanced capability of the biofilm to form meta-autunite in comparison to the planktonic cells was proven. Conclusively, the *P. fluorescens* biofilm is more efficient in U(VI) detoxification.
In conclusion, Mont Terri Opalinus Clay contains bacterial communities, that may influence the speciation and hence the migration behavior of selected An/Ln under environmental conditions.

Zusammenfassung

Erstmalig konnte aus 50 g unbehandeltem Mont Terri Opalinus-Ton mikrobielle Gesamt-DNA isoliert werden. Auf der Basis dieser Gesamt-DNA konnte gezeigt werden, dass Vertreter von *Firmicutes*, *Beta-Proteobakterien* und *Bacteriodetes* die 16S rRNA Klonbibliothek der unbehandelten Tonprobe dominieren. Wird der Ton mit einem Medium (R2A) zur Stimulierung von Mikroben behandelt, überwiegen Vertreter von *Firmicutes*. Bakterielle Isolate, die *Firmicutes* zuzuordnen sind, wurden aus Mont Terri Opalinus-Ton auf R2A Medium kultiviert: *Sporomusa* spp., *Paenibacillus* spp. und *Clostridium* spp.. Alle weiteren Untersuchungen konzentrierten sich auf die Isolate *Sporomusa* sp. MT-2 und *Paenibacillus* sp. MT-2. Zellen von *Sporomusa* sp. und *Paenibacillus* sp. wurden umfassend analysiert bezüglich des Wachstums, der Zellwandstruktur, der Morphologie, und der funktionellen Gruppen der Zellmembran.
Es wurden starke Actiniden(An)/Lanthaniden(Ln)-Wechselwirkungen der Opalinus-Ton Isolate und des Äspö-Bakteriums *Pseudomonas fluorescens* (CCUG 32456) innerhalb eines breiten pH-Bereichs (2-8) bestimmt. Die Anbindung der Metalle erfolgt in Abhängigkeit des pH an Hydrogenphosphat-, Carboxyl- und Phosphorylgruppen der jeweiligen Zellmembran. Die thermodynamischen Stabilitätskonstanten der An/Ln mit den Opalinus-Ton Isolaten und dem Äspö-Bakterium *P. fluorescens* wurden bestimmt und sind in Modellierungsprogrammen einsetzbar. Entsprechend dem eingesetzten An wurden abweichende Wechselwirkungsmechanismen mit den Zellen festgestellt (U(VI): Biosorption, teilweise Biomineralisation; Cm(III): Biosorption, Tendenzen für eingelagertes Cm(III); Pu: Biosorption, Bioreduktion und Tendenzen für eingelagertes Pu). Beim Vergleich der U(VI)-Ergebnisse für *P. fluorescens* zeigte sich, dass die Zellen unterschiedliche Strategien zur Bewältigung des U(VI)-Stresses entwickeln je nachdem ob sie planktonisch (reine Biosorption) oder in Form eines Biofilms (Bildung von Meta-Autunit-Strukturen) vorkommen.
Zusammenfassend kann festgestellt werden, dass der Mont Terri Opalinus-Ton bakterielle Gemeinschaften enthält, welche die Speziation und somit auch das Ausbreitungsverhalten ausgewählter An/Ln unter umweltrelevanten Bedingungen beeinflussen können.

Content

1 Introduction

Besides the prominent processes influencing the migration of actinides in the environment, e.g. sorption onto mineral surfaces, there is growing attention to the influence of indigenous microorganisms on actinide speciation. The concept of geological disposal comprises a detailed knowledge concerning potential host rock formations. One of such formations are the Opalinus Clay formations of the Mont Terri underground rock laboratory (URL), Switzerland which is under investigation to test their suitability as host rock for future disposal of radioactive waste since almost 20 years (Thury and Bossart 1999). It is well known that bacteria indigenous to such subterranean soil environments can affect the speciation and hence the mobility of actinides (e.g., Lloyd and Gadd 2011, Brookshaw et al. 2012), dominant bacterial strains from sites destined for future nuclear waste deposition have to be investigated regarding their interaction mechanisms with soluble actinide ions (e.g., Anderson et al. 2011). The so isolated bacterial populations can have considerable impact on actinide mobility and retardation both by direct and indirect pathways (e.g., Lovley et al. 1991, Kalinowski et al. 2004, Merroun et al. 2008, Moll et al. 2004, 2008, 2013, Lütke et al. 2012). The understanding of the speciation and the structure of the actinide (An)/lanthanide (Ln) complexes formed in presence of indigenous bacteria over a range of geochemical parameters (e.g., pH, metal concentration) becomes indispensable for eventually predicting the safety of a planned nuclear waste repository.

The starting point of our project was the detection of bacteria and organics in deep clay formations (Boivin et al. 1996) and also in Opalinus Clay of the Mont Terri URL (Stroes-Gascoyne et al. 2007). However due to difficulties in isolating the total microbial DNA (tDNA) the bacterial diversity in Mont Terri Opalinus Clay was still unknown.

Our project is focused on broaden the knowledge concerning the bacterial diversity in Mont Terri Opalinus Clay by applying direct molecular culture-independent retrievals and cultivation experiments. After cultivation and characterization of dominant bacterial populations we want to investigate their influence on the geo-chemical behavior of selected actinides (uranium, plutonium, and curium). The indirect (e.g., actinide mobilization by microbially produced bioligands) and direct (e.g., biosorption, bioaccumulation, biotransformation) influence of microorganisms on migration processes of actinides has to be taken into account for the risk assessment of potential high level nuclear waste disposal sites. Within our last project (02 E 9985) we investigated indirect interaction paths of the Äspö-strain *Pseudomonas fluorescens* (Moll et al. 2009) in terms of complexation studies of the secreted pyoverdins with selected actinides whereas this new study is concentrated on direct

interactions of *P. fluorescens* cells with selected actinides. This approach could be used to rate the influence of both actinide interaction paths on one microorganism. The experiments were performed with planktonic cells and *P. fluorescens* cells fixed in a biofilm. To summarize, the main goals of the project are:

i) Direct investigations of the microbial diversity in Mont Terri Opalinus Clay.
ii) Cultivation and characterization of Mont Terri Opalinus Clay specific bacteria.
iii) Investigations to characterize the interactions of selected actinides (uranium, curium, plutonium) with bacterial isolates from Mont Terri Opalinus Clay.
iiii) Interaction studies with the Äspö-strain *P. fluorescens* a) planktonic cells with uranium, curium, and plutonium and b) *P. fluorescens* biofilms with uranium.

The indigenous microbial diversity of geological formations destined for storage of nuclear waste may play an important role in the mobility and retardation of actinides. Thus the investigation of locally isolated strains and their interaction mechanisms with actinides becomes indispensable for a site safety assessment. The obtained results should help to improve the scientific basis for the performance assessment and safety of nuclear waste repositories.
The scientific results of this project are described in detail in the following sections.

2 Bacterial diversity in Mont Terri Opalinus Clay

As mentioned above, it is of interest to know which bacteria are present in the host rock of a potential nuclear waste disposal site and to analyze bacterial interactions with actinides.

Over the last years a couple of studies were done about the microbial diversity in the Opalinus Clay (Stroes-Cascoyne et al. 2007, Poulain et al. 2008). Sulphate-reducing bacteria and unknown species of *Sphingomonas* and *Alicyclobacillus* were isolated from these samples. Additionally, phospholipid fatty acids were extracted, which suggested the presence of viable cells. However, no PCR-amplifiable DNA from the core samples could be extracted (Stroes-Cascoyne et al. 2007).

For the analysis of the bacterial diversity in Opalinus Clay we used successfully culture-independent approaches (2.1) and cultivation experiments (2.2).

2.1 Direct molecular culture-independent retrievals

The first step for this analysis is the extraction of high molecular weight DNA. A method evolved by Selenska-Pobell and co-workers (Selenska-Pobell et al. 2001) combines a very effective direct lysis of microorganisms in environmental samples and the precipitation of the extracted DNA with polyethyleneglycol, with the final purification steps based on the use of AXG-100 cartridges (Macherey-Nagel, Düren, Germany). This method was successful in isolating high molecular weight DNA from Opalinus Clay of the Mont Terri URL by using 50 g of sample material.

Due to the tight binding of the DNA to the clay particles, DNA recovery from clay samples is especially difficult (Yankson and Steck 2009). In order to increase the efficiency of the DNA extraction by alkaline cells lysis at 70 °C, this step was performed four times. To increase the total DNA yield, the elution step was preformed twice with additional volume from the elution buffer. Due to the expected low yield, the recovered DNA was dissolved finally in 25 to 30 µL TE buffer, pH 8. For quick and reliable estimation of the bacterial community structure the Ribosomal IntergenicLSpacer Amplification (RISA) approach was used as described earlier, using the primer pair $16S_{969F}$-$23S_{130R}$ (Selenska-Pobell et al. 2001). Three different samples were analyzed: the inner part of the core (MT-2), the surface part of the core (MT-2-SF) and the R2A-treated sample (MT-2-R2A).

As evident from the results presented in Figure 2.1, the RISA patterns obtained for the MT-2-SF sample did not match with those of the MT-2 sample. This result indicates that the core surface sample is occupied by bacteria not or barely presented in the parallel sample MT-2

from the inner part of the core. With other words, clay material from the inner part of the core should be analyzed to avoid contaminants which might penetrate into the core during the sampling. Applying RISA to the R2A medium treated sample MT-2-R2A we obtained a very different profile that indicates shifting in the bacterial community structure due to the addition of nutrients.

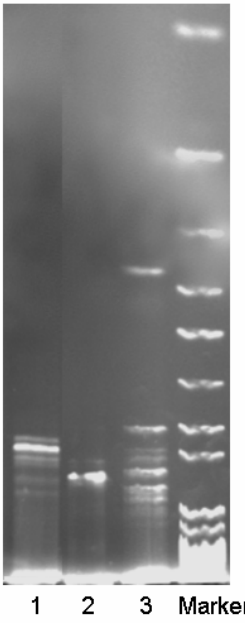

Fig. 2.1 RISA analysis of the samples: (1) inner part of the core MT-2; (2) the surface part of the core MT-2-SF; and (3) the R2A treated sample MT-2-R2A.

2.1.1 Unperturbed Mont Terri Opalinus Clay sample

The Opalinus Clay core samples used in this study were collected in April 2009 from the borehole BHT-1 of the Mont Terri URL. In order to distinguish the indigenous clay bacteria from any contaminants, which might be introduced into the core samples during the drilling, we analyzed two parallel samples – one containing material from the inner part of the core (MT-2) and a second one – from the surface part (MT-2-SF).

16S rRNA genes were amplified from the extracted high molecular weight DNA by Polymerase Chain Reaction (PCR) with the primers $16S_{7F}$ und $16S_{1513R}$ (Lane 1991) and a clone library was established (TOPO TA cloning kit (Invitrogen)). The analysis of the clone library was performed by restriction fragment length polymorphism (RFLP), followed by sequencing and phylogenetic analysis of representatives of the RFLP groups. As shown in Figure 2.2 an unexpected variety of nine different bacterial groups was found in the unperturbed MT-2 sample. The largest group in the sample includes rather diverse representatives of *Frimicutes*, which were affiliated with five distinct clostridial families. The

second largest group in the MT-2 sample was, in contrast, very uniform and it was closely related to *Acidovorax* sp., belonging to the *Betaproteobacteria*. Representatives of *Acidovorax* are nitrate reducers able to reduce U(VI) to U(IV) as well (Nyman et al. 2006). The third predominant group was affiliated with *Bacteroidetes*, which are widely distributed in water, soils and sediments and are characterized as a bacterial group which is very adaptive to changes in the nutrient conditions in the environment. Small populations of *Alpha-*, *Gamma-*, and *Deltaproteobacteria* as well as *Acidobacteria* and *Actinobacteria* were also identified in the MT-2 sample.

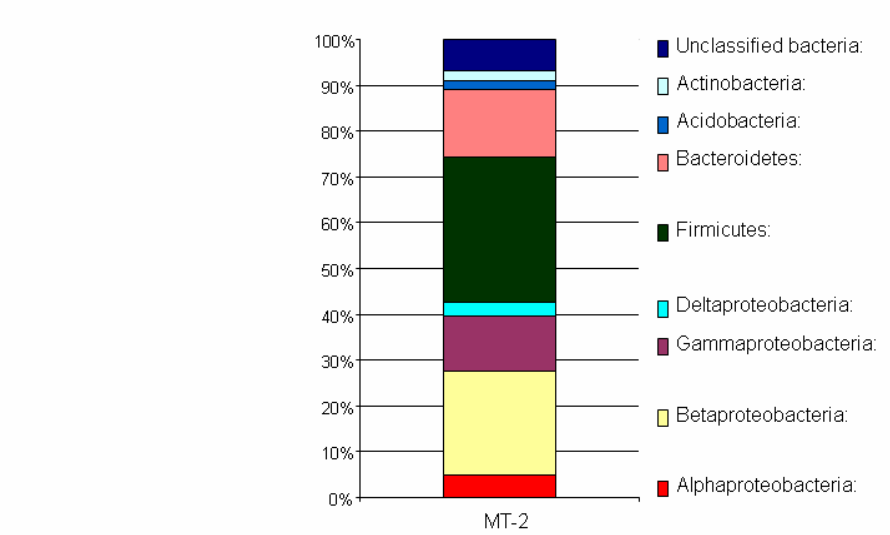

Fig. 2.2 Bacterial diversity of the unperturbed Opalinus Clay sample MT-2.

In contrast, the bacterial community in sample MT-2-SF consisted only of diverse members of *Betaproteobacteria* (*Ralstonia* spp. and *Burkholderia* spp.) (not shown).

Interestingly, the *Betaproteobacteria* detected in the inner part of the core (MT-2) were mainly *Acidovorax* spp., which are different than the ones found in the surface part.

These results suggest that in the inner part of the core the indigenous clay bacteria were analyzed, whereas the bacteria found in the surface part can be contaminants, which might be introduced into the core samples during the drilling. For further investigations it is suggested to remove the outer part of the core und just use the inner part for the analysis.

2.1.2 R2A treated Mont Terri Opalinus Clay sample

To study the response of the natural bacterial community to the addition of nutrients one sample from the inner part of the core was treated for two weeks with R2A medium (MT-2-R2A). The treatment with R2A medium lead to stimulation of only two groups of *Firmicutes* in the sample MT-2-R2A which completely overgrew the rest of the bacterial populations

characteristic for the unperturbed original sample MT-2 (Fig. 2.2). About 50 % of the retrieved 16S rRNA genes in the MT-2-R2A sample were affiliated with *Paenibacillus* spp. and 45 % with the non-pathogenic clostridial group of *Sporomusa* spp. It is noticeable that both of these species were not identified in the unperturbed sample MT-2. Only about 5 % of the clones of the MT-2-R2A library were categorized as individual.

2.1.3 Mont Terri pore water

The pore water sample HT3 from the Mont Terri URL was collected until June 2011. Immediately after arriving, 50 ml of the sample was successively filtered through 0.45 µm, 0.22 µm, and 0.1 µm sterile filters. The filters were frozen at −20 ºC for DNA extraction.

After a successful DNA extraction and an amplification of 16S rRNA genes, a clone library with 100 clones was constructed and analyzed. As shown in Figure 2.3, *Alpha-*, *Beta-* and *Gammaproteobacteria* were present in the sample, whereas *Gammaproteobacteria* especially *Pseudomonas* sp. dominated the bacterial community. *Agrobacterium* sp. as represenatives from the *Alphaproteobacteria* and *Limnobacter* sp. as representatives from the *Betaproteobacteria* were identified.

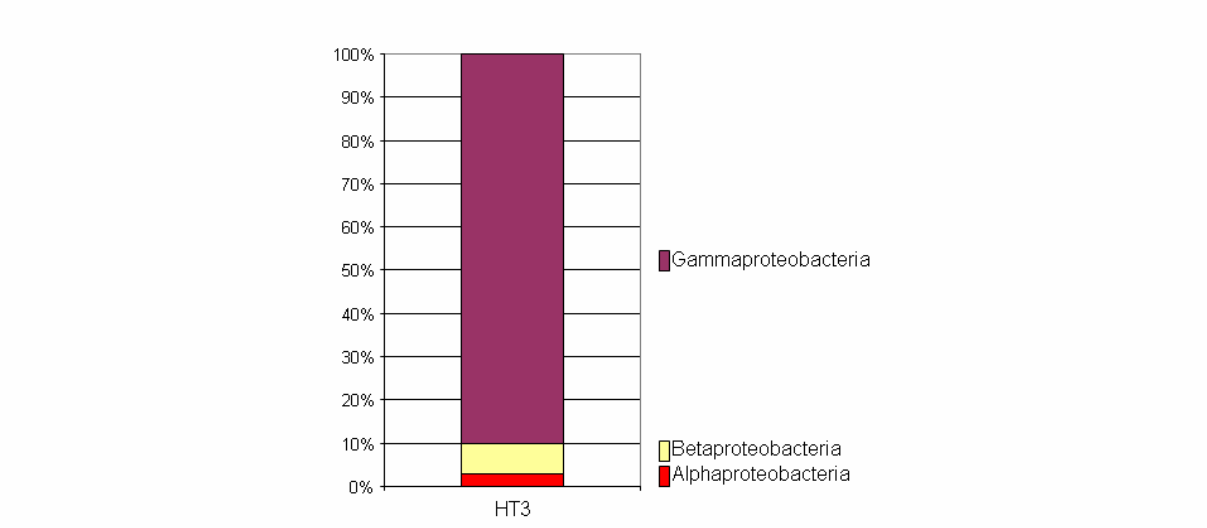

Fig. 2.3 Bacterial diversity in the pore water from Mont Terri URL.

2.2 Cultivation/Enrichment experiments

2.2.1 Isolation of bacteria from Mont Terri Opalinus Clay

Bacteria were cultured from 200 g of the sample MT-2, which was incubated initially in 200 mL sterile autoclaved dH_2O at room temperature and in anaerobic jar with Anaerocult® - A (Merck). After 5 days of incubation the extracted water was collected and subsequently

filtrated through filters with different size of the pores. The filters were stored at −20 °C for further analysis. Samples before each filtration were collected, serial dilutions were prepared, and 0.1 mL aliquots were plated on R2A agar medium. The filtrated water was used for preparation of R2A liquid medium instead of dH_2O. The rest of the clay sample was incubated in the R2A medium. This procedure was repeated every 2 weeks.

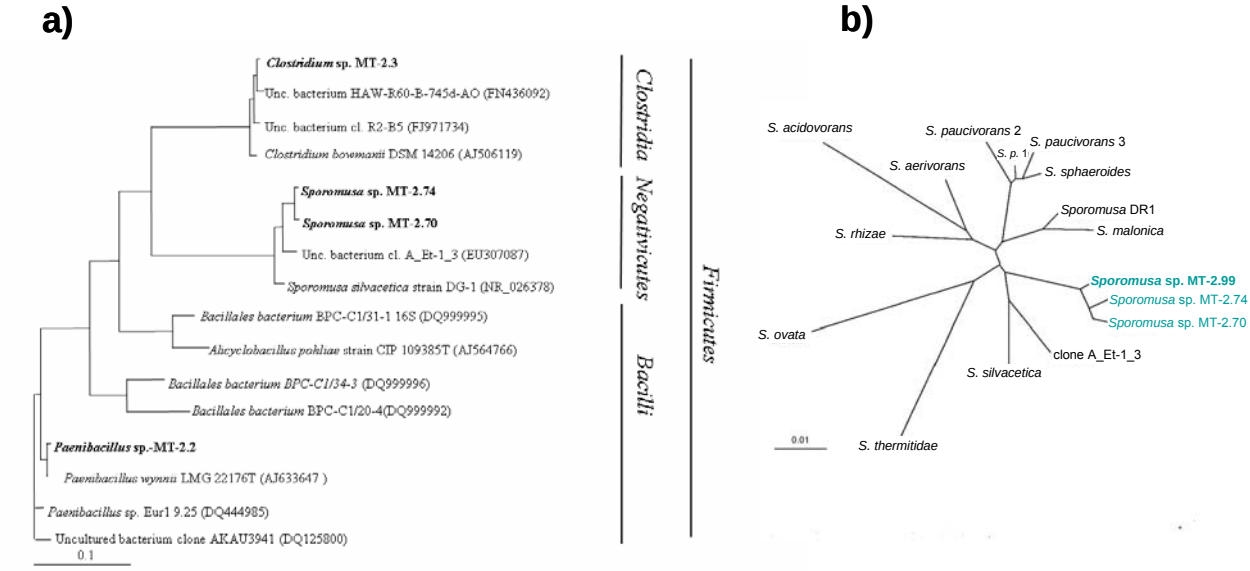

Fig.2.4 a) Phylogenetic dendrogram of the 16S rRNA genes of the isolates, obtained from the sample MT-2 under anaerobic conditions on R2A agar plates. b) Phylogenetic dendrogram of the 16S rRNA genes of all *Sporomusa* isolates in detail.

The first colonies, observed have appeared after 4 weeks of incubation on R2A agar medium. The colonies were white or yellow colored, circular shaped but with different size. Microscopic analysis has shown presence of rod shaped cells with a length of ~2 µm and a width of about 0.5 µm, as well small rods or spheres at about 0.1 µm. 16S rRNA genes of the isolates were amplified via *in-situ* PCR, following up sequencing and phylogenetic analysis. As demonstrated in the phylogenetic dendrogram (Fig. 2.4 a), 16S rRNA genes of the isolates affiliated within the *Firmicutes* with the classes – *Clostridia*, *Negativicutes* and *Bacilli*. The isolate MT-2.3 cultivated in our study was affiliated with *Clostridium bowmanii* DSM14206 (AJ506119) which is a psychrophilic bacterium found in the area around the Lake Fryxell, Antarctica (Spring et al. 2003). Interestingly, the isolates MT-2.70, MT-2.74, and MT-2.99 (see Fig. 2.4 b) were related to the uncultured bacterium clone A_Et-1_3 (EU307087) retrieved from Fe(III)-reducing enrichment culture (Hansel et al. 2008) and *Sporomusa silvacetica* strain DG-1 (NR_026378) an obligately anaerobic and sporulating bacteria, which was isolated from a well-drained, aggregated forest soil (pH 6.0) in east-central Germany (Kuhner et al. 1997). The isolate MT-2.2 was closely affiliated with *Paenibacillus wynnii*

LMG 22176T (AJ633647), which was found on Mars oasis on Alexander island, Antarctica (Rodríguez-Díaz et al. 2005). It is important to notice that all the *Clostridia*-affiliated isolates were related to nonpathogenic representatives. Up to date, we were able to isolate representatives of three bacterial lineages. This limited diversity could be interpreted with the unfavorable living conditions, characterizing the Opalinus Clay. However, the capability of representatives of *Bacilli*, *Negativicutes* and *Clostridia* to form spores gives them a potential to survive in unfavorable conditions. On the other hand the use of the R2A medium in our experiments, which is specific for oligotrophic microorganisms, could also explain the limited diversity observed in our study. The treatment of the Opalinus Clay with an iron-reducing and a sulphate-reducing media was tried as well. However, no distinct growth could be detected in the enrichment culture. An Opalinus Clay specific *Sporomusa* sp. isolate and *Paenibacillus* sp. isolate was chosen for further analyses (see 3.2.1 and 3.2.2) and the study of the interaction mechanisms with U(VI), Cu(III)/Eu(III) and Pu (see 4.2.1 and 4.2.2).

2.2.2 Isolation of bacteria from Mont Terri pore water

The filtrates of the pore water HT3 as well as a portion of the original water were used for the culture-dependent analysis. 0.1 mL aliquots of the water were spread on 50 % R2A agar plates or G1M1 agar plates (Heylen et al. 2006) and incubated at room temperature or 30 ºC under anaerobic conditions.

By using these two different media, we were able to enrich and isolate bacteria from the pore water of the Mont Terri URL. After 4 weeks of incubation the observed colonies were picked and transferred to new agar plates. The colonies were white or yellow colored, circular shaped but with different size. The 16S rRNA gene of the isolates was amplified with the primers $16S_{7f}$ and $16S_{1513r}$ with an *in-situ* PCR, sequenced and phylogenetic analyzed to get some information about these isolates. All the isolates enriched and isolated from 50 % R2A media were affiliated with *Betaproteobacteria* (Fig. 2.5). The 16S rRNA gene of isolate HT3-12 was 99 % similar to the 16S rRNA gene of the uncultured *Acidovorax* sp. A19, which was retrieved from a low-grade copper bioleaching heap, and *Acidovorax facilis* 228. Interestingly, 16S rRNA genes of *Acidovorax* spp. were also detected in the clone library of sample MT-2 (see clones MT-2-81 and MT-2-113 in Fig. 2.5 and chapter 2.1.1). In this case, we could identify *Acidovorax* spp. by a culture-dependent method in the pore water and a culture-independent method in the clay sample. In addition, the isolate HT3-8 (Fig. 2.5) was closely affiliated with the betaproteobacterium *Cupriavidus campinensis* WS2, the type strain of *Cupriavidus campinensis*.

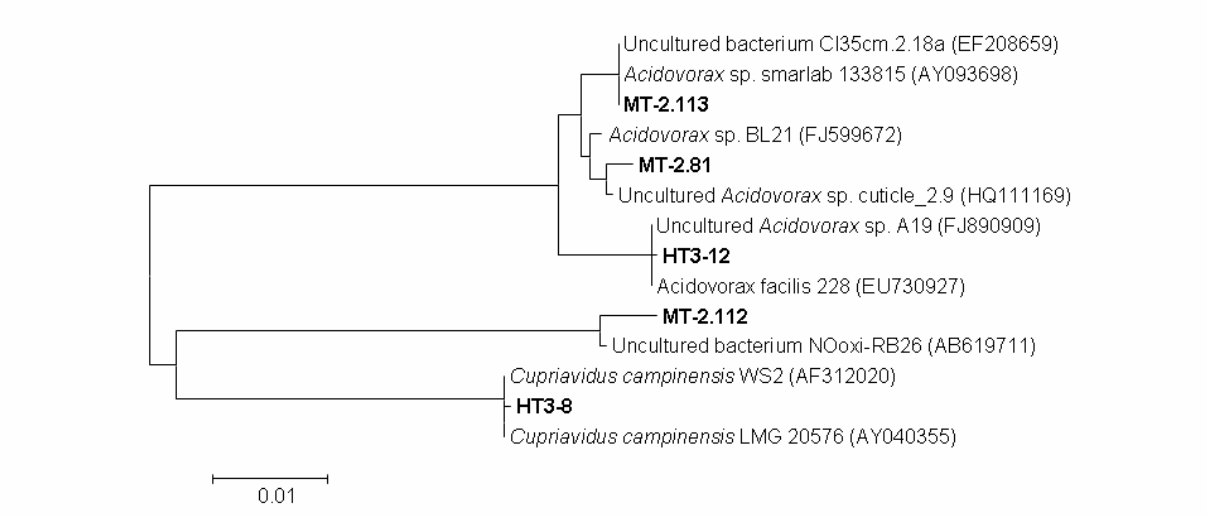

Fig. 2.5 Phylogenetic dendrogram of the 16S rRNA genes of the betaproteobacterial isolates obtained from the Mont Terri pore water HT3 and sequences retrieved from the clone library of sample MT-2.

From the MT-2 sample were also bacteria isolated on R2A media but with a slightly different method (see 2.2.1). As mentioned above *Bacilli* and *Clostridia* were in comparison to the pore water detected in the Opalinus Clay sample.

A nitrite reducing media (G1M1) was also used to isolate bacteria from the pore water. In comparison to the R2A media, only representatives of *Gammaproteobacteria* were enriched on the G1M1 media. The 16S rRNA genes of these isolates were similar to the 16S rRNA gene of *Pseudomonas stutzeri*, a well known denitrifier, which was dominating the pore water sample by culture-independent 16Sr RNA gene retrieval (see 2.1.3).

The limited bacterial diversity observed by the culture-dependent method in the pore water from the Mont Terri URL can be explained by the unfavorable living conditions in the Opalinus Clay. In addition, we could demonstrate that it also depends on the used media, what kind of bacteria can be enriched and isolated from the sample. The used R2A media is specific for oligotrophic microorganisms, whereas the G1M1 media is specific for nitrite reducing bacteria.

3 Cultivation and characterization of bacterial isolates from Mont Terri URL and from Äspö HRL

3.1 Experimental

Cultivation of bacterial isolates

The Mont Terri isolates *Paenibacillus* sp. MT-2.2 and *Sporomusa* sp. MT-2.99 were grown at anaerobic conditions (N_2 atmosphere) in R2A medium (DSMZ medium 830) at 30°C. The cells were grown to the late exponential growth phase to an OD_{600} of 0.08 - 0.09 for two days and separated from the growth medium by centrifugation (8000g). For An/Ln interaction experiments (see chapter 4) the cells were washed three times and suspended in degassed analytical grade 0.1 M $NaClO_4$ or 0.9 % NaCl (Sigma-Aldrich, Germany), respectively. The biomass of the cell stock suspension was determined by measuring the OD_{600} which was then converted to the dry biomass according to the following equations:

a) *Sporomusa* sp. $[dry\ biomass] = 0.280 \cdot OD_{600}$ (3.1);

b) *Paenibacillus* sp. $[dry\ biomass] = 0.336 \cdot OD_{600}$ (3.2).

The Äspö isolate *P. fluorescens* (CCUG 32456 A) was grown in batch cultures under aerobic conditions at 30°C. The strain was grown in two different media depending on the designated experiment. The nutrient broth (NB) medium (DSMZ medium 1a: 5 g/L peptone, 3 g/L meat extract, pH 7.0) was used for experiments with metabolically inactive cells. The cells were grown to the mid-exponential growth phase to an optical density at 600 nm (OD_{600}) of 1.0 - 1.2 and then separated from the growth medium by centrifugation (8000g). The standard succinate medium (SSM) (Albrecht-Gary et al. 1994) as a minimal medium was used for investigating the interaction of metabolically active cells. The SSM's initial amount of phosphate was reduced to 0.5% to reduce U(VI) phosphate precipitation. The optical density at 600 nm (OD_{600}) was found to be correlated to the [dry biomass] in (g/L) according to the following equation:

$[dry\ biomass] = 0.290 \cdot OD_{600}$ (3.3).

The equations 3.1 to 3.3 were used for dry biomass determinations.

Purity control and microbiological characterization of the bacterial isolates

To ensure the purity of the used bacterial strains light microscopy, plating on respective agar (colony homogeneity) and *in situ* PCR with RFLP were employed. In case of the investigated Mont Terri strains additionally sequencing was done to provide the correct genus and species

of this novel isolates. The PCR was done directly from freshly grown cells using the universal primer pair 8F 1513R. The PCR mixture with a final volume of 20 µL contained 0.9 µL template DNA, 1.3 mM $MgCl_2$, 2.5 nmol each of the four desoxynucleoside triphosphates (dNTPs), 7 pmol each of the forward and reverse primer, 1 U Taq DNA polymerase and 2 µL of the corresponding 10x Taq polymerase buffer (Promega, Mannheim, Germany). The PCR amplification was carried out using a Biometra thermocycler (Göttingen, Germany). Generated PCR amplicons were digested with the endonucleases *Hae*III and *Rsa*I in the corresponding buffers (Promega, Mannheim, Germany) overnight at 37°C. Restriction fragments were separated electrophoretically in a 3 % low melt agarose gel (Biozym, Oldenburg, Germany), stained with ethidium bromide and viewed under UV illumination. The resulting RFLP profiles were partly compared with the theoretical ones which were calculated using the software Restriction Mapper.

To characterize the bacterial cell walls as an influencing factor in actinide binding, *Sporomusa* sp. MT-2.99, *Paenibacillus* sp. MT-2.2 and *P. fluorescens* were analysed employing microbiological techniques such as Gram staining, KOH test and aminopeptidase test.

Cell surface characterization by potentiometry

Potentiometric titration was employed to determine the pK_a values and surface site densities of the bacterial isolates as a basis for eventually determining the stability of the An/Ln complexes formed. At first the cells were washed three times with a solution containing 0.099 M NaCl and 0.001 M HCl. The cells were then suspended in the same solution to yield a final total volume of 40 mL, a dry biomass concentration of max. 0.3 $g_{dry\ weight}/L$ and a pH of about 3. Prior to the titration bacterial suspensions were degassed for 20 min with N_2. Titrations were carried out manually and in triplicate under N_2 atmosphere in a glove box at 25°C. The bacterial suspensions were titrated from pH 3 to 10.6 using CO_2-free 0.042 M NaOH. Higher pH values result in base hydrolysis of the cells. The exact titrant concentration was determined by counter titration with standard 0.100 M HCl (Merck, Germany). The pH was measured using a glass electrode (InLab Solids, Mettler-Toledo, Giessen, Germany) calibrated with standard buffers and a pH meter (InoLab720, WTW, Weinheim, Germany). The titration curves consisted of 85 data points with an average pH interval of 0.08 units. Each titration curve was evaluated using the program HYPERQUAD (Gans et al. 1996).

3.2 Results and discussion

3.2.1 The Mont Terri Opalinus Clay isolate *Sporomusa* sp.

Purity control

RFLP profiles were used to monitor the microbiological purity of the bacterial isolates used for An/Ln experiments. In the following the restriction digests of the 16S rRNA of *Sporomusa* sp. MT-2.99 with *Hae*III and *Msp*I are shown (Fig. 3.1).

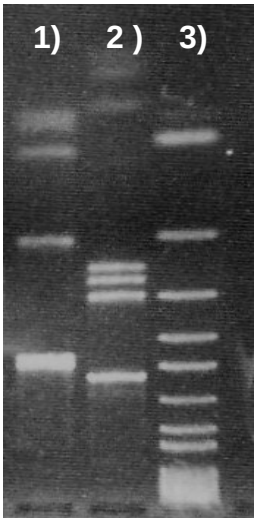

Fig. 3.1 RFLP profiles of *Sporomusa* sp. MT-2.99, lane 1) digest with *Hae*III, lane 2) digest with *Msp*I, lane 3): size marker.

Cell morphology

The isolated *Sporomusa* sp. strain MT-2.99 is an obligate anaerobe as all other members of the genus *Sporomusa*. Unique morphological features were observed for this isolate depending on the growth phase, as shown in Figure 3.2.

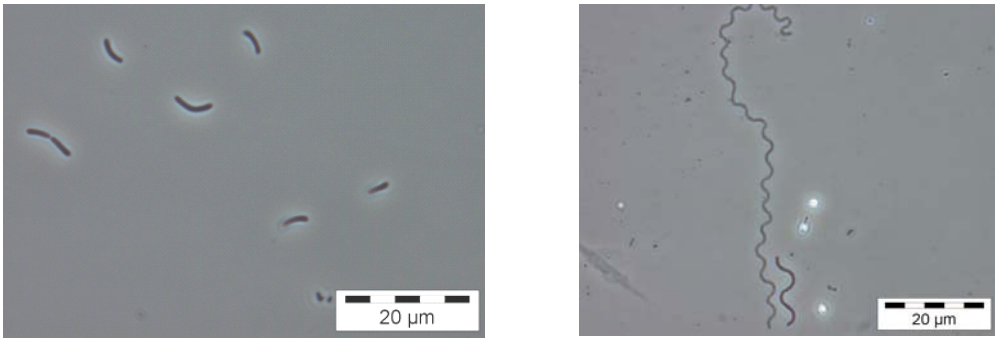

Fig. 3.2 Characteristic morphological features of *Sporomusa* sp. MT-2.99 – banana-shaped rods in early exponential growth phase (left) and formation of elongated cells and endospores in stationary phase (right).

In the early exponential growth phase a banana-shaped cell morphology typical for members of the *Sporomusa* genus was observed. To our knowledge unique for a strain of this genus was the appearance of strongly elongated spiral-shaped cells in the stationary growth phase (Fig. 3.2 right), 0.7 µm in diameter and maximum observed length 103 µm.

In order to appropriately assess the An (Ln) binding to the cell surfaces of the different bacterial strains different microbiological methods were employed to characterize the bacterial cell walls: the amino peptidase test, Gram staining, and the KOH test. The results of the former two tests for *Sporomusa* sp. cells are displayed in Figure 3.3.

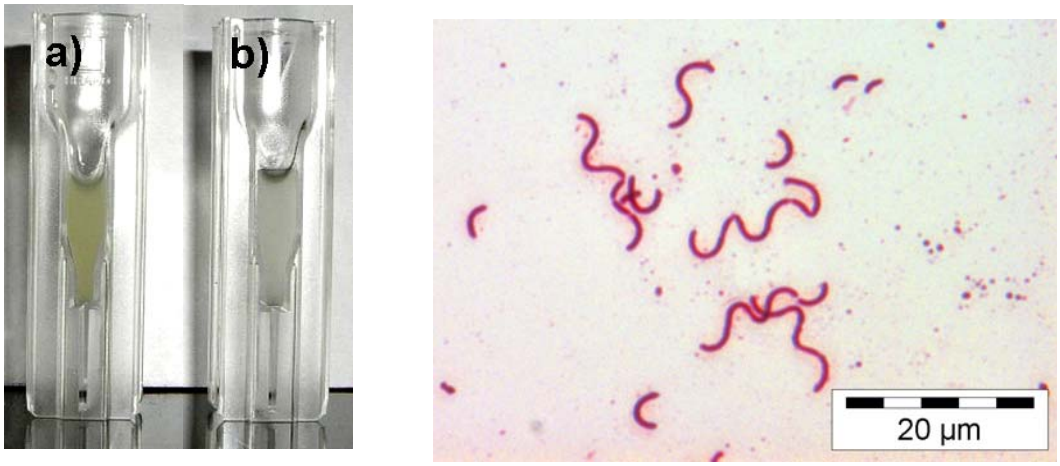

Fig. 3.3 Assessment of cell wall structure of *Sporomusa* sp. MT-2.99 by means of amino peptidase test (left) and Gram staining (right). The left image displays the *L*-alanine 4-nitroanilide conversion by *Sporomusa* sp. MT-2.99 (a) compared to *Paenibacillus* sp. MT-2.2 (b).

The amino peptidase test is based on that almost all Gram-negative bacteria are able to convert *L*-alanine nitroanilide to nitroanilide (yellow). *Sporomusa* sp. was able to convert *L*-alanine nitroanilide in contrast to *Paenibacillus* sp. cells, the second investigated Mont Terri isolate. Hence the *Sporomusa* sp. isolate can be classified as Gram-negative, while *Paenibacillus* sp. MT-2.2 is Gram-positive. Also the Gram staining and KOH test indicated *Sporomusa* sp. to be Gram-negative. However, a definite classification of the cell wall is difficult for *Sporomusa*. Because *Sporomusa* belongs to *Negativicutes* a class of firmicute bacteria, whose members have a peculiar cell wall composition which stains Gram-negative, unlike most other members of the *Firmicutes*.

Characterization of cell surface functional groups

The titration curves of the bacterial strains were all fitted with a three-site model using HYPERQUAD (Gans et al. 1996). The application of HYPERQUAD is a novel approach. Hitherto, for evaluation the codes Protofit (Turner and Fein 2006) and FITEQL (Westall

1982) have been used. The description of the bacterial cell wall with three major global binding sites is a common approach (Fein et al. 1997, Yee et al. 2004, Dittrich and Sibler 2005, Fang et al. 2009). As described in detail by (Moll et al. 2013b) and shown in Figure 3.4 the fit of the titration curve of *Sporomusa* sp. cells with HYPERQUAD delivered a very good result also in view of the determined σ^2 values of the fit.

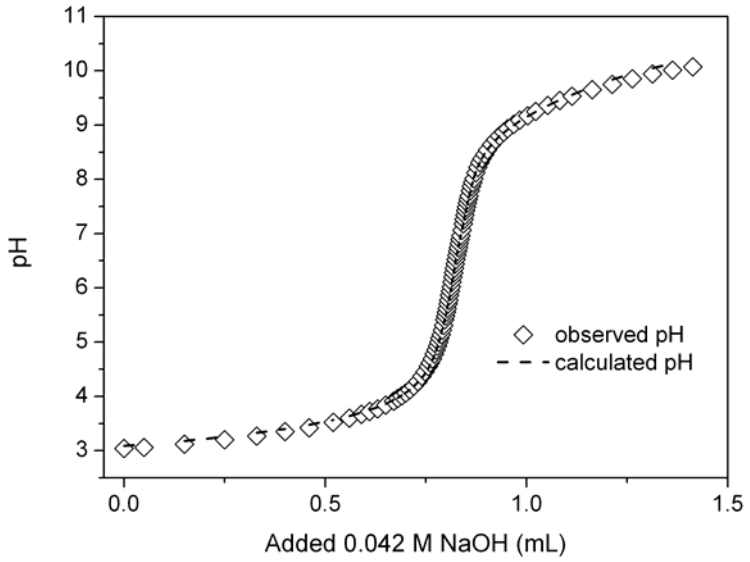

Fig. 3.4 Titration of 0.3 $g_{dry\ weight}$/L *Sporomusa* sp. cells with 0.042 M NaOH and fit with HYPERQUAD.

Calculated pK_a values and site densities of the binding sites amounted to 4.80 ± 0.06 (0.53 ± 0.08 mmol/$g_{dry\ weight}$), 6.68 ± 0.06 (0.35 ± 0.03 mmol/$g_{dry\ weight}$), and 9.01 ± 0.08 (0.48 ± 0.05 mmol/$g_{dry\ weight}$). By comparing these values to the pK_a ranges of different functional groups reported in (Cox et al. 1999), the respective surface functional groups can be attributed to carboxyl, phosphate and amine moieties. The determined pK_a values of the major global binding sites are in a very good agreement to those determined for a strain of the Gram-negative genus *Calothrix* (Yee et al. 2004). The agreement of our results with the literature also signifies that HYPERQUAD analysis as a novel approach is appropriate for modelling surface site reactions of bacterial cell walls.

3.2.2 The Mont Terri Opalinus Clay isolate *Paenibacillus* sp.

Purity control

The RFLP pattern shown in Figure 3.5 demonstrates the microbiological purity of the *Paenibacillus* sp. isolate used for An experiments. Its RFLP pattern is shown in comparison to the one of *Paenibacillus wynnii* LMG 22176T (Rodriguez-Diaz et al. 2005), the closest phylogenetic affiliate.

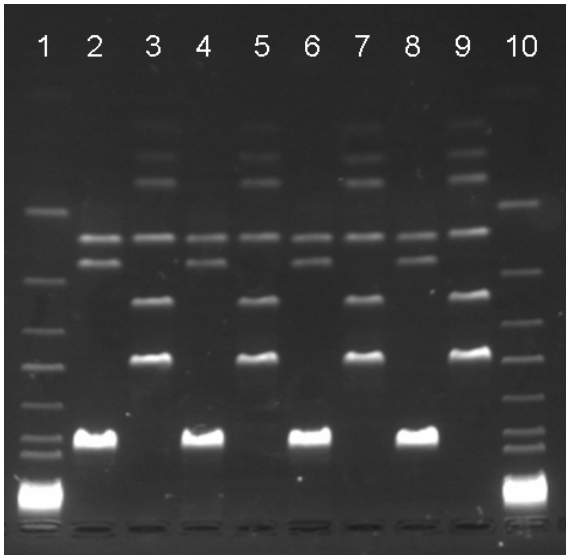

Fig. 3.5 Comparison of the RFLP profiles of the Opalinus Clay isolate *Paenibacillus* sp. (6-9) and *Paenibacillus wynnii* LMG 22176^{T} (2-5). Lane 2, 4, 6, 8 are digests with *Hae*III, lane 3, 5, 7, 9 those with *Rsa*I. Lane 1 & 10: size marker.

Cell morphology

The *Paenibacillus* sp. clay isolate was found to be facultative anaerobic. The formation of endospores typical for strains of the genus *Paenibacillus* was also observed. Cells were rod-shaped, 0.7 µm in diameter, and occurred partly strongly elongated (up to 144 µm). Figure 3.6 exemplarily illustrates mentioned morphological features.

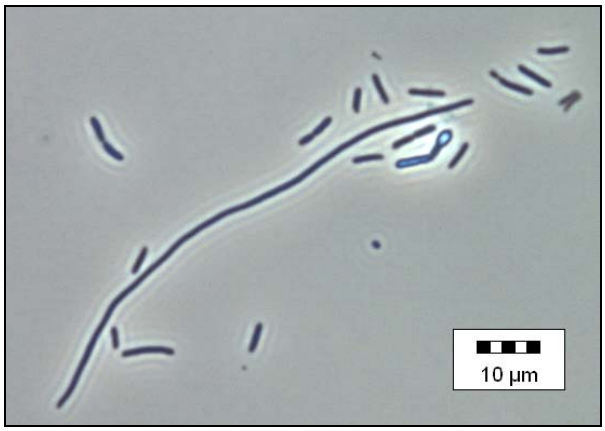

Fig. 3.6 Characteristic morphological features of *Paenibacillus* sp. MT-2.2 - formation of elongated cells and endospores.

In view of the size of vivid, reproducing cells of this strain, cell viability inside the compact clay seems questionable. While the vivid bacteria are at least several µm in size, the clay pores are only in the nm range. Remarkable is that all the isolates recovered from the Mont Terri clay are pronounced endospore formers. Since endospore match the size of the pores it

is assumed that the recovered isolates have endured the harsh conditions inside the clay over large periods in time in a dormant state in the form of spores.

The capability of vivid *Paenibacillus* sp. cells to form elongated cells as shown in Figure 3.6 differentiates the isolate from the closest affiliate *Paenibacillus wynnii* LMG 22176T.

The study of the cell wall structure with Gram staining indicated the strain to be weakly Gram-positive (Fig. 3.7). In the KOH test no lysis of the cell walls was observed which also signified that the Mont Terri isolate is Gram-positive.

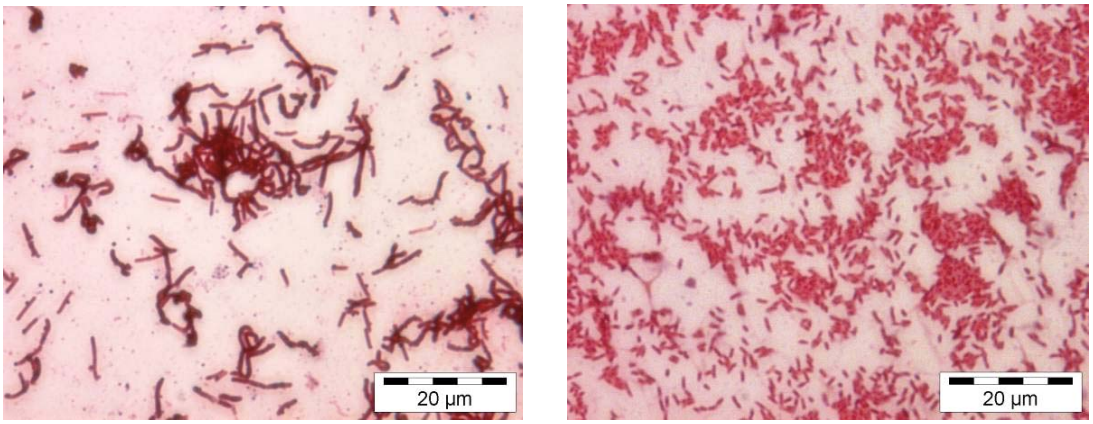

Fig. 3.7 Gram staining of *Paenibacillus* sp. MT-2.2 (left) in comparison to *E. coli* (Gram-negative reference strain) (right).

The inability of *Paenibacillus* sp. cells to cleave *L*-alanine from *L*-alanine nitroanilide in the amino peptidase test was illustrated previously (Fig. 3.3) and also indicated the strain to be Gram-positive.

Characterization of cell surface functional groups

As described previously for the other Mont Terri isolate *Sporomusa* sp. MT-2.99, the potentiometric data of the *Paenibacillus* sp. isolate was fitted with a three-site-model using HYPERQUAD. Calculated pK_a values and densities of the surface functional groups of *Paenibacillus* sp. cells amounted to 4.90 ± 0.05 (0.55 ± 0.12 mmol/$g_{dry\ weight}$), 6.66 ± 0.10 (0.24 ± 0.01 mmol/$g_{dry\ weight}$), and 9.20 ± 0.03 (1.19 ± 0.26 mmol/$g_{dry\ weight}$) (Lütke et al. 2013b). Again an excellent agreement can be found comparing our results to the ones published by (Yee et al. 2004), who reported pK_a values of 4.7 ± 0.4, 6.6 ± 0.2, and 9.1 ± 0.3 investigating cyanobacteria.

3.2.3 The Äspö-strain *Pseudomonas fluorescens* (CCUG 32456)

Purity control

Investigating planktonic cells and biofilms of *P. fluorescens*, the microbiological purity of the strain was checked frequently by *in situ* PCR and subsequent RFLP, as previously described. Figure 3.8 exemplarily shows the agreement of both, the experimental and the theoretical RFLP profiles, for *P. fluorescens* using the endonucleases *Hae*III and *Rsa*I.

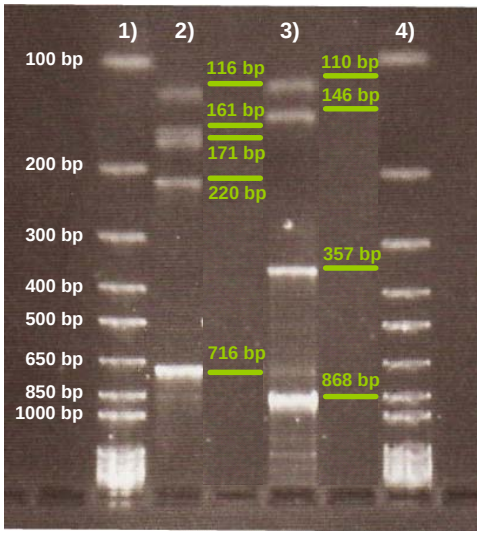

Fig. 3.8 RFLP profiles of digests with *Hae*III (2) and *Rsa*I (3) compared to the one of the marker (1, 4). Calculated theoretical RFLP profiles are given in green to the right of the respective lane.

Furthermore an indication for culture purity is that the sizes of the digest fragments add roughly up to the amplicon size of about 1500 bp. This procedure was applied to all bacterial stock suspensions used for actinide interaction experiments and used for biofilm generation and also to monitor the purity of the generated biofilm.

3.2.3.1 Planktonic cells

Cell morphology

A characteristic light microscopic image of planktonic cells of the here investigated strain *P. fluorescens* CCUG 32456A is presented in Figure 3.9. Since for the Äspö isolate *P. fluorescens* the exact phylogenetic classification has been determined before it was almost certain that the strain is Gram-negative. Hence the microbiological cell wall characterization of this strain is given here in brief. Same tests were applied as for the Mont Terri isolates. The Gram staining reaction was negative. In the KOH test lysis was observed also indicating the cell walls to be Gram-negative. These findings were confirmed by the amino peptidase test in

which the strain was able to convert *L*-alanine nitroanilide. Overall the original assumption of *P. fluorescens* being Gram-negative could be proven.

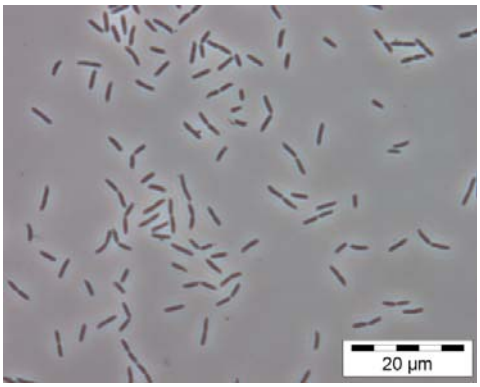

Fig. 3.9 Phase contrast light microscopic image of *P. fluorescens* (CCUG 32456A) in the mid-exponential growth phase.

Characterization of cell surface functional groups

Analogous to the evaluation of *Sporomusa* sp. and *Paenibacillus* sp. titration data the titration curve of *P. fluorescens* (CCUG 32456A) was fitted with a three-site model with HYPERQUAD. Based on the residues and sigma a three-site model here also provided a very good fit of the experimental data. Calculated pK_a values and site densities of the binding sites were 4.65 ± 0.13 (0.82 ± 0.06 mmol/$g_{dry\ weight}$), 6.62 ± 0.13 (0.36 ± 0.09 mmol/$g_{dry\ weight}$), and 9.18 ± 0.02 (0.78 ± 0.24 mmol/$g_{dry\ weight}$). The parameters determined for surface functional groups of *P. fluorescens* (CCUG 32456 A) are comparable to those obtained for another strain of this bacterium, *P. fluorescens* (ATCC 55241) (Yoshida et al. 2004).

3.2.3.2 Biofilms

For the biofilm formation a *P. fluorescens* (CCUG32456) strain was cultivated in a synthetic nutrient medium consisting in 5 g/L peptone and 3 g/L meat extract with a pH 7 ± 0.2 in the absence of glucose. The phosphate amount was low ($[PO_4^{3-}]$ = 12.7 mg/L). The culture was harvested in the mid-exponential growth phase. The optical density was adjusted to 0.2 at 600 nm. A volume of 3.6 mL of the *P. fluorescens* culture was added to 400 mL of the synthetic nutrient medium, kept in a glass plunger in air atmosphere under sterile condition. After seven days the *P. fluorescens* strain formed a 400 µm thick slimy biofilm as homogeneous surface pellicle on the interface between air and nutrient medium. After plating the strain on NB agar and with *in situ* PCR with subsequent RFLP the purity of the strain was analyzed with light microscopy.

4 The interaction of bacterial isolates from Mont Terri Opalinus Clay with selected actinides

Bacteria are known to interact with actinides through versatile processes thereby influencing the actinide speciation and hence migration (Lovley et al. 1991, Panak et al. 2002, Moll et al. 2004, Renninger et al. 2004, Merroun and Selenska-Pobell 2008, Sheng et al. 2011, Moll et al. 2013) in the environment. Therefore it is of importance to identify relevant interaction processes occurring with dominant bacterial strains isolated from mentioned sites destined for instance for the safe disposal of nuclear waste and to assess the resulting actinide speciation. Bacteria belong to the most widely spread organisms in nature. Besides archaea, these organisms represent the only form of life which can inhabit hostile environments of e.g. high salinity (Oren 2002), temperature (Takai et al. 2008) and radiation (Makarova et al. 2001), like in designated nuclear waste disposal sites.

In general, the versatile interactions between microbes and actinides can be classified into two major categories, the direct and indirect interaction mechanisms. Direct interactions include the processes uptake, biosorption, biomineralization, and biotransformation (Figure 4.1).

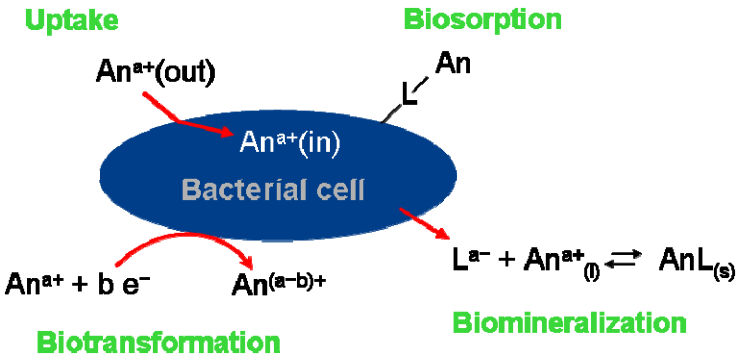

Fig. 4.1 Interaction mechanisms between bacteria and actinides (An).

Uptake means the incorporation of the actinide inside the cell. With biosorption is meant that a pure binding of the actinide to cell surface functional groups occurs. Biomineralization refers to the cellular liberation of inorganic ligands leading to the formation of a precipitate, e.g. meta-autunite. Biotransformation is a very general term referring to a microbe-mediated conversion of the oxidation state (oxidation or reduction) of the respective actinide. Indirect interaction refers to the release of cellular ligands which bind to the actinides in solution. A prominent example is the release of siderophores of the pyoverdin type by *P. fluorescens*

which have shown to possess great binding potential towards U(VI), Cm(III) and Np(V) (Moll et al. 2008, 2010).

The diversity of interaction mechanisms is due to the variety of metabolism and cell surface structures among microbes. The cell walls of bacteria represent a highly efficient matrix for metal sorption offering mainly carboxylic, phosphoryl and amine moieties for metal complexation (Beveridge and Doyle 1989). It has been proposed that bacteria freely suspended in solution may even have a radionuclide-sorbing capacity higher than that of the surrounding mineral phases (Pedersen and Albinsson 1992, Bencheikh-Latmani et al. 2003, Ohnuki et al. 2005).

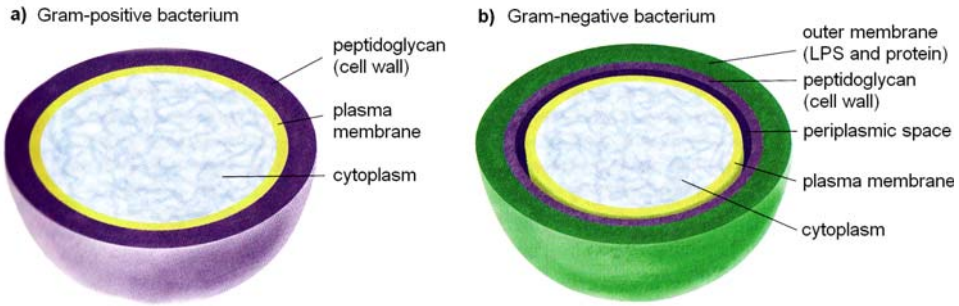

Fig. 4.2 Types of bacterial cell walls, adapted from (Voet et al. 2002).

The composition of the cell wall differs for Gram-negative and Gram-positive bacterial strains. Since strains of the genera *Pseudomonas*/*Sporomusa* and *Paenibacillus* differ by that, with the present work the influence of the cell wall structure on actinide binding can be assessed. The cell walls of Gram-negative bacteria like *Sporomusa* sp. / *P. fluorescens* possess an outer membrane of lipopolysaccharide (LPS), a periplasm consisting of a thin layer of peptidoglycan (PG), and an inner cytoplasmic membrane (phospholipid bilayer) (Fig. 4.2b). The LPS offers carboxyl, phosphoryl, hydroxyl and amino groups as binding sites for metals (Beveridge and Doyle 1989). The PG polymeric framework itself is rich in carboxylate groups. In the PG framework teichoic and teichuronic acids are interconnected, which contain also phosphate groups. In contrast to *Pseudomonads*, strains of the genus *Paenibacillus* are Gram-positive. In Gram-positive bacteria the major and very outer cell wall component is peptidoglycan (see Fig. 4.2a) which can make up to 90 % of the dry weight of the bacterial cells. As explained previously, in PG also carboxyl and phosphoryl moieties are relevant for metal complexation. PG contains teichoic acids which are basically glycerol phosphate polymers. In the following sections when discussing the bacterial An/Ln interaction results a closer description of the cell wall structures of the discussed strains will be given as well as the state-of-the-art concerning bacterial U(VI), Cm(III)/Eu(III) and Pu interactions.

4.1 Experimental

Preparation of actinide bacteria solutions

U(VI) biosorption by the Mont Terri isolates was investigated in dependence on $[U(VI)]_{initial}$, and pH at anaerobic conditions (N_2 atmosphere). The U(VI) binding in dependence on $[U(VI)]_{initial}$ was investigated at pH 4, 6, and 7. For all U(VI) experiments a stock solution of 0.1 M $UO_2(ClO_4)_2$ was used. U(VI) accumulation experiments were carried out in 0.1 M $NaClO_4$ (Sigma-Aldrich, Germany). The pH adjustments were made with $HClO_4$ or NaOH both from Merck, Germany. The pH was measured using an InLab Solids electrode (Mettler-Toledo, Giessen, Germany) calibrated with standard buffers and a pH meter (InoLab720, WTW, Weinheim, Germany). The pH was adjusted with a precision of 0.03 units. To investigate U(VI) sorption in dependence on $[U(VI)]_{initial}$ the dry biomass was set to 0.2 $g_{dry\ weight}$/L, while [U(VI)] was varied from 0.4 to max. 48 mg/L.

The adsorption of UO_2^{2+} onto the reaction vessel as source of error of this experiment was investigated. Therefore after the U(VI) interaction experiment the reaction tubes were rinsed 3 times with Milli-Q water and then incubated for 2 days with 1 M HNO_3 to desorb U(VI). Solutions where then analysed with ICP-MS regarding [U(VI)]. All experiments were done in duplicate.

In addition to the analysis of the supernatants regarding [U(VI)], selected samples were also analysed regarding the release of inorganic phosphate in dependency on the pH and $[U(VI)]_{initial}$ by means of ion exchange chromatography (IEC). To judge to which extent phosphate release occurs without U(VI) added furthermore pure bacterial solutions were analysed.

Time-resolved laser-induced fluorescence spectroscopy (TRLFS) samples were prepared analogously to the samples of the U(VI) binding experiments. The [U(VI)] and [dry biomass] were set to $1 \cdot 10^{-4}$ M and 0.2 $g_{dry\ weight}$/L, respectively. Investigated pH values were also chosen analogously to the biosorption studies. In addition, the influence of $[U(VI)]_{initial}$ on U(VI) binding by *Paenibacillus* sp. cells was investigated at pH 5.

Prior to the TRLFS measurement, the U(VI)-loaded cells were washed three times in 0.1 M $NaClO_4$ at the appropriate pH to remove loosely bound U(VI). Besides the U(VI)-loaded cells also the corresponding supernatants were measured with TRLFS.

The interaction of trace amounts of Cm(III) ($3 \cdot 10^{-7}$ M) with *Sporomusa* sp. and *Paenibacillus* sp. cells was investigated in dependency on pH. A stock solution of the long-lived curium isotope ^{248}Cm was used. This solution had the following composition: 97.3% ^{248}Cm, 2.6% ^{246}Cm, 0.04% ^{245}Cm, 0.02% ^{247}Cm, and 0.009% ^{244}Cm in 1.0 M $HClO_4$. An europium(III)

stock solution was prepared by dissolving $EuCl_3$ in water. The experiments were performed in a glove box under an N_2 atmosphere at 25ºC. As a background electrolyte, analytical grade 0.1 M $NaClO_4$ (Merck, Darmstadt, Germany) was used. To prevent the carbonate complexation of curium(III) and europium(III), carbonate-free water and a NaOH solution were used. The pH was measured using an InLab Solids combination pH puncture electrode (Mettler-Toledo, Giessen, Germany) calibrated with standard buffers. The pH was changed by adding analytical grade NaOH (Merck) or $HClO_4$ (Merck) with an accuracy of ± 0.02 units. TRLFS measurements were performed at different biomass concentrations (0.01 - 200 $mg_{dry\ weight}/L$) within a pH-range of 8.0-2.0. Three series of experiments were performed at 3 µM Eu^{3+} to explore its interaction behavior with *Sporomusa* sp. . Here the biomass concentration was kept constant at 0.02 $g_{dry\ weight}/L$, while varying pH between 8.0-2.0. In order to obtain information on the binding strength and the reversibility of the biosorption process, the Cm(III)/Eu(III) on the biomass was extracted with 0.01 M EDTA solution (pH 5) as described by Panak and Nitsche 2001.

Bacterial An (Ln) surface species characterized by potentiometry

For titrations with Eu(III) the experimental setup was the same as described previously for the titration of pure bacterial suspensions. The final [Eu(III)] was set to $1 \cdot 10^{-4}$ M. The titrations of U(VI) and bacteria were carried out analogously. The only difference existed in the used background electrolyte, which was 0.1 M $NaClO_4$ for titrations of solutions containing U(VI). For this purpose cells were washed three times in 0.1 M $NaClO_4$ as background electrolyte and then suspended in the same solution. The [dry biomass] and [U(VI)] were set to 0.3 $g_{dry\ weight}/L$ and $1 \cdot 10^{-4}$ M UO_2^{2+}, respectively. A starting pH of about 3 was established by adding a defined quantity of $HClO_4$. As titrant CO_2-free 0.042 or 0.050 M NaOH was used. To calculate the stability constants of the U(VI) and Eu(III) surface complexes from the titration data HYPERQUAD (Gans et al. 1996) was employed.

Experimental setup of the applied spectroscopic techniques

Time-resolved laser-induced fluorescence spectroscopy

For U(VI) measurements a pulsed Nd:YAG laser (Minilite, Continuum Inc., Santa Clara, USA) with an emission wavelength of 266 nm and a repetition rate of 10 Hz was used for excitation of the uranyl ion. By means of a fiber optic cable the luminescence emission signal was focused onto a spectrograph (iHR 550, Yobin-Ivon Horiba). The luminescence spectra were measured with an intensified CCD camera (Yobin-Ivon Horiba). Using an internal delay

generator, time-resolved spectra were recorded from 300 ns up to a maximum delay of 10.3 µs and with a maximum increment of 200 ns. The spectra were recorded from a delay time of 300 ns to avoid measuring the fluorescence of cellular organic matter. The spectra were recorded from 371 to 674 nm, averaging three spectra with 100 laser shots per spectrum. A pulse width of 2 µs was applied. The TRLFS setup has been described in detail elsewhere (Geipel et al. 1996).

For Cm(III)/Eu(III) the time-resolved luminescence spectra were recorded using a unique pulsed flash lamp pumped Nd:YAG-OPO laser system (Powerlite Precision II 9020 laser equipped with a Green PANTHER EX OPO from Continuum, Santa Clara, CA, USA). The laser pulse energy, which was between 1.5 and 2.5 mJ depending on the excitation wavelength used, was monitored using a photodiode. The luminescence spectra were detected using an optical multi-channel analyzer-system, consisting of an Oriel MS 257 monochromator and spectrograph with a 300 or 1200 line mm^{-1} grating and an Andor iStar ICCD camera (Lot-Oriel Group, Darmstadt, Germany). The TRLFS setup has been described in detail elsewhere (Moll et al. 2008a, 2013a). A constant time window of 1 ms length was applied. For Cm(III) measurements an excitation wavelength of 396 nm was used whereas for Eu(III) an excitation wavelength of 394 nm was applied. For time-dependent emission decay measurements, the delay time between laser pulse and camera gating was scanned with time intervals of 10, 15, or 20 µs. The excitation spectra of Cm(III) in *Sporomusa* sp. suspensions were scanned over the 350-410 nm range with a resolution of 1 nm. All TRLFS spectra were measured after an equilibration time of 20 minutes.

U(VI) binding by X-ray absorption spectroscopy (XAS)

Uranium L_{III}-edge x-ray absorption spectroscopy was carried out at the Rossendorf Beamline (ROBL) at the European Synchrotron Radiation Facility (ESRF) in Grenoble, France (Matz et al. 1999). For measurement a water-cooled Si(111) double-crystal monochromator and Si-coated mirrors for focusing and rejection of higher harmonics in channel cut mode (5-35 keV) were used. The extended X-ray absorption fine structure spectroscopy (EXAFS) spectra were recorded in fluorescence mode using a 13-element Ge solid-state detector as well as in transmission mode using ionization chambers. Energy calibration was done measuring the K-edge spectrum of an Y foil and defining the first inflection point as 17038 eV. Spectra were analyzed using the programs Sixpack/ Samview (Webb 2005) and WinXAS version 3.1 (Ressler 1998). The theoretical backscattering phases and amplitude functions for analysis of the data were created using the FEFF8 code (Ankudinov et al. 1998). As model structures

either that of meta-autunite (Makarov and Ivanov 1960, Locock and Burns 2003) or a combined structural model of uranyl acetate (Ramos Silva et al. 1999) and uranyl adenosine monophosphate (Szabó et al. 2005) was used. All fits included the four-legged multiple scattering (MS) path of the UO_2^{2+} ion, $U \rightarrow O_{ax} \rightarrow U \rightarrow O_{ax}$. The radial distance R and Debye-Waller factor σ^2 of the MS path were correlated to the corresponding single scattering (SS) path by multiplying R and σ^2 of the latter with two (Hudson et al. 1996). During the fit the coordination number N of the $U \rightarrow O_{ax}$ SS path was fixed to 2. For all fits the amplitude reduction factor S_0^2 was held constant at 0.95. The fit was carried out in R-space.

TRLFS: evaluation of Cm(III)/Eu(III) luminescence spectra

The spectra were base-line corrected, energy corrected and normalized using the ORIGIN 6.1G (OriginLab Corporation, USA) code. The lifetime of luminescent species was obtained also with this software. In the case of europium(III) normalization was applied only to the peak area of the $^5D_0 \rightarrow {}^7F_1$ band because the luminescence of this transition is a magnetic dipole and therefore not influenced by the chemical environment of the metal ion. In the case of europium(III) the relative peak intensity ratio ($R_{E/M}$) was defined as:

$$R_{E/M} = I\,(^5D_0 \rightarrow {}^7F_2) / I\,(^5D_0 \rightarrow {}^7F_1) \qquad (4.1)$$

where I ($^5D_0 \rightarrow {}^7F_2$) and I ($^5D_0 \rightarrow {}^7F_1$) were calculated from the peak areas. The number of coordinated water molecules was calculated using the empirical equations given by Kimura et al. 1994, 1996, 1998:

$$n_{H2O} \pm 0.5 = 0.65 \times 1/\tau - 0.88 \text{ for curium(III)} \qquad (4.2)$$

$$n_{H2O} \pm 0.5 = 1.07 \times 1/\tau - 0.62 \text{ for europium(III)} \qquad (4.3)$$

Luminescence data were evaluated by the factor analysis technique, a powerful tool for the determination of the number of independent absorbing/emitting species in a series of mixtures. In the past we could demonstrate the successful application of a respective software, SPECFIT (Binstead et al. 2004), to describe the complexation of Cm^{3+} and Eu^{3+} with a variety of ligands by luminescence data (e.g., Moll et al. 2005, 2008, 2012, Glorius et al. 2008, Heller et al. 2009, 2012, Barkleit et al. 2013). Input parameters for the data fitting were the known and calculated total concentrations of Cm^{3+}/Eu^{3+} and of the functional groups located at the cell envelope of *Sporomusa*/*Paenibacillus* sp. (biomass concentration in $g_{dry\ weight}$/L and pK_a's and corresponding site densities), the pH of each sample, the known stability constants of the curium(III)- and europium(III) hydroxides, that have been derived from (Guillaumont et al. 2003, Plancque et al. 2003) and corrected for I = 0.1 M, respectively, and the normalized

sample spectra. Accompanying speciation calculations were done with the program MEDUSA (Puigdomenech 2002).

Pu biosorption, absorption spectroscopy, solvent extraction

The starting compound to obtain the ^{242}Pu stock solution was a green-brown powder of PuO_2 (AEA technology QSA GmbH) with the following composition: 0.009 % of Pu-238, 0.008 % Pu-239, 0.020 % Pu-240, 0.017 % Pu-241, 99.945 % Pu-242, and 0.001 % Pu-244. The problem is that this substance is chemically highly inert and dissolves extremely slowly in acids (Keller 1971). We performed an oxidative dissolution of $^{242}PuO_2$ in HNO_3 in the presence of $AgNO_3$ and $K_2S_2O_8$. Finally the $^{242}Pu(VI)$ stock solution in 3 M $HClO_4$ was prepared by electrolysis.

The plutonium oxidation state distribution was determined by solvent extraction in combination with absorption spectroscopy (UV-vis-NIR). The absorption spectroscopy measurements were performed using a CARY5G UV-vis-NIR spectrometer (Varian Co.) at a temperature of 22 ± 1 °C. Because of the low absorption coefficients of Pu(IV), Pu(V), and Pu(IV)-polymers (Keller 1971, Wilson et al. 2005, Ockenden 1956) and the low concentration of Pu in the solutions, the quantification of the different Pu oxidation states was performed by solvent extraction. The extractions were performed rapidly and in parallel. All plutonium concentrations were measured by liquid scintillation counting (LSC) using a LS counter, Wallac system 1414 (Perkin Elmer). For this, defined sample volumes (0.1 to 1 mL) were mixed with 15 mL of Ultima Gold scintillation cocktail. The solvent extraction experiments demonstrated that the acidic Pu stock solution still contained, besides approximately 70 % Pu(VI), approximately 21 % Pu(IV)-polymers due to the synthesis procedure. The Pu-*Sporomusa* sp. experiments were performed at [dry biomass] of 0.33 ± 0.01 $g_{dry\ weight}/L$ and pH 6.2 under N_2 atmosphere at 25 °C in 0.1 M $NaClO_4$ solution. $[^{242}Pu]_{initial}$ was varied between 0.2 and 110 mg/L. The ^{242}Pu present in blank (no cells added), supernatant, and washed biomass suspension at pH 0 was analyzed using UV-vis-NIR spectroscopy, solvent extraction, and LSC as described in Moll et al. 2006. Detailed investigations of the distribution of the different Pu oxidation states were made at a fixed concentration of Pu, $[^{242}Pu]_{initial}$ of 15 ± 0.9 mg/L. Samples were taken after defined time steps. The separation of cells from the supernatant solution was performed by centrifugation (5000g).

4.2 Results and discussion

4.2.1 Actinide interactions with *Sporomusa* sp.

4.2.1.1 Interaction with U(VI)

U(VI) biosorption studies

The biosorption efficiency of a microbial strain is a key parameter for judging the retardation of the respective actinide caused by the strain. Furthermore such knowledge might be used for developing remediation strategies of contaminated sites. U(VI) biosorption of *Sporomusa* sp. cells was studied depending on $[U(VI)]_{initial}$ and pH (Fig. 4.3).

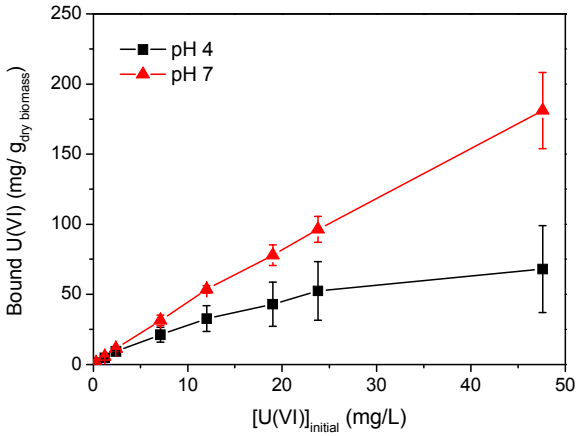

Fig. 4.3 U(VI) binding onto *Sporomusa* sp. MT-2.99 (0.2 $g_{dry\ weight}$/L) in dependence on $[U]_{initial}$ at different pH values in 0.1 M $NaClO_4$. U(VI) interaction time = 48 h.

Sporomusa sp. cells display a pronounced affinity for U(VI) while U(VI) binding is strongly pH-dependent. Almost three times as much U(VI) is immobilized at pH 7 compared to pH 4.

Potentiometric titrations

The bacterial surface functional groups are the primary binding partner for metal ions. Hence potentiometric titration has been employed for the determination of the U(VI) complexes with the bacterial surface functional groups. Figure 4.4 illustrates the titration curve of U(VI) with *Sporomusa* sp. cells and the fit with HYPERQUAD using a three-site model. The fit included the pK_a values and densities of the major global binding sites of the bacterial cell surfaces. In addition the following hydrolytic uranyl species and their stability constants were included in the fit: $(UO_2)_2(OH)_2^{2+}$, $(UO_2)_3(OH)_5^{+}$, $(UO_2)_4(OH)_7^{+}$ (Guillaumont et al. 2003). The titration curve could be modeled with a very good fit result when the complexes $R{-}COO{-}UO_2^{+}$, $R{-}O{-}PO_3H{-}UO_2^{+}$, $R{-}O{-}PO_3{-}UO_2$, and $(R{-}O{-}PO_3)_2{-}UO_2^{2-}$ were considered, as can be seen

from the HYPERQUAD fit result. The corresponding stability constants are summarized and compared to literature data in Table 4.1.

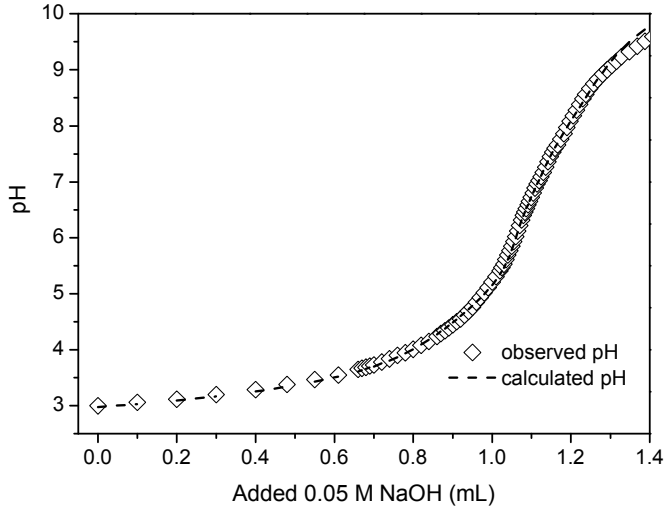

Fig. 4.4 Titration of $1 \cdot 10^{-4}$ M UO_2^{2+} and 0.3 $g_{dry\ weight}$/L cells in 0.1 M $NaClO_4$ with 0.050 M NaOH and fit with HYPERQUAD.

Table 4.1 Calculated stability constants of UO_2^{2+} complexes with *Sporomusa* sp. surface functional groups and comparison to literature.

Species	Complex	xyz [a]	log β_{xyz} (± SD)	Method	Reference
Sporomusa sp.	R-COO-UO_2^+	110	4.75 ± 0.98	PT	this work
	R-O-PO_3-UO_2	110	8.58 ± 0.04		
	R-O-PO_3H-UO_2^+	111	13.07 ± 0.06		
	$(R\text{-}O\text{-}PO_3)_2$-$UO_2^{2-}$	120	13.30 ± 0.09		
Peptidoglycan	R-COO-UO_2^+	110	7.28 ± 0.03 // 6.90 ± 0.20	PT // TRLFS	(Barkleit et al. 2009)
Lipopoly-saccharide	R-COO-UO_2^+	110	5.93 ± 0.17	PT	(Barkleit et al. 2008)
	R-O-PO_3-UO_2	110	7.50 ± 0.30 // 7.53 ± 0.25	PT // TRLFS	
	R-O-PO_3H-UO_2^+	111	11.66 ± 0.30 // 12.01 ± 0.10	PT // TRLFS	
	$(R\text{-}O\text{-}PO_3)_2$-$UO_2^{2-}$	120	13.80 ± 0.37	TRLFS	
Bacillus subtilis	R-COO-UO_2^+	110	5.4 ± 0.2	Adsorption experiment	(Fowle et al. 2000)
	R-O-PO_3H-UO_2^+	111	11.8 ± 0.2		

[a] metal / ligand / H^+.

As it can be seen from Table 4.1, a moderate to strong interaction of U(VI) with the surface functional groups of *Sporomusa* sp. can be found. The affinity of uranyl to phosphoryl groups is much higher than that to carboxylic sites. Since lipopolysaccharide (LPS) is a major and the very outer part of the cell wall of Gram-negative bacteria, the determined complex stability constants have been compared to UO_2^{2+} interacting with LPS (Barkleit et al. 2008). Besides LPS, the results on UO_2^{2+} interacting with peptidoglycan (PG) (Barkleit et al. 2009) are also listed for comparison (Table 4.1). PG is the second outer cell wall polymer and hence can not be excluded to interact with U(VI). The third comparison is made to the stability constants of U(VI) bound to surface functional groups of *Bacillus subtilis* (Fowle et al. 2000). Although *B. subtilis* is Gram-positive, this strain was chosen because at present this is the only literature source on thermodynamic data on U(VI) surface complexation onto bacteria which can be compared. The determined stability constant of the R-COO-UO_2^+ complex signifies that interaction of U(VI) with carboxylic sites of the *Sporomusa* sp. cell surface is weaker than with carboxylic sites of *B. subtilis* or for instance peptidoglycan. On the other hand, and increased stability of the phosphoryl coordination of U(VI) compared to the literature is observable. This is the first successful use of the program HYPERQUAD for calculating stability constants for metal ions sorbed to bacterial surfaces at all. The determined complex stability constants have been used to calculate the U(VI) speciation in presence of *Sporomusa* sp. cells. The results are presented in the following.

The U(VI) speciation influenced by Sporomusa sp.

Based on the determined stability constants of the U(VI) complexes formed at the cell surface and the relevant U(VI) hydrolytic species (Guillaumont et al. 2003) a U(VI) species distribution in presence of the cells was calculated with the HySS 2009 code (Alderighi et al. 1999) (Fig. 4.5). The U(VI) species distribution in presence of *Sporomusa* sp. reveals that in the acidic pH range below pH 4 U(VI) binds to the cell surface mainly via protonated phosphoryl groups. The results gained by (Fowle et al. 2000) on the interaction of U(VI) with *B. subtilis* have demonstrated that the best fit for uranium binding at low pH is the one including adsorption onto protonated phosphoryl sites, thus supports the calculated U(VI) speciation in presence of *Sporomusa* sp. cells. From the calculated speciation it can also be seen that U(VI) binding by carboxylic sites only plays a minor role which is due to the low stability of the U(VI) carboxylic complex. Between pH 4.5 and 6.5 U(VI) is mainly coordinated by deprotonated phosphoryl groups of the cell surface.

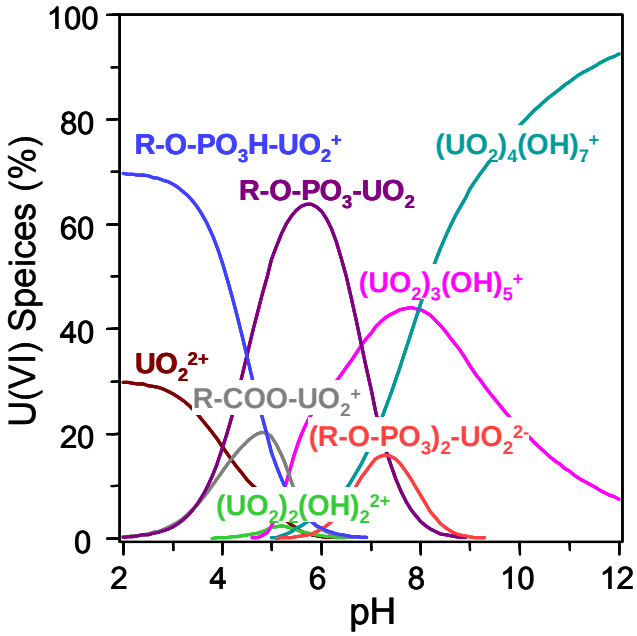

Fig. 4.5 U(VI) species distribution in presence of *Sporomusa* sp. cells in dependence on pH calculated using HySS 2009 (Alderighi et al. 1999), [U(VI)] = $1 \cdot 10^{-4}$ M, [dry biomass] = 0.2 g/L.

If the pH is increased further uranyl hydroxides dominate the U(VI) speciation in aqueous solution (in a CO_2-free system). The U(VI) interactions with bacterial surface functionalities suppressed and hence shifted the U(VI) hydrolysis towards higher pH (approximately by two pH units).

Within pH 4 to 7, preliminary TRLFS measurements with U(VI) loaded *Sporomusa* sp. cells showed red shifted emission maxima compared to the abiotic controls. At pH ≥ 6, the emission maxima (main band at 519 nm) of the U(VI) loaded cells indicated an increased influence of deprotonated phosphoryl groups in U(VI) binding. Hence, the TRLFS measurements confirmed the results obtained with potentiometric titration.

U(VI)-Sporomusa sp. system: X-ray absorption fine structure (XAFS) spectroscopy

The Mont Terri isolate *Sporomusa* sp. was investigated regarding its interaction with U(VI) in 0.1 M $NaClO_4$ in dependency on pH. Hence primarily metabolically rather inactive cells were studied. Three U(VI)-*Sporomusa* sp. samples were investigated in order to determine structural parameters of the formed bacterial surface species. The samples can be described as follows. In sample A *Sporomusa* sp. cells were contacted with 0.2 mM U(VI) at pH 4. In samples B the pH was changed to pH 7 and in sample C the [U(VI)] was decreased to 0.1 mM. All samples were prepared under N_2 atmosphere.

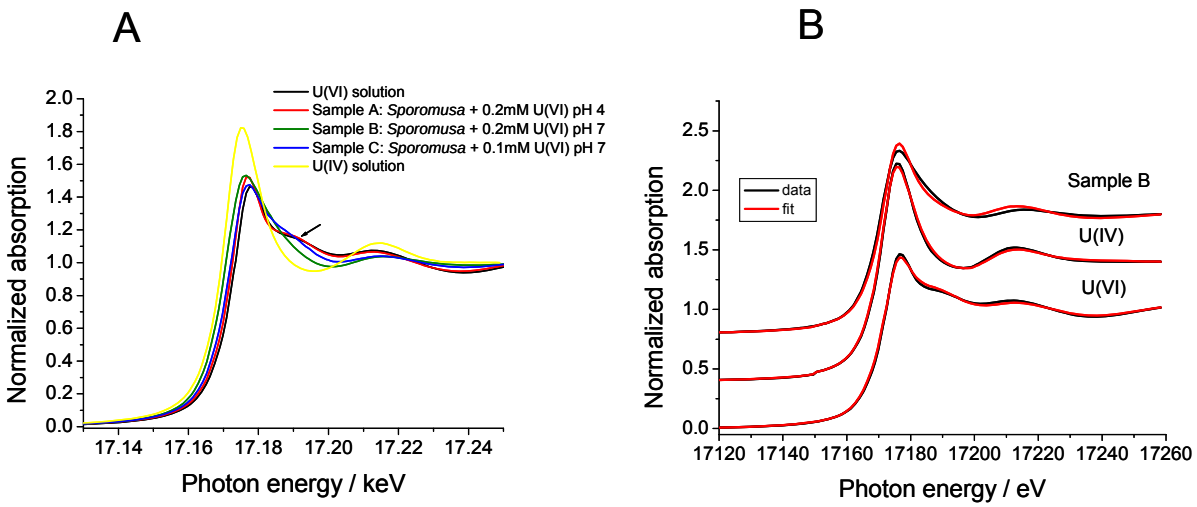

Fig. 4.6 A) Summary of the measured U L_{III}-edge XANES spectra within the U(VI)-*Sporomusa* sp. system. B) XANES spectra of 0.03 M U(IV) and 0.04 M U(VI) reference solutions in 1 M $HClO_4$ and after interaction with *Sporomusa* sp. (sample B).

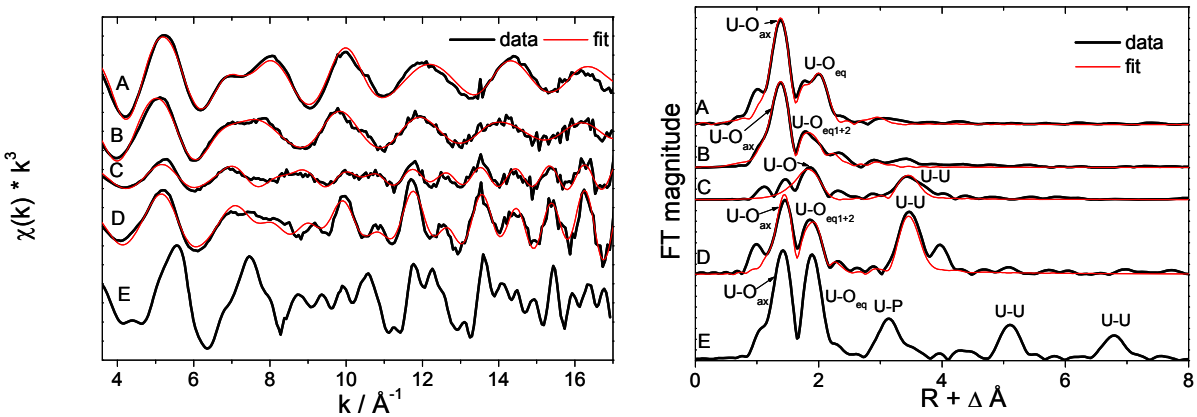

Fig.4.7 Uranium L_{III}-edge k^3-weighted EXAFS spectra (left) and the corresponding Fourier transformations (right) of the U(VI) complexes formed with *Sporomusa* sp. in 0.1 M $NaClO_4$ at pH 4 and 7 (B to D, respectively) compared to the free uranyl ion at pH 2 (A) and the meta-autunite-like structure observed for *P. fluorescens* (E). $[U(VI)]_{initial}$ = 0.1 - 0.2 mM, $[dry\ biomass]_{initial}$ = 0.2 g/L. Black = experimental data, red = fit.

X-ray absorption near edge spectroscopy (XANES) is one method to distinguish between different oxidation states of an absorbing atom. U(VI) samples can be easily detected by a characteristic shoulder approximately 20 eV above the white line. This feature (marked with an arrow in Fig. 4.6 A) results from multiple scattering processes within the linear uranyl unit (O=U=O). It is only present in the case of uranium(VI). The reduced amplitude of this shoulder of the bacterial samples B and C indicated the presence of uranium(IV) formed by the activity of the cells. This was unexpected and occurred in both samples prepared at pH 7. The mechanism of the U(VI) reduction by *Sporomusa* sp. cells is not understood up to know. Sample A prepared at pH 4 showed no indications for the occurrence of U(IV). To determine the amounts of U(IV) and U(VI) present in the bacterial samples B and C, we applied the

Factor Analysis described by Rossberg et al. 2003. The calculations revealed mixtures containing 50% U(IV) and 50% U(VI) in sample B, whereas samples C contained only 10 % U(IV) besides 90 % U(VI).

Table 4.2 EXAFS results on U(VI) interaction with *Sporomusa* sp. Coordination numbers N, bond distances R, and Debye-Waller factors σ^2 are given. For comparison the structural parameters of the free uranyl ion and the meta-autunite phase formed with *P. fluorescens* in SSM with phosphate are listed.

Sample composition	**Path**	**N** [a]	**R (Å)** [b]	**σ^2 (Å^2)** [c]	**ΔE_0 (eV)**	**Comments**
A)	U-O_{ax}	2[d]	1.77	0.0013	10.6	T = 298 K
0.05 M U(VI), pH 2	U-O_{eq}	5.2	2.41	0.0071		
B)	U-O_{ax}	2[d]	1.78	0.0023	8.7	T = 15 K
Sporomusa sp. + 0.2 mM	U-O_{eq1}	4.0	2.38	0.0061		
U(VI), pH 4	U-O_{eq2}	1.0	2.53	0.0010		
C)	U-O	2.2	2.34	0.0051	6[d]	T = 15 K
Sporomusa sp. + 0.2 mM	U-U	0.5	3.63	0.0010		
U(VI), pH 7						
D)	U-O_{ax}	2[d]	1.81	0.0010	6.6	T = 15 K
Sporomusa sp. + 0.1 mM	U-O_{eq1}	2.2	2.34	0.0013		
U(VI), pH 7	U-O_{eq2}	3.2	2.47	0.0068		
	U-U	1.2	3.75	0.0010	-33.6	
E)	U-O_{ax}	2[d]	1.79	0.0016	13.0	T = 15 K
P. fluorescens	U-O_{eq}	4[d]	2.29	0.0018		
+ 0.2 mM U(VI),	U-P	4[d]	3.63	0.0049		
0.5%-phosphate-SSM,	U-U	4[d]	5.24	0.0032		
pH 7	U-U	4[d]	6.88	0.0016		

a) errors in coordination numbers are ± 25%, *b)* errors in bond distances are ± 0.02 Å, *c)* Debye-Waller factor, *d)* parameter was fixed during fit.

The k^3-weighted $\chi(k)$ spectra and corresponding FTs of U(VI)-loaded *Sporomusa* sp. cells at pH 4 and 7 are illustrated in comparison to that of the free uranyl ion and the meta-autunite-like structure observed for *P. fluorescens* in contact with U(VI) in SSM with phosphate in Figure 4.7. The corresponding structural parameters of the best fits obtained are summarized in Table 4.2. Investigating the sorption of U(VI) onto *Sporomusa* sp. cells by EXAFS spectroscopy at pH 4 (sample B) a split equatorial oxygen shell was found indicating the contribution of two different O-donors to UO_2^{2+} coordination. U-O_{eq} bond lengths of 2.38 Å and 2.53 Å were calculated. The shorter bond distance a complexation of the uranyl ion by organic phosphate groups is suggested, while the longer bond distance points towards U(VI) interaction with carboxyl groups. Especially in contrast to the highly crystalline m-autunite structure determined in the U(VI)–*P. fluorescens*–0.5%-P-SSM system (sample E) the observed features indicate biosorption of U(VI) to the bacterial cell wall functional groups

which was also found using TRLFS. The evaluation of the EXAFS oscillations measured for samples C and D is difficult because here different uranium oxidations states are existing in one biological sample. Therefore the structural interpretations are only shortly described here. No axial oxygen shell could be determined in sample C. Hence U(IV) contributions dominated the overall EXAFS oscillation. The U-O shell at 2.35 Å and the U-U distance at 3.63 Å could point to the formation of biogenic UO_2 as published by Singer et al. 2009. However the U-U distance is approximately 0.22 Å shorter compared to biogenic nanoparticulate UO_2. In similarity to *Paenibacillus* sp. (see Table 4.10 sample C) the structural parameters ($U\text{-}O_{ax}$ and U-U distances) observed for the sample C allow the interpretation by two possibilities. First an additional formation of a schoepite-like phase seems possible. However, the structural parameters in terms of N and R deviate from those of a precipitate formed at pH 7 in a bacteria-free system (Moll et al. 2000). Therefore the formation of polynuclear U(VI) surface species might occur.

4.2.1.2 Interaction with Cm(III)/Eu(III)

The Sporomusa sp. Eu(III) system – potentiometric titrations

Due to similar ionic radii Eu(III) was investigated to resemble Cm(III) coordination chemistry. The titration of Eu(III) and *Sporomusa* sp. cells and the corresponding fit with HYPERQUAD is shown in the following (Fig. 4.8).

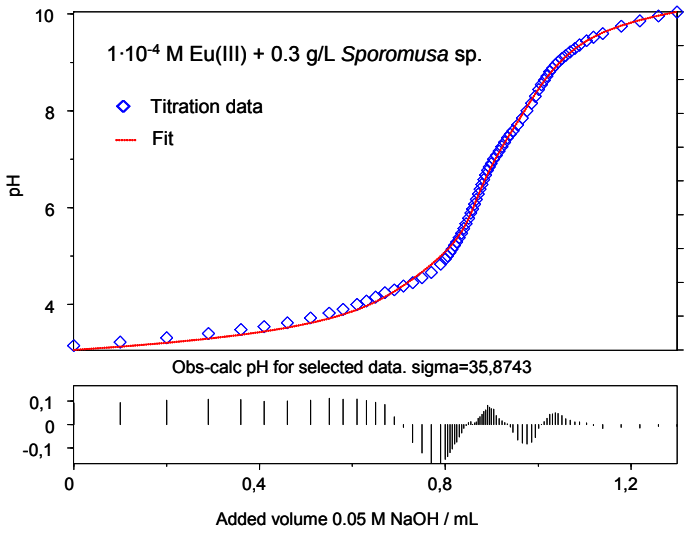

Fig. 4.8 Titration of 0.1 mM Eu^{3+} and 0.3 $g_{dry\ weight}$/L cells in 0.1 M NaCl titrated with 0.05 M NaOH and fit.

Fitting the titration data of bacterial cells and Eu^{3+}, the following hydrolytic europium(III) species and their stability constants could be included in the fit: $Eu(OH)^{2+}$, and $Eu(OH)_2^{+}$ (Plancque et al. 2003).

Table 4.3 Calculated stability constants of Cm^{3+}/Eu^{3+} complexes with surface functional groups of *Sporomusa* sp., *P. fluorescens*, and *Paenibacillus* sp. cells and comparison to literature.

Species	Complex	xyz[a]	log β_{xyz}	Reference
Sporomusa sp. MT-2.99	R–COO–Cm^{2+}	110	8.06 ± 0.61[b]	This work
	R–O–PO_3H–Cm^{2+}	111	13.90 ± 0.90[b]	
	R–COO–Eu^{2+}	110	6.66 ± 0.48[b]	
	R–O–PO_3H–Eu^{2+}	111	13.38 ± 0.48[b]	
	R–COO–Eu^{2+}	110	6.89 ± 0.62[c]	
	R–O–PO_3–Eu^{+}	110	7.71 ± 0.33[c]	
	R–O–PO_3H–Eu^{2+}	111	15.49 ± 0.19[c]	
Pseudomonas fluorescens	R–COO–Cm^{2+}	110	6.11 ± 0.51[b]	This work
	R–O–PO_3H–Cm^{2+}	111	12.74 ± 0.58[b]	and
	R–COO–Eu^{2+}	110	7.26 ± 0.08[c]	Moll et al. 2013a
	R–O–PO_3H–Eu^{2+}	111	14.95 ± 0.12[c]	
Paenibacillus sp. MT-2.2	R–O–PO_3H–Cm^{2+}	111	13.94 ± 0.18[b]	This work
	R–COO–Eu^{2+}	110	5.70 ± 0.25[c]	and
	R–O–PO_3H–Eu^{2+}	111	13.64 ± 0.30[c]	Lütke 2013
Bacillus subtilis	R–COO–Eu^{2+}	110	7.13 ± 0.40[b, c]	Markai et al. 2003
	R–O–PO_3–Eu^{+}	110	8.14 ± 0.50[b, c]	
EDTA	$CmEDTA^{-}$	110	18.41[b]	Choppin et al. 2006
	$EuEDTA^{-}$	110	17.52[b]	Thakur et al. 2009
Organic phosphoryl ligands				
Adenosine 5'-Triphosphate	CmATPH	111	13.23 ± 0.10[b]	Moll et al. 2005
	$CmATP^{-}$	110	8.19 ± 0.16[b]	
Phosphoryl / carboxyl / amino groups containing bioligands				
LPS (*P. aeruginosa*)[d]	R–COO–Cm^{2+}	110	7.0 ± 0.5[b]	Moll et al. 2009
	R–O–PO_3H–Cm^{2+}	111	13.0 ± 0.6[b]	
Carboxyl / hydroxyl /amino groups containing bioligands				
PG (*B. subtilis*)[d]	R–COO–Cm^{2+}	110	5.21 ± 0.19[b]	Moll et al. 2009
Polyelectrolytes (carboxyl groups)				
Humic acid	CmHA		6.24 ± 0.28[b]	Kim et al. 1993

a: xyz = metal / ligand / H^{+}; b: from TRLFS, c: from potentiometric titrations, d: own measurements; recalculated in this study. ATP: adenosine 5'-triphosphate, EDTA: ethylenediaminetetraacetic acid, LPS: lipopolysaccharide, PG: peptidoglycan.

The titration curve could be modeled with a very good fit result when the bacterial surface complexes R–COO–Eu^{2+}, R–O–PO_3H–Eu^{2+}, and R–O–PO_3–Eu^{+} were considered, as can be seen from the HYPERQUAD fit result (Fig. 4.8). The respective calculated stability constants are summarized and compared to literature data in Table 4.3. From the stability constants

listed in Table 4.3 it can be seen that overall Eu(III) can form fairly stable complexes with the surface functional groups of *Sporomusa* sp. cells. Furthermore the interaction with phosphoryl sites are characterized by stability constants several orders of magnitude greater than that of carboxyl site interaction. Our results have been compared to Eu^{3+} interacting with Gram-negative (*P. fluorescens* in Moll et al. 2013a) and Gram-positive bacteria (*Paenibacillus* sp. in Lütke 2013a, and *B. subtilis* in Markai et al. 2003). Our reported stability constant of the R–COO–Eu^{2+} complex is in good agreement with the stability constant of the 1:1 complex of Eu(III) interacting with carboxylic groups of the *B. subtilis* cell surface published by Markai et al. 2003, respectively. In our previous study (Moll et al. 2013a) on the Eu(III) interaction with carboxylic sites of the *P. fluorescens* (CCUG 32456 A) cell envelope a slightly higher log β value of 7.26 was determined (see also chapter 5). Considering the given standard deviations still both constants are in a fairly good agreement. Eu(III) forms more stable bacterial surface complexes with phosphoryl sites of the *Sporomusa* sp. cell envelope. The *Sporomusa* sp. R–O–PO_3H–Eu^{2+} complex exhibits a comparable stability constant with the corresponding value of the *P. fluorescens* complex. *Paenibacillus* sp. forms a R–O–PO_3H–Eu^{2+} complex with lower thermodynamic stability. Possibly here differences in the cell wall structures are reflected in the stability of the formed complexes. Individual cell wall structures influencing the strength of the formed Eu(III) complexes might also be the cause for the deviation of the stability constants of the R–COO–Eu^{2+} complexes of *Sporomusa* sp. (log β = 6.89) and *Paenibacillus* sp. (log β = 5.70). The comparison of the determined stability constants for deprotonated phosphoryl interaction, in specific of the R–O–PO_3–Eu^{+} complex, to the literature revealed again a fairly good agreement with the result gained by Markai et al. 2003.

The Sporomusa sp. Eu(III) system – TRLFS

The luminescence spectrum of Eu^{3+} displays the typical changes upon cell addition and pH change which points to complexation with bacterial surface functionalities: The intensity of the hypersensitive $^5D_0 \rightarrow {}^7F_2$ transition at about 617 nm increases strongly (with increasing pH), the symmetry-forbidden $^5D_0 \rightarrow {}^7F_0$ transition at around 579 nm appears (see Fig. 4.9), and the luminescence decay changes to bi-exponential with prolonged lifetimes (see Table 4.4). The luminescence spectrum of the Eu^{3+} aqua ion is characterized by emission bands at 585-600 nm (magnetic dipole transition $^5D_0 \rightarrow {}^7F_1$) and 610-625 nm (hypersensitive transition $^5D_0 \rightarrow {}^7F_2$). The intensity ratio according to equation (4.1) of 0.5 and the measured lifetime of

110 ± 5 µs corresponding to 9 water molecules in its first coordination sphere are in good agreement with the literature (e.g., Horrocks et al. 1979, Kimura et al. 1994, Kim et al. 1994, Moulin et al. 1999, Plancque et al. 2003, Heller et al. 2009, 2012, Barkleit et al. 2013). Even when it is proposed that the $^7F_1$ peak should be not influenced by complexation, we observed in all bacterial suspensions independent of pH a slight decrease in intensity combined with a broadening of this transition. The interaction of Eu^{3+} with *Sporomusa* sp. cells is primarily pronounced in the $^7F_2$ peak.

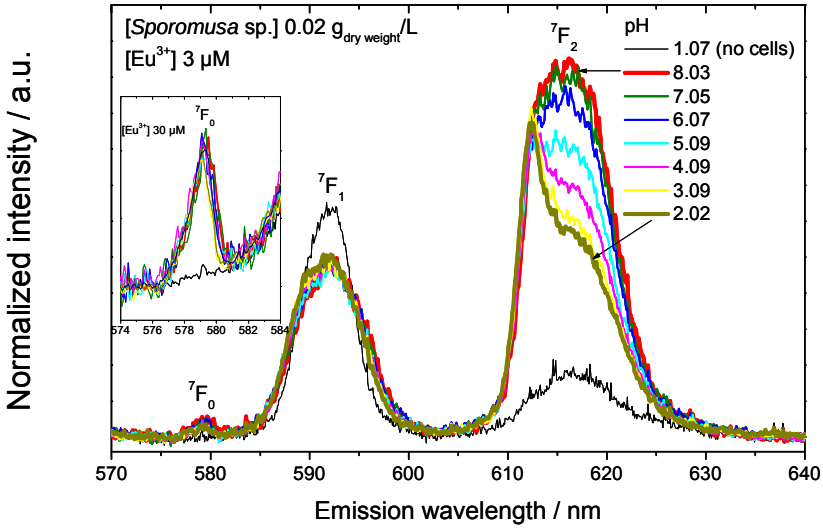

Fig. 4.9 Luminescence emission spectra of 3 µM europium(III) in 0.1 M $NaClO_4$ measured as a function of pH at a fixed biomass concentration of 0.02 $g_{dry\ weight}$/L (inset: [Eu^{3+}] 30 µM).

Table 4.4 Spectroscopic properties of the identified europium(III) species.

	Eu^{3+} (aq)	**R–O–PO_3H–Eu^{2+}**	**R–COO–Eu^{2+}**
Emission (nm)			
$^7F_0$	-	579.0 (1.50)	579.2 (1.60)
$^7F_1$	589.0 (3.50)[a]	588.7 (2.90)	588.8 (4.33)
	592.2 (5.20)	592.1 (7.40)	592.5 (7.45)
$^7F_2$	616.8 (10.30)	612.3 (2.65)	613.0 (3.80)
	-	616.5 (9.30)	616.9 (8.35)
$R_{E/M}$[b]	0.50	1.81	3.27
Lifetime (µs)	110 ± 5	170 ± 23	**170 ± 23**
		515 ± 73	515 ± 73

[a] Values in parentheses are full width at half- maximum; [b] Intensity ratio of the $^7F_2$ (electric dipole transition) over the $^7F_1$ (magnetic dipole transition) luminescence band.

Two bacterial Eu^{3+} species can be easily distinguished. Between pH 2 and 4.1, the $^7F_2$ band exhibits a sharp shoulder at 612 nm (see Fig. 4.9) and an enhanced $R_{E/M}$ value of 1.90 ± 0.10. This observation demonstrates that also *Sporomusa* sp. interacts with Eu(III) from acidic

solutions. This is in agreement with earlier results based on large log K_d values for europium(III) observed at pH 3 and 4 by Ozaki et al. 2004. This class of spectra can be attributed to the formation of Eu^{3+}–*Sporomusa* sp. species 1. In the higher pH region between 6.07 and 8.03 the $^7F_2$ band is characterized by a broad maximum at 616 nm with a larger $R_{E/M}$ value of 2.53 ± 0.11. The characteristic feature at 612 nm disappeared. This second class of spectra can be attributed to the formation of Eu^{3+}–*Sporomusa* sp. species 2. The spectrum at pH 5.09 displays a transition state between both types of spectra. The pH-dependent change of the emission data of the Eu^{3+}–*Sporomusa* sp. system implies the involvement of two functional groups located at the cell envelope structure.

Table 4.5 Luminescence lifetimes of the Eu^{3+}–*Sporomusa* sp. system including those of relevant model systems for comparison.

Species	Lifetime / µs	Comments	Reference
Eu^{3+} (aq)	110 ± 5	monoexponential decay	This work
Eu^{3+}–*Sporomusa* sp. complexes			This work
Eu^{3+}– *Sporomusa* sp. species 2: R–COO–Eu^{2+}	170 ± 23	bi-exponential	
Eu^{3+}– *Sporomusa* sp. Species 1: R–O–PO_3H–Eu^{2+}	515 ± 73	decay	
$EuCl_3$/$Eu_2(SO_4)_3$/$Eu(NO_3)$–*Pseudomonas aeruginosa* complexes			Texier et al. 2000
Carboxyl sites	98-254	bi-exponential	
Phosphoryl sites	534-677	decay	
Eu^{3+}–*B. subtilis* complexes			Markai et al. 2003
Carboxyl sites	230 ± 20	bi-exponential	
Phosphoryl sites	730 ± 30	decay	
Eu^{3+} + Citric acid		monoexponential	Heller et al. 2012
EuHCit	165 ± 10		
Eu(HCitH)$HCit^{2-}$	250 ± 5		
$Eu(HCit)_2^{3-}$	490 ± 20		
$Eu(Cit)_2^{5-}$	676 ± 5		
Eu^{3+} + Salicylic acid		monoexponential	Barkleit et al. 2013
$Eu(Sal)^{2+}$, $Eu(Sal)_2^+$, $Eu(Sal)_3$	305 ± 5		
Eu^{3+}–glycerol-2-phosphate	704 ± 30	monoexponential	Markai et al. 2003
$Eu(PO_4)$	745	monoexponential	Texier et al. 2000

ICP-MS analyses of the supernatants after separating the cells in the acidic and alkaline pH-region ([Eu(III)] 3 and 30 µM, 0.02 $g_{dry\ weight}$/L) showed that approximately 7 % of the total Eu(III) concentration remained in solution independent of pH. Hence ≥ 90 % of the Eu(III) is always associated on the biomass. These findings could be confirmed by measuring the

Eu(III) luminescence intensities in the corresponding supernatants and Eu(III) loaded biomasses after washing with 0.1 M $NaClO_4$.

To obtain information on the reversibility and the binding strength of bacterial Eu(III) surface complexes, we extracted the cell-bound Eu(III) with 0.01 M EDTA solution (pH 5). At $[Eu(III)]_{initial}$ of 30 µM independent from pH, 60 ± 7 % of the europium(III) was released from the cells. The majority of Eu(III) seemed to concentrate extracellularly on the cell envelope. Hence the main process is reversible and confirms the formation of surface complexes with functional groups of the cell envelope. These bacterial complexes are less stable than the europium(III)–EDTA complex (see Table 4.3). However, there is an measurable amount of Eu(III) which cannot be removed from the biomass with EDTA. This points to strongly irreversibly bound Eu(III) most likely within the complex cell envelope structure of this Gram-negative bacterium (minor process).

In all bacterial samples a bi-exponential luminescence decay behavior was measured. The occurrence of two lifetimes suggests that two distinct chemical environments contribute to the speciation of the accumulated Eu(III) by the biomass. The averaged value of the shorter lifetime was calculated to be 170 ± 23 µs, whereas the component with the longer lifetime was calculated to be 515 ± 73 µs. These lifetimes correspond to 6.0 and 1.5, respectively, remaining water molecule in the Eu(III) first coordination sphere. By comparing our lifetime and later discussed speciation results with literature data on bacterial Eu^{3+} interaction studies (see Tab. 4.5), the longer lifetime can be assigned to Eu^{3+}–*Sporomusa* sp. species 1, whereas the shorter lifetime corresponds to Eu^{3+}–*Sporomusa* sp. species 2.

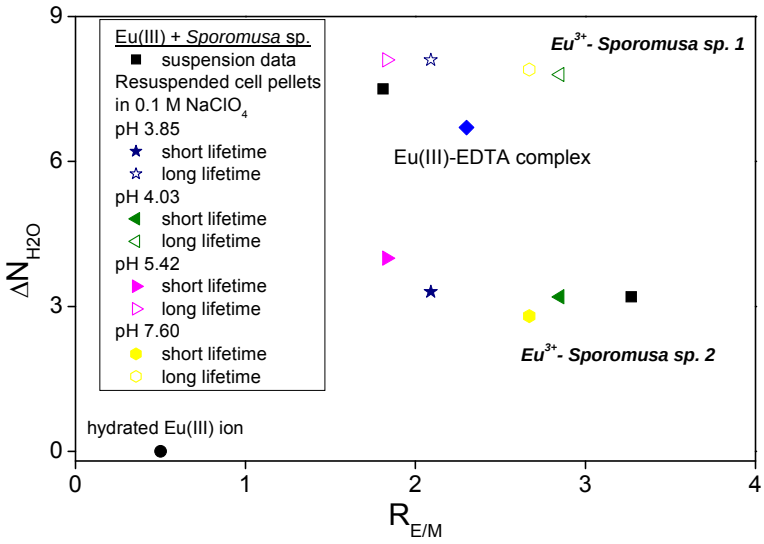

Fig. 4.10 CE diagram of europium(III) bound to *Sporomusa* sp. cells.

Figure 4.10 shows the Coordination-Environment diagram (CE diagram) for Eu(III) associated with cells of *Sporomusa* sp.. The CE diagram was constructed as described by Ozaki et al. 2002. The interpretation on the basis of the CE diagram implies that Eu(III) interacts with the coordination site characterized by the short lifetime in complex with both outer-spherical and inner-spherical properties (carboxyl sites: Eu^{3+}–*Sporomusa* sp. species 2). The interaction with the coordination site characterized by the long lifetime is clearly an inner-spherical complex (phosphoryl sites: Eu^{3+}–*Sporomusa* sp. species 1).

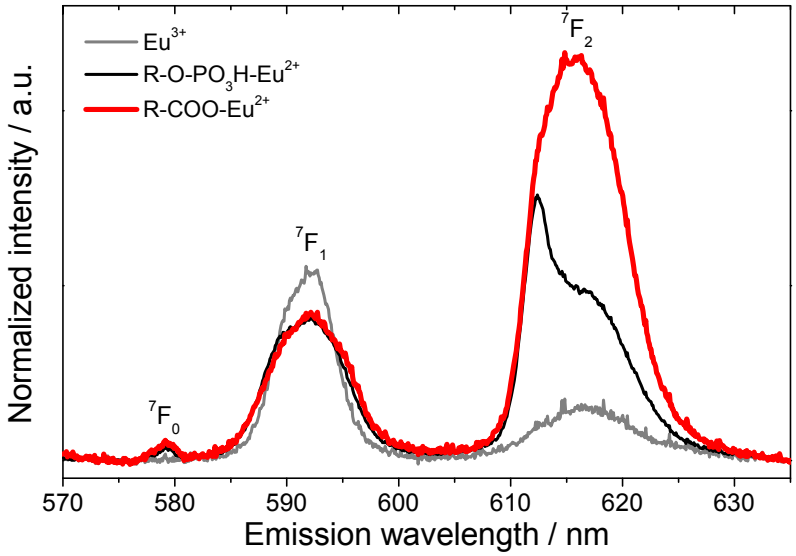

Fig. 4.11 Luminescence emission spectra of the single components in the Eu^{3+}–*Sporomusa* sp. system as derived by peak deconvolution using SPECFIT.

The program SPECFIT was used to extract the bacterial europium(III) surface complexation constants (Tab. 4.3) and the single component spectra (Fig. 4.11). The calculation procedure is based on the formal complex formation equation for discrete binding sites

$$x\ Eu^{3+} + y\ R{-}A_i^- + z\ H^+ \rightleftharpoons [(Eu)_x(R{-}A_i)_yH_z]^{[x(2x-y+z)]+}, \qquad (4.4)$$

and the appropriate mass action law, which represents the complex stability constant log $\log \beta_{xyz}$:

$$K = \frac{[(Eu)_x(R-A_i)_yH_z]}{[Eu^{3+}]^x[R-A_i]^y[H^+]^z} \qquad (4.5)$$

The pH dependent change of the emission data (see Fig. 4.9) in the presence of *Sporomusa* sp. cells could be described by the formation of two Eu(III) surface complexes. Within the

investigated pH range, most likely bacterial carboxyl and phosphoryl groups are responsible for Eu(III) coordination on the cell envelope. Due to the strong interactions detected already in the acidic pH region a protonated europium(III) phosphoryl complex is likely to occur followed by a carboxyl complex at higher pH. The best fits were obtained with two 1 : 1 complexes, R–O–PO_3H–Eu^{2+} (Eu^{3+}–*Sporomusa* sp. species 1) and R–COO–Eu^{2+} (Eu^{3+}–*Sporomusa* sp. species 2). The surface complexation constants were calculated to be log $ß_{111}$ = 13.38 ± 0.48 for the protonated phosphoryl complex, and log $ß_{110}$ = 6.66 ± 0.48 for the carboxyl coordination (see Table 4.3). The presented single component spectra were averaged from the individual spectra calculated for every run (see Fig. 4.11). The single component spectra of the bacterial Eu(III) surface complexes are characterized by the occurrence of the $^7F_0$ transition and the changes in shape and the intensity of the $^7F_2$ transition compared to the findings for the Eu^{3+} ion.

The spectroscopic properties of the identified Eu^{3+}–*Sporomusa* sp. species were summarized in Table 4.4. A detailed characterization of aqueous Eu^{3+}–*Sporomusa* sp. species based on the changes of the intrinsic luminescence of Eu^{3+} was not reported before. Moreover europium(III) surface complexation constants of bacterial cells are limited.

The Sporomusa sp. Cm(III) system – TRLFS

A strong decrease in the emission band of the free Cm^{3+} at 593.8 nm could be detected already at pH 1.95 and a low biomass concentration of 0.02 $g_{dry\ weight}$/L (Fig. 4.12 A).

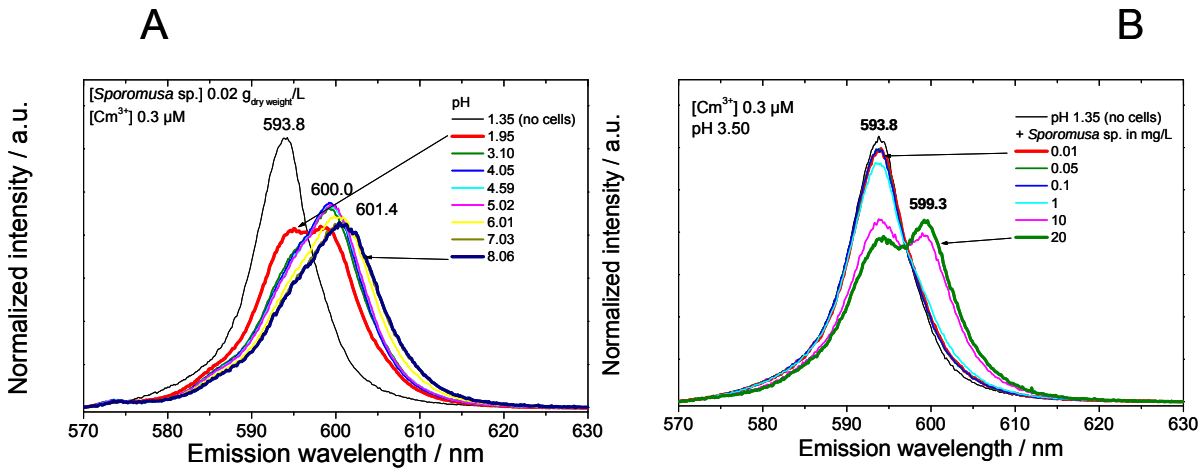

Fig. 4.12 Luminescence emission spectra of 0.3 µM curium(III) in 0.1 M $NaClO_4$ measured: A) as a function of pH at a fixed biomass concentration of 0.02 $g_{dry\ weight}$/ and B) as a function of the biomass concentration at pH 3.5.

A new red-shifted emission band at around 600 nm occurred simultaneously showing the influence of a first Cm^{3+}–*Sporomusa* sp. species (Fig. 4.12 A). It demonstrates that *Sporomusa* sp. interacts also with Cm(III) from acidic solutions. This is in agreement with earlier results based on large log K_d values for curium(III) observed at pH 3 and 4 by Ozaki et al. 2004 and also with our findings for *P. fluorescens* (CCUG 32456 A) published in Moll et al. 2013a. The dependencies found in the TRLFS spectra (Fig. 4.12 A) suggested the occurrence of two individual Cm^{3+}–*Sporomusa* sp. species between pH 1.9 and 8.1 having emission maxima at ca. 600 (Cm^{3+}–*Sporomusa* sp. species 1), and 601.4 nm (Cm^{3+}–*Sporomusa* sp. species 2). Figure 4.12 B presents the changes observed in the emission spectra at pH 3.5 and 0.3 µM Cm(III) as a function of the biomass concentration. The presence of the emission band at 599.3 nm at biomass concentrations greater than 1 $mg_{dry\ weight}/L$ indicates the formation of Cm^{3+}–*Sporomusa* sp. species 1. By contrast, all Cm(III) already exists as Cm^{3+}–*Sporomusa* sp. species 2 at a very low biomass concentration of 0.01 $mg_{dry\ weight}/L$ at pH 6.5 indicated by the emission maximum at 601.4 nm (data not shown). The pH-dependent change of the emission data of the Cm^{3+}–*Sporomusa* sp. system implies the involvement of two functional groups located at the cell envelope structure.

TRLFS of the supernatants and the Cm(III) loaded biomass after washing with 0.1 M $NaClO_4$ (0.02 $g_{dry\ weight}/L$) showed that 21 ± 3 % of the total Cm(III) luminescence intensity remained in solution independent of pH. Hence approximately 80 % of the Cm(III) was always associated with the biomass. This points to the possibility of a release of complexing agents possibly phosphates by the cells.

To obtain information on the reversibility and the binding strength of bacterial curium(III) surface complexes, we extracted the cell-bound Cm(III) with 0.01 M EDTA solution (pH 5). At pH 4.6 and 6.4 and a biomass concentration of 0.02 g/L and similar to Eu(III) 73% of the adsorbed Cm(III) was easily desorbed with an 0.01 M EDTA solution. The majority of Cm(III) seemed to concentrate extracellularly on the cell envelope. Hence the major process is reversible and confirms the formation of surface complexes with functional groups of the cell envelope. The bacterial complexes are less stable than the curium(III)–EDTA complex (see Table 4.3). However, there is a measurable amount of Cm(III) which cannot be removed from the biomass with EDTA. This points to strongly irreversibly bound Cm(III) probably within the complex cell envelope structure of this Gram-negative bacterium (minor process).

Again in all bacterial samples a bi-exponential luminescence decay behavior was measured. The occurrence of two lifetimes suggests that two distinct chemical environments contribute to the speciation of the accumulated Cm(III) by the biomass. The averaged value of the

shorter lifetime was calculated to be 108 ± 15 µs, whereas the component with the longer lifetime was calculated to be 252 ± 46 µs. These lifetimes correspond to 5.0 and 2.0, respectively, remaining water molecules in the curium(III) first coordination sphere. In general we found a stronger contribution of the long lifetime to measured sum lifetimes in the acidic pH region. In contrast the short lifetime contributed most in the neutral to alkaline pH region. Due to these findings and by comparison to relevant literature values (see Tab. 4.6) the longer lifetime can be assigned to Cm^{3+}–*Sporomusa* sp. species 1, whereas the shorter lifetime corresponds to Cm^{3+}–*Sporomusa* sp. species 2.

Table 4.6 Luminescence emission data of the Cm^{3+}–*Sporomusa* sp. system including those of relevant model systems for comparison.

Species	Emission peak maxima/nm	Lifetime / µs	Reference
Cm^{3+} (aq)	593.7	67 ± 2	This work
Cm^{3+}–*Sporomusa* sp. Complexes			This work
Cm^{3+}– *Sporomusa* sp. species 2: R–COO–Cm^{2+}	601.6	108 ± 15	
Cm^{3+} – *Sporomusa* sp. species 1: R–O–PO_3H–Cm^{2+}	599.8	252 ± 46	
Cm^{3+}–*Pseudomonas fluorescens* complexes			Moll et al. 2013a
R–COO–Cm^{2+}	601.9	121 ± 10	
R–O–PO_3H–Cm^{2+}	599.6	390 ± 78	
Cm^{3+}–*Desulfovibrio aespoeensis* complex	600.1	162 ± 5	Moll et al. 2004
Cm^{3+}–*Paenibacillus* sp. Complex			This work and
R–O–PO_3H–Cm^{2+}	598.8	477 ± 73	Lütke 2013a
Cm^{3+}– organic phosphoryl complexes			
$CmATPH_2^+$	598.6	89	Moll et al. 2005
CmATPH	600.3	92	
$CmATP^-$	601.0	187	
Cm^{3+} + bioligands with phosphoryl / carboxyl / amino groups			
LPS (*Pseudomonas aeruginosa*)[a]			Moll et al. 2009
R–COO–Cm^{2+}	602.3	100 and 214	
R–O–PO_3H–Cm^{2+}	599.9	150	
Cm^{3+} + bioligands with carboxyl / hydroxyl / amino groups			
PG (*Bacillus subtilis*)[a]			Moll et al. 2009
R–COO–Cm^{2+}	602.0	230	
Cm^{3+} + polyelectrolytes with carboxyl groups			
CmHA	601.0	72 and 145	Kim et al. 1993

a: own measurements; recalculated in this study.

PYO: pyoverdins, ATP: adenosine 5'-triphosphate, LPS: lipopolysaccharide, PG: peptidoglycan, HA: humic acid.

The excitation spectra measured in the curium(III)–*Sporomusa* sp. system were characterized by sharp, well-resolved absorption bands coming from intense transitions to the H-, G-, and F-states (see Fig. 4.13). Depending on the pH and hence on the speciation different excitation spectra were detected, with representative examples presented in Fig. 4.13.

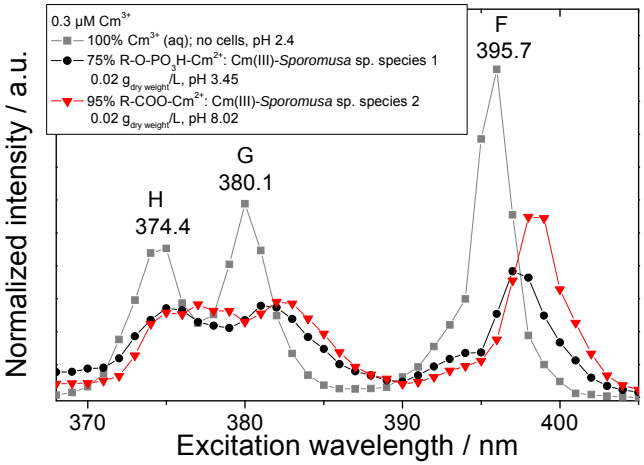

Fig. 4.13 Excitation spectra of curium(III) measured in the *Sporomusa* sp. system.

Compared to the spectrum of the Cm^{3+} aquo ion a strong red shift of about 2.5 nm was detected for the cell-bound curium(III). The red shift of the absorption bands was combined with an increase in luminescence line widths of the H, G, and F absorption bands, e.g. F band: 397.5 (4.2) nm for Cm^{3+}–*Sporomusa* sp. species 1 and 398.5 (3.6) nm for Cm^{3+}–*Sporomusa* sp. species 2 compared with 395.7 (2.4) nm for Cm^{3+} (see Table 4.7). The excitation spectra clearly support our conclusions drawn from the luminescence emission measurements concerning the speciation of aqueous curium(III) in the *Sporomusa* sp. system.

Table 4.7 Spectroscopic properties of the identified curium(III) species.

	Cm^{3+} (aq)	**R–O–PO_3H–Cm^{2+}**	**R–COO–Cm^{2+}**
Excitation (nm)	374.4 (3.3)[a]	350.4 (32.0)[b]	353.3 (17.3)[c]
	380.1 (2.9)	375.2 (4.8)	376.4 (6.2)
	395.7 (2.4)	381.7 (6.2)	382.7 (5.9)
		397.5 (4.2)	398.5 (3.6)
Emission (nm)	**593.7 (8.2)**	586.1 [d]	588.5 [d]
		593.9 [d]	596.2 [d]
		599.8 (7.4)	**601.6** (8.6)
Lifetime (µs)	67 ± 2	108 ± 15	**108 ± 15**
		252 ± 46	252 ± 46

[a] Values in parentheses are full width at half- maximum.
[b] In 0.02 $g_{dry\ weight}$/L *Sporomusa* sp. at pH 3.45 (75% R–O–PO_3H–Cm^{2+} = Cm^{3+}– *Sporomusa* sp. species 1).
[c] In 0.02 $g_{dry\ weight}$/L *Sporomusa* sp. at pH 8.00 (95% R–COO–Cm^{2+} = Cm^{3+}– *Sporomusa* sp. species 2).
[d] Shoulder.

The program SPECFIT was used to extract the bacterial curium(III) surface complexation constants (Tab. 4.3) and the single component spectra (Fig. 4.14).

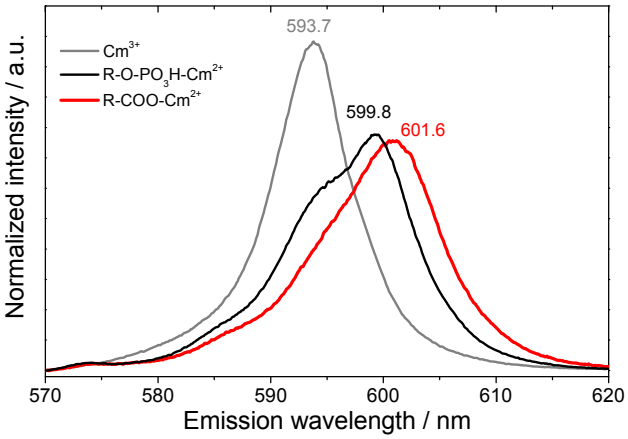

Fig. 4.14 Luminescence emission spectra of the single components in the Cm^{3+}–*Sporomusa* sp. system, as derived by peak deconvolution using SPECFIT.

The calculation procedure is based on the formal complex formation equation for discrete binding sites (equation 4.4) and the appropriate mass action law, which represents the complex stability constant log β_{xyz} (equation 4.5). The variations observed in the emission data (see Fig. 4.12 A, B) could be described by the formation of two Cm(III) surface complexes. Because of the strong interactions detected in the acidic pH region, a protonated curium(III) phosphoryl complex likely occurred followed by a carboxyl complex at higher pH. The best fits were obtained with two 1 : 1 complexes, R–O–PO_3H–Cm^{2+} (Cm^{3+}–*Sporomusa* sp. species 1) and R–COO–Cm^{2+} (Cm^{3+}–*Sporomusa* sp. species 2). The surface complexation constants were calculated to be log $ß_{111}$ = 13.90 ± 0.90 for the protonated phosphoryl complex, and log $ß_{110}$ = 8.06 ± 0.61 for the carboxyl coordination (see Table 4.3). The presented single component spectra were averaged from the individual spectra calculated for every run (see Fig. 4.14). The emission peak maximum is shifted from 593.7 nm for the Cm^{3+} aquo ion to 599.8, and 601.6 nm when curium(III) occurs in the two identified 1 : 1 Sporomusa sp. complexes. The spectroscopic properties of the identified Cm^{3+}–*Sporomusa* sp. species are summarized in Table 4.7. A detailed characterization of aqueous Cm^{3+}–*Sporomusa* sp. species based on the changes of the intrinsic luminescence of Cm^{3+} has not been reported before.

The Sporomusa sp. Eu(III)/Cm(III) system – Summary

For curium(III) slightly larger log ß values for the bacterial surface complexes were measured compared to europium(III). However we could also show that Eu(III) can be used as a non-radioactive analogon to mimic bacterial interactions of An(III). Both metals exhibited a similar interaction behavior with *Sporomusa* sp. cells. We were able to identify a Eu(III) surface complex with deprotonated phosphoryl groups, $R–O–PO_3–Eu^+$, by potentiometric titration. Both species $R–COO–Eu^{2+}$ and $R–O–PO_3–Eu^+$ coexist in the same pH region 4-8. Here we could see the limitations of TRLFS. A differentiation of two individual species was not possible in this pH range in the spectroscopic titrations by TRLFS. In contrast to TRLFS speciation studies of Cm(III) with organic phosphoryl ligands like ATP (Moll et al. 2005) this technique seems to have difficulties in order to distinguish bacterial phosphoryl species ($R–O–PO_3H–Cm^{2+}$ and $R–O–PO_3–Cm^+$) which differ only in the number of protons. From an Cm^{3+}–*Paenibacillus* sp. study by TRLFS (see chapter 4.2.2 and Lütke 2013a) we got indications that both Cm(III) phosphoryl species exhibited emission maxima at 598.3 and 599.3 nm. This difference of roughly 1 nm is too small for a safe prediction of two Cm(III) phosphoryl species. It follows that the stability range of Cm(III)/Eu(III) carboxyl interactions might be over-determined by TRLFS for the *Sporomusa* sp. system. In contrast in the Eu^{3+}–*P. fluorescens* system a $R–O–PO_3–Eu^+$ species was not identified by potentiometric titrations.

4.2.1.3 Interaction with Pu

The Sporomusa sp. Pu system – Accumulation experiments

The amount of Pu sorbed by *Sporomusa* sp. increased with time as shown in Fig. 4.15 B. Steady state conditions were reached after approximately 220 h. The kinetic data (see Fig. 4.15 A) could be successfully fitted to a bi-exponential law ($y = y_0 + A\ 1\ e^{-(x/t1)} + A\ 2\ e^{-(x/t2)}$). This suggests that at least two different processes occur after adding Pu to the biomass. The kinetic fits showed that the overall process consists of at least two parts: a fast process having a time frame of ~ 0.5 h (e.g., biosorption) and a much slower process with a time frame of ~ 300 h (e.g., bioreduction). We observed an increased amount of Pu at contact times > 300 h. This can be interpreted by a larger Pu binding capacity of the dead biomass. It could be demonstrated that the $[^{242}Pu]_{initial}$ influences the amount of Pu associated with cells of *Sporomusa* sp..

At an initial Pu concentration of 4.2 mg/L, we observed a removal efficiency of 97 %. Whereas at $[^{242}Pu]_{initial}$ of 109 mg/L, the removal efficiency decreased to a level of 24 % (see

Fig. 4.16 left). Similar observations were made in our earlier study with *Desulfovibrio aespoensis* (Moll et al. 2006).

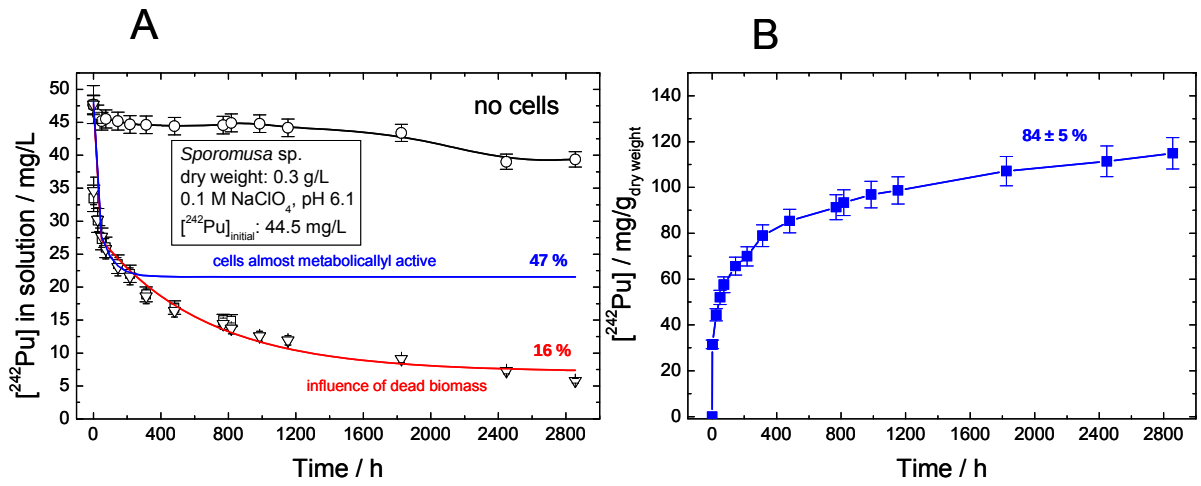

Fig. 4.15 (A) Decrease of the ^{242}Pu concentration in solution and (B) increase of the amount of accumulated ^{242}Pu by the cells of *Sporomusa* sp.

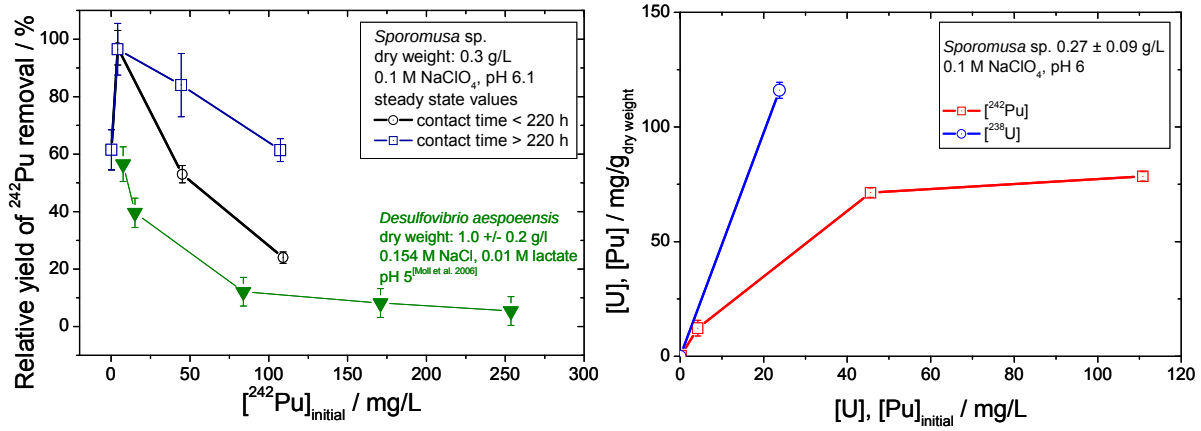

Fig. 4.16 Removed uranium and plutonium from the test solutions by cells of *Sporomusa* sp. as a function of the initial actinide concentration at pH 6.1.

As depicted in Fig. 4.16 (left) *Sporomusa* sp. cells are more effective in binding Pu at pH 6.1 compared to *D. aespoeensis*. Comparing the plutonium results with uranium (see Fig. 4.16 right), the measurements indicate that the cells accumulating less plutonium. One explanation could be a higher stress to the cells caused by the higher toxicity/radiotoxicity of ^{242}Pu compared to ^{238}U. The maximum concentration of accumulated Pu by the biomass was 75 ± 5 $mg/g_{dry\ weight}$.

The Sporomusa sp. Pu system – Pu oxidation state distribution

First insights in the Pu oxidation state distribution were obtained by absorption spectroscopy (see Fig. 4.17).

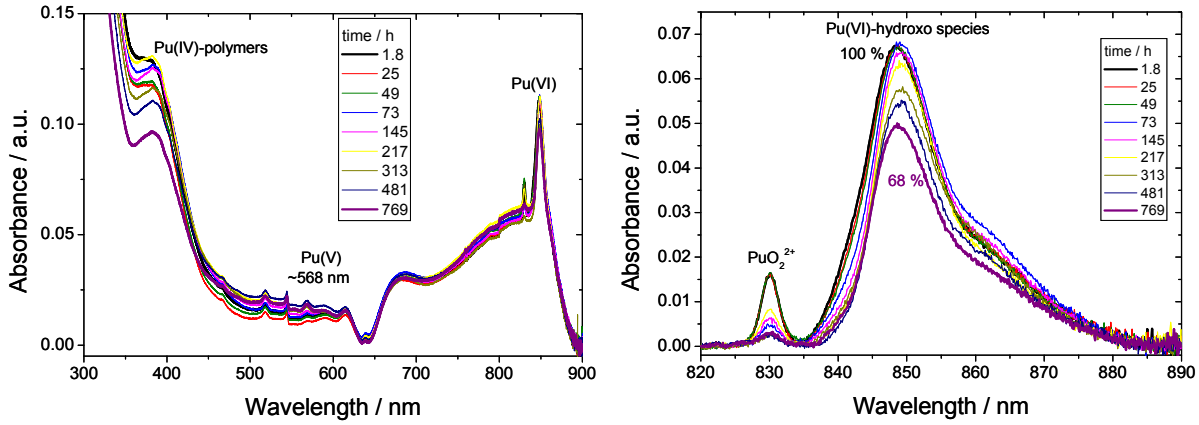

Fig. 4.17 Absorption spectra of the blank solutions as a function of time ([^{242}Pu]: 107 mg/L, 0.1 M $NaClO_4$, pH 6.1).

The overall absorption spectra depicted left gave evidence for Pu(VI), Pu(IV)-polymers in the lower wavelength region, and Pu(V) due to the weak absorption band at 568 nm. A decrease of Pu(VI) from 100 % to about 68 % was observed within the investigated time range, most likely due to abiotic reduction processes. The Pu(VI) speciation is dominated by different Pu(VI)-hydroxo species: $(PuO_2)_2(OH)_2^{2+}$/$(PuO_2)_2(OH)_4^0$ (aq) at 849 nm and $PuO_2(OH)_3^-$ at 863 nm according to Reilly and Neu 2006.

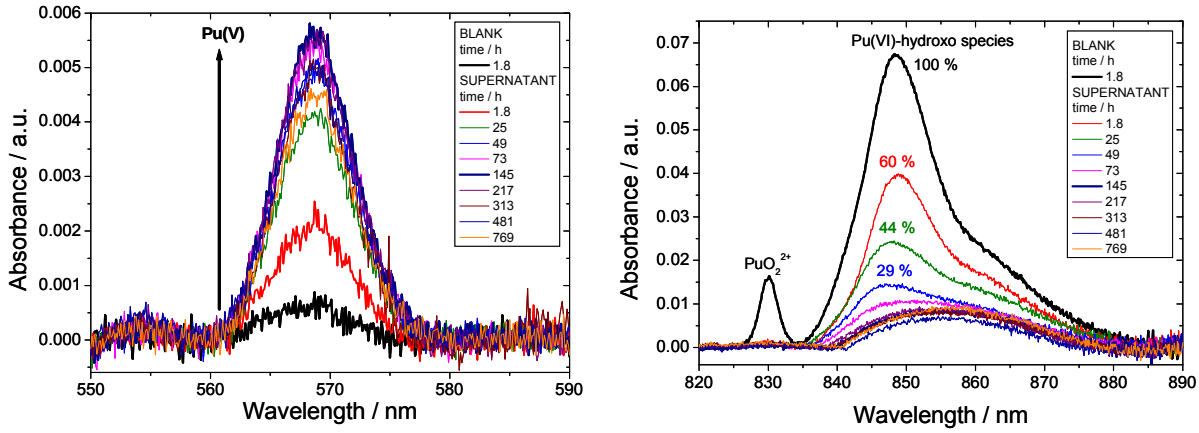

Fig. 4.18 Absorption spectra of the supernatants after separating the cells by centrifugation as a function of time ([^{242}Pu]: 107 mg/L, [BTM] 0.3 g/L, 0.1 M $NaClO_4$, pH 6.1).

Figure 4.18 depicts the results obtained with the supernatants after separating the *Sporomusa* sp. cells by centrifugation ([^{242}Pu]: 107 mg/L, [BTM] 0.3 g/L, 0.1 M $NaClO_4$, pH 6.1). A very

fast decrease of the PuO_2^{2+} absorption band at 830.1 nm could be observed (biosorption). Moreover and due to the activity of the biomass the amount of Pu(VI)-hydroxo species decreased at 71 % within the first 49 h of contact time. The decrease of the Pu(VI) signals is associated with an increase of the absorption band at 569 nm. This can be interpreted by an enrichment of Pu(V) in the supernatants. This Pu(V) might be the result of a biotic Pu(VI) reduction by *Sporomusa* sp. cells.

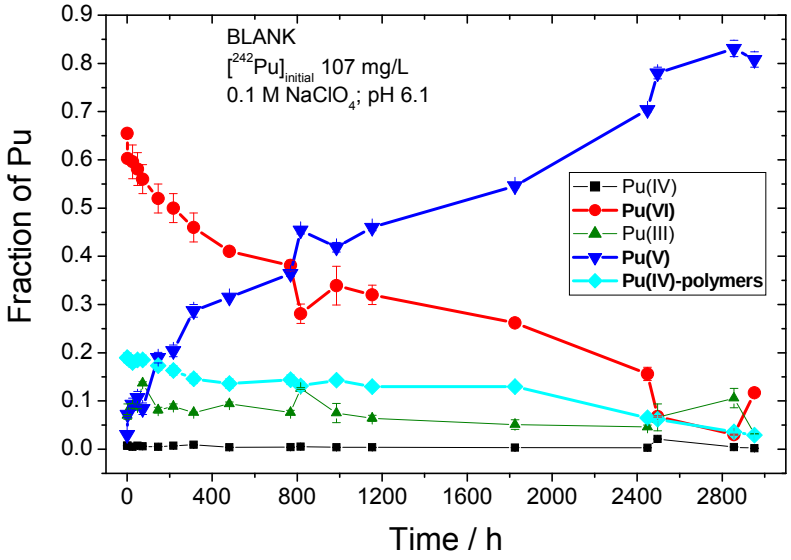

Fig. 4.19 ^{242}Pu oxidation state distributions in the blank samples determined by solvent extraction as a function of time ([^{242}Pu]: 107 mg/L, 0.1 M $NaClO_4$, pH 6.1).

To describe the interaction mechanism of Pu with *Sporomusa* sp., the time dependent Pu oxidation state distribution was determined in the blanks where no cells were added, in the supernatants after separating the cells and finally in the acidic biomass suspension. In the beginning of the experiments it can be seen in Figure 4.19 that the dominating Pu species in the blanks are Pu(VI), 62 ± 3 %, and Pu(IV)-polymers, 19 ± 1 %. Within the first 72 h of interaction time the Pu oxidation state distribution remained relatively unchanged. But we could see a slow tendency of an abiotic reduction of Pu(VI) forming Pu(V) in all of our experiments. This could be partly the result of α-radiation processes where Pu(V) is formed. After around 800 h the amount of Pu(VI) decreased from 65 % to 33 %.

A significant change of the Pu oxidation state distribution was observed in the supernatant as shown in Fig. 4.20. Already after a contact time of 25 h, the amount of Pu(VI) decreased from 65 to 22 %, whereas the Pu(V) content increased from 8.3 to 71 %. After 73 h, the Pu(VI) and Pu(V) concentrations reached steady state conditions with average values of 2.0 ± 1.3 % and

89 ± 5 %, respectively. This indicates a fast reduction of Pu(VI) to Pu(V) most likely due to the activity of the cells.

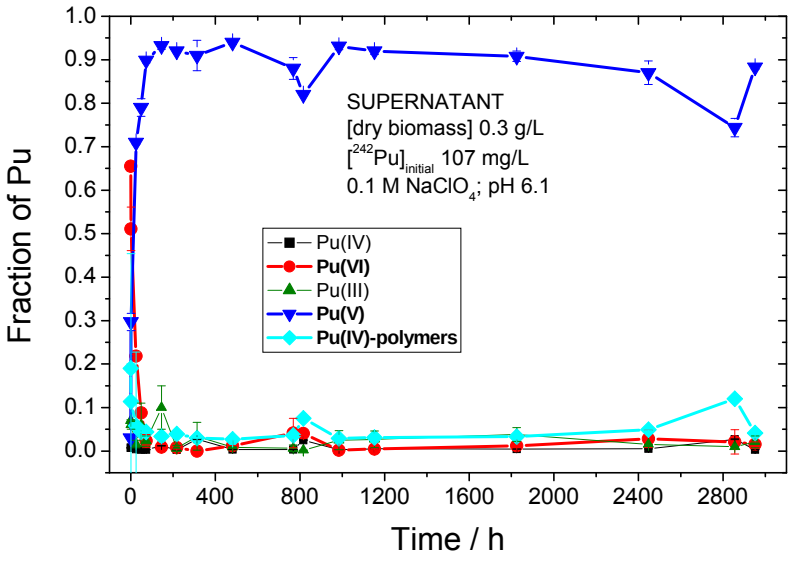

Fig. 4.20 ^{242}Pu oxidation state distributions in the supernatants after separation of the cells determined by solvent extraction as a function of time ([^{242}Pu]: 107 mg/L, [dry biomass] 0.3 g/L, 0.1 M $NaClO_4$, pH 6.1).

As a result and without adding an electron donor *Sporomusa* sp. cells were able to reduce 66 % of the initially Pu(VI) to Pu(V). To compare with the aerobic soil heterotrophs *B. spaericus* and *P. stutzeri* could reduce one third of the initially present Pu(VI) within the first 24 h of incubation (Panak and Nitsche 2001), the sulfate reducer *D. äspöensis* were able to reduce 97 % of the initially Pu(VI) to Pu(V) (Moll et al. 2006). The bioreduction process of Pu(VI) to Pu(V) by cells of *Sporomusa* sp. is not understood at the moment, it could take place via an enzymatic reduction where the dead part of the bacterial culture provides electron donors to the actively reducing part. After the interaction the majority of the Pu(V) was detected in solution. We assume that this happens due to the comparable weak complexing properties of the PuO_2^+ ion which is related with a release from the cell envelope. Similar observations were made in the past (Panak and Nitsche 2001, Moll et al. 2006). The reducing properties of *Sporomusa* sp. suspensions could be proven by E_h measurements. Detailed measurements of the experimental run with $[^{242}Pu]_{initial}$ of 15 mg/L showed a relatively stable redox potential in the blanks of 790 ± 73 mV, whereas the corresponding value in the biomass containing samples dropped down to 330 ± 26 mV within the first 312 h of contact time. The amount of Pu(IV)-polymers decreased from 19 to 4.5 % after 49 h and is then, 4.5 ± 2 %, independent from the contact time. This suggests good binding properties of the cell envelope towards Pu(IV)-polymers (biosorption). The results of the solvent extractions could be confirmed by

UV-vis absorption spectroscopy (see Fig. 4.17 and 4.18). The formed Pu(V) is relatively stable after removing the cells from solution.

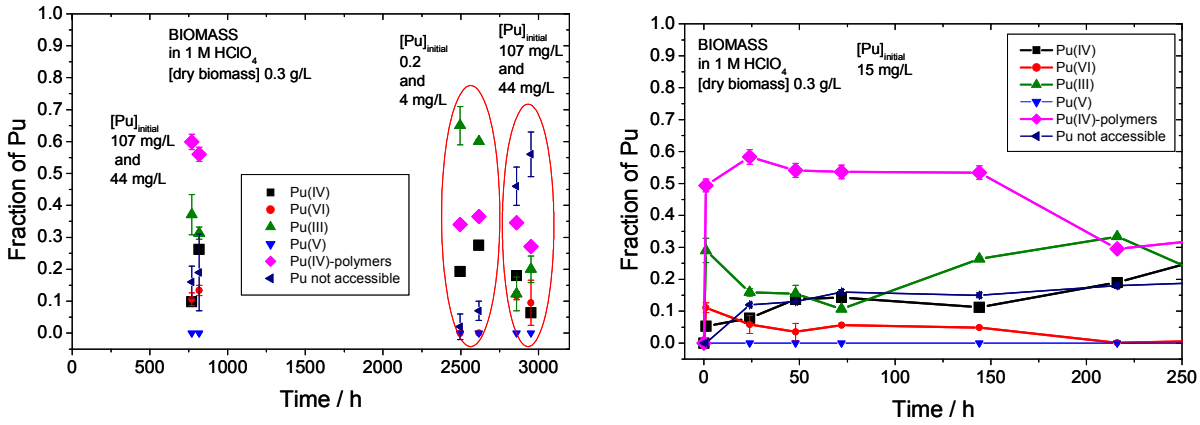

Fig. 4.21 ^{242}Pu oxidation state distributions in the biomass by solvent extraction over the time ([^{242}Pu]$_{varied}$: 0.2 to 107 mg/L, [dry biomass] 0.3 g/L, 0.1 M $NaClO_4$, pH 6.1).

After separating the supernatant from the cells, the bacteria were washed twice with 0.1 M $NaClO_4$. The washed biomass was acidified to pH 0 by adding 1 M $HClO_4$. ^{242}Pu concentration measurements by LSC in the supernatant acidic solution after separating the cells showed that always a certain amount of the accumulated ^{242}Pu remains with the biomass after a contact time of 1 h. After 2500 h of interaction between the cells and [^{242}Pu]$_{initial}$ < 5 mg/L, this amount of strongly bound plutonium amounts to about 11 %. In contrast at [^{242}Pu]$_{initial}$ > 5 mg/L, this amount of strongly bound plutonium increased to about 60 %. Therefore, the solvent extractions were performed with the acidified biomass suspensions. The increase of the strongly bound Pu correlates with the amount of inaccessible Pu in the extraction experiments (see Fig. 4.21).

In the following, the results of the oxidation state distribution measurements of the cell bound plutonium are described. After a contact time of 1 h, the amount of Pu(VI) associated with the biomass was determined to be approximately 11 % ([^{242}Pu]$_{initial}$ 15 mg/L). This shows the biosorption and fast reduction of Pu(VI) to Pu(V). The formed Pu(V) gets very fast dissolved from the cell envelope because the amount of Pu(V) associated with the cells was below the detection limit. The Pu(IV)-polymers are dominating the Pu oxidation state distribution, ~ 60 %, at contact times < 1000 h. The decreased amount of detectable Pu(IV)-polymers from 60 to 30 % in the time range above 1000 h, possibly indicates an accumulation inside the bacterial cells. A further argument for an accumulation of Pu inside the cells might be the increased amount of Pu which is not accessible for the solvent extraction. This effect is much more pronounced at [^{242}Pu]$_{initial}$ > 5 mg/L. Especially in all samples with [^{242}Pu]$_{initial}$ < 107 mg/L an increase of Pu(IV) up to 25 % could be observed. Interestingly we found that the

cells were able to form Pu(III) up to 60 % at low plutonium concentrations 5 mg/L and at long contact times (see Fig. 4.21). The observed tendency of a higher capacity of *Sporomusa* sp. cells to form Pu(III) at lower initial plutonium concentrations is correlated with significantly lower redox potentials of 145 mV (0.2 and 4.1 mg/L) compared to 424 mV (44 mg/L) and 633 mV (107 mg/L).

4.2.2 Actinide interactions with *Paenibacillus* sp.

4.2.2.1 Interaction with U(VI)

U(VI) biosorption studies

The U(VI) sorption experiments with *Paenibacillus* sp. were carried out anaerobically (N_2 atmosphere) to mimic the conditions at Mont Terri. The dependency of the U(VI) binding on $[U(VI)]_{initial}$ and pH as well as the cell-mediated phosphate liberation were studied and the results are presented in the following.

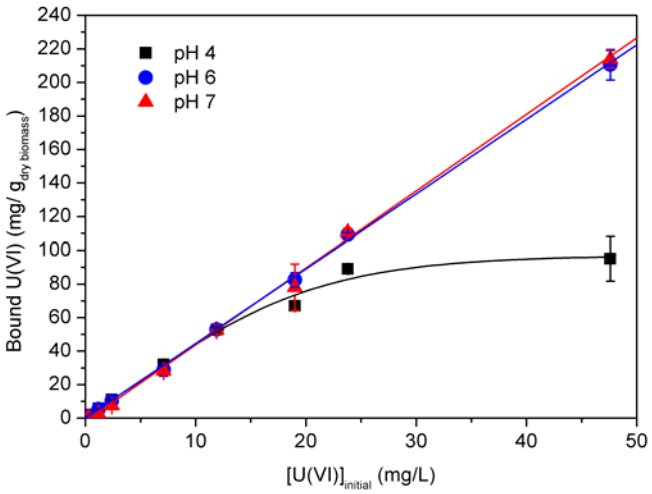

Fig. 4.22 U(VI) binding onto *Paenibacillus* sp. cells in dependence on $[UO_2^{2+}]_{initial}$ at different pH values in 0.1 M $NaClO_4$, [dry biomass] = 0.2 g/L, U(VI) interaction time = 48 h.

As can be seen from Figure 4.22, *Paenibacillus* sp. cells also have a pronounced affinity for U(VI). The study of the pH-dependent adsorption of U(VI) to the reaction tube walls revealed a loss of maximum 11% of the initial amount of U(VI). This loss was accounted for in the calculation of the amount of U(VI) bound per g dry biomass. At an initial [U(VI)] of about 48 mg/L at pH 6 and 7 more than two times as much U(VI) is bound as at pH 4. Interestingly, for pH 6 and 7 the dependency of the sorption on the initial [U(VI)] can be described in both

cases by a linear correlation and almost identical sorption efficiencies were found. At pH 4 on the contrary the sorption shows an asymptotic behaviour with increasing $[U(VI)]_{initial}$. This finding can possibly be explained by a smaller degree of deprotonation of the cell surface functional groups at pH 4 in comparison to pH 6 or 7 resulting in a fewer number of functional groups available for U(VI) complexation.

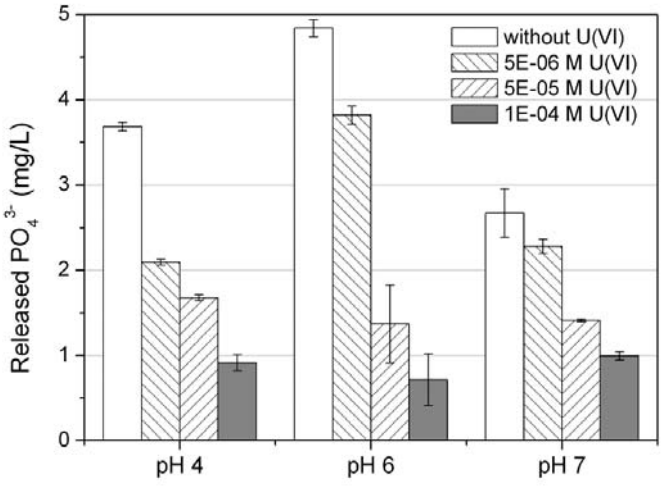

Fig. 4.23 Inorganic phosphate liberation in dependence on $[U(VI)]_{initial}$ at different pH values in 0.1 M $NaClO_4$, [dry biomass] = 0.2 g/L, U(VI) interaction time = 48 h.

That phosphate release can be an active process of microorganisms and altered through external conditions has been discovered very early (Shapiro 1967). Figure 4.23 illustrates the dependency of the inorganic phosphate release by *Paenibacillus* sp. cells on the initial U(VI) concentration and pH. It can be seen that phosphatase activity is maximum at pH 6. At a [U(VI)] as low as $5 \cdot 10^{-6}$ M inorganic phosphate liberation is already markedly decreased in comparison to the samples without any U(VI) added. This effect is strongest at pH 4. Phosphatase activity of *Paenibacillus* sp. is already drastically reduced at an initial [U(VI)] of $1 \cdot 10^{-6}$ M. Upon increasing $[U(VI)]_{initial}$ the phosphate decrease becomes more drastic. This finding might be explainable by either the inhibition of phosphatase activity through U(VI) or the cells switching to the phosphorylation of other compounds (e.g. creation of organophosphates like ATP). These samples were investigated with TRLFS to prove the formation of aqueous uranyl phosphate species.

Potentiometric titration

This method was employed to calculate the stability constants of the U(VI) and Eu(III) complexes formed with the surface functional groups of the studied bacterial strains. Fitting

the titration data of *Paenibacillus* sp. and UO_2^{2+} with HYPERQUAD the hydrolytic uranyl species $(UO_2)_2(OH)_2^{2+}$, $(UO_2)_3(OH)_5^{+}$, $(UO_2)_4(OH)_7^{+}$ (Guillaumont et al. 2003) could be included. Likewise, the best fit result was obtained when the bacterial surface complexes R-COO-UO_2^{+}, R-O-PO_3H-UO_2^{+}, R-O-PO_3-UO_2, and (R-O-PO_3)$_2$-UO_2^{2-} were considered, as can be seen from the HYPERQUAD fit result (Figure 4.24). The respective calculated stability constants are summarized and compared to literature data in Table 4.8.

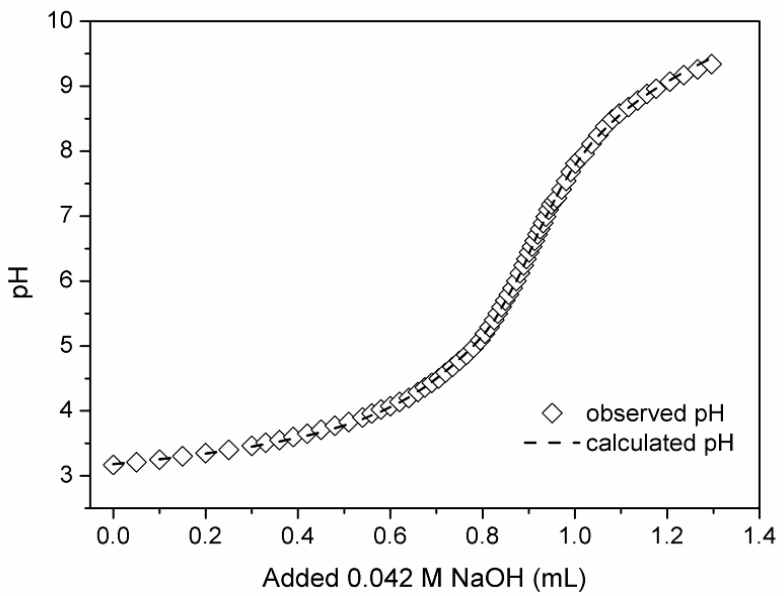

Fig. 4.24 Titration of $1 \cdot 10^{-4}$ M UO_2^{2+} and 0.3 $g_{dry\ weight}$/L cells in 0.1 M $NaClO_4$ with 0.042 M NaOH and fit.

From the stability constants listed in Table 4.8 it can be seen that overall U(VI) can form fairly stable complexes with the surface functional groups of *Paenibacillus* sp. cells. Furthermore the interaction with phosphoryl sites are characterized by stability constants several orders of magnitude greater than that of carboxyl site interaction. The results have been compared to UO_2^{2+} interacting with peptidoglycan (PG) (Barkleit et al. 2009) because PG is the major and very outer part of the cell wall of Gram-positive bacteria. The results were also compared to UO_2^{2+} interacting with glycerol phosphate (Koban and Bernhard 2004) as structural unit of cell wall-inherent teichoic acids of Gram-positive bacteria offering phosphoryl binding sites. Additionally a comparison is made to the stability constants of U(VI) bound to surface functional groups of the Gram-positive strain *B. subtilis* (Fowle et al. 2000). The reported stability constant of the R-COO-UO_2^{+} complex is in very good agreement with the stability constant of the 1:1 complex of U(VI) interacting with carboxylic groups of the *B. subtilis* cell surface published by (Fowle et al. 2000). However, if compared to the results published by Barkleit et al. on the U(VI) interaction with peptidoglycan (Barkleit et al.

2009), where the R-COO-UO_2^+ complex with a log β value of 4.02 was specifically attributed to UO_2^{2+} interacting with glutamic acid groups, deviates somewhat.

Table 4.8 Calculated stability constants of UO_2^{2+} complexes with surface functional groups of *Paenibacillus* sp. cells and comparison to literature.

Species	Complex	xyz [a]	log β_{xyz} (± SD)	Method	Reference
Paenibacillus sp.	R-COO-UO_2^+	110	5.33 ± 0.08	PT	this work,
	R-O-PO_3-UO_2	110	8.89 ± 0.04		(Lütke et al. 2013b)
	R-O-PO_3H-UO_2^+	111	12.92 ± 0.05		
	$(R\text{-}O\text{-}PO_3)_2$-$UO_2^{2-}$	120	13.62 ± 0.08		
Peptidoglycan	R-COO-UO_2^+	110	4.02 ± 0.02	PT	(Barkleit et al. 2009)
Glycerol 1-phosphate	R-O-PO_3-UO_2	110	6.23 ± 0.09// 6.15 ± 0.05	PT // TRLFS	(Koban and Bernhard 2004)
	$(R\text{-}O\text{-}PO_3)_2$-$UO_2^{2-}$	120	10.22 ± 0.13		
Bacillus subtilis	R-COO-UO_2^+	110	5.4 ± 0.2	Adsorption	(Fowle et al. 2000)
	R-O-PO_3H-UO_2^+	111	11.8 ± 0.2	experiment	

a) stoichiometry of metal: ligand: H.

The comparison of the determined stability constants for phosphoryl interaction, in specific of the R-O-PO_3H-UO_2^+ complex, to the literature revealed again a fair agreement with the result gained by (Fowle et al. 2000). Some discrepancy to the literature is observable when comparing the results on U(VI) interaction with deprotonated bacterial phosphoryl sites to the results gained with the model compound glycerol 1-phosphate. Both complexes, the 1:1 and 1:2 complex, were found, but the reported stability constants are significantly lower. Nevertheless, it should be noted that glycerol 1-phosphate is a model compound for the glycerol phosphate polymer (teichoic acid) occurring in the Gram-positive cell wall, which might be an explanation for the deviation.

Bacterial impact of Paenibacillus sp. on U(VI) speciation

Two different sets of conditions were used for the HySS 2009 (Alderighi et al. 1999) speciation calculation. On the one hand, a U(VI) species distribution was calculated according to the TRLFS conditions in order to interpret the results gained with this technique (a). On the other hand, to predict the U(VI) speciation in the field of a nuclear waste repository,

repository or environmentally relevant U(VI) concentrations were used as input parameters (b). Furthermore the relevant U(VI) hydrolytic species and their stability constants were included in the calculation. In specific, these were the hydroxyl complexes which could be included in the fit of the titration data: $(UO_2)_2(OH)_2^{2+}$, $(UO_2)_3(OH)_5^{+}$, and $(UO_2)_4(OH)_7^{+}$ (Guillaumont et al. 2003).

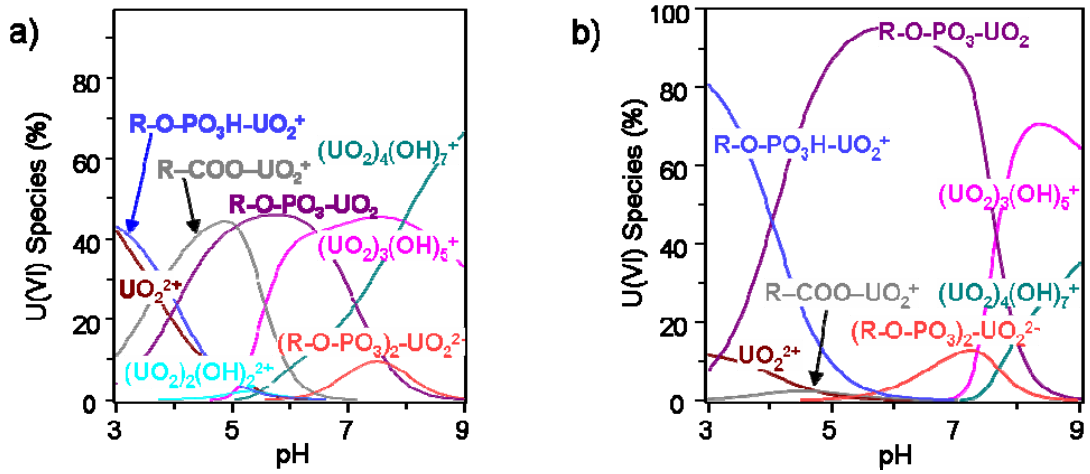

Fig. 4.25 U(VI) species distributions in presence of *Paenibacillus* sp. cells in dependence on pH calculated using HySS 2009 at a) TRLFS conditions: [U(VI)] = $1 \cdot 10^{-4}$ M, [dry biomass] = 0.2 g/L, and b) environmentally relevant concentrations: [U(VI)] = $1 \cdot 10^{-6}$ M, [dry biomass] = 0.02 g/L. CO_2-free system.

Here also the two mentioned cases, TRLFS and environmental conditions ([U(VI)] = $1 \cdot 10^{-6}$ M) were examined (Figure 4.25 a and b, respectively). At the concentrations related to the TRLFS measurements the U(VI) speciation in the acidic pH range (pH 3) is determined majorily by UO_2^{2+} being coordinated to hydrogen phosphoryl sites (Fig. 4.25 a). This finding coheres well to what was reported by Fowle et al. 2000: the best fit of data obtained from U(VI) binding to *B. subtilis* was achieved by considering U(VI) bound via H-phosphoryl groups at low pH. Nevertheless, at pH 3 for instance there is an almost equal portion of non-complexed U(VI) in the cell supernatant, which should be detectable using TRLFS. The species distribution diagram furthermore shows that upon increasing pH an increasing coordination of UO_2^{2+} to carboxylic and deprotonated phosphoryl sites occurred. At a pH greater than 7 uranyl hydroxides dominate the speciation in a CO_2-free system. If environmentally relevant U(VI) concentrations are regarded (Fig. 4.25 b) the coordination to deprotonated phosphoryl and H-phosphoryl sites becomes quite dominant in comparison to the coordination to carboxylic sites which is greatly suppressed. This seems logical since at lower U(VI) first the more stable phosphoryl complexes form. With increasing U(VI) surface load the carboxyl complexes form later on. This was also found by Barkleit et al. investigating

the interaction of U(VI) with lipopolysaccharide (Barkleit et al. 2008). The influence of released cellular ligands on the U(VI) speciation was repressed in the speciation calculations.

TRLFS measurements

The interaction of the Mont Terri isolate with U(VI) was studied to prove the corresponding results gained with potentiometry. In addition especially the occurrence of free UO_2^{2+} at acidic pH should be proven.

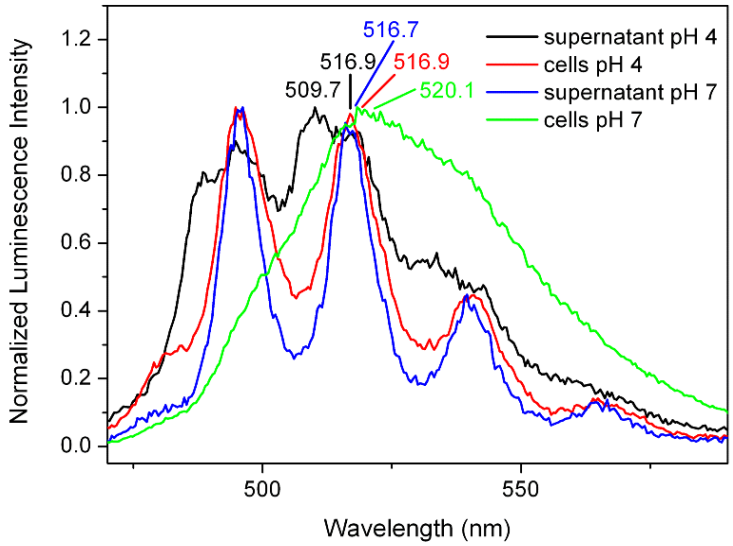

Fig. 4.26 Luminescence spectra of U(VI)-loaded *Paenibacillus* sp. cells and U(VI) in the cell supernatants at pH 4 and 7 in 0.1 M $NaClO_4$. $[U(VI)]_{initial} = 1 \cdot 10^{-4}$ M, [dry biomass] = 0.2 g/L, U(VI) interaction time = 48 h.

From both, the cells and the corresponding cell supernatants at pH 4 and 7, U(VI) luminescence spectra were collected and compared (Fig. 4.26). Luminescence emission maxima and calculated lifetimes related to the spectra shown in Figure 4.26 are summarized and compared to the appropriate literature in Table 4.9. From Figure 4.26 it becomes obvious that the speciation at the cell surface changes in dependence on the pH. With a pH shift from 4 to 7 the main luminescence emission band is slightly red-shifted by roughly 3 nm and also the spectral pattern changes.

The pH dependency of the U(VI) speciation at the cell surface already became obvious from the presented species distribution which had been calculated from the potentiometric titration results. Furthermore the emission maxima of U(VI) in the supernatant at pH 4 indicate the occurrence of at least two luminescent species having quite distinct emission maxima. An emission band located at 509.7 nm and the associated lifetime of 1.03 ± 0.02 µs clearly indicates a spectral contribution of the free UO_2^{2+} ion.

Table 4.9 Main luminescence emission bands and lifetimes related to spectra shown in Figure 4.26 in comparison to literature data.

Species/ complex	Emission maxima (nm)				Lifetimes (µs)	Reference
UO_2^{2+} (100%), pH 1	488.9	510.5	533.9	559.4	1.8 ± 0.2	(Geipel et al. 2000)
U(VI), pH 4: UO_2^{2+}, $(UO_2)_2(OH)_2^{2+}$ [a]	488.0	509.1	532.2	557.0	1.3 ± 0.1, 8.0 ± 0.7	this work
U(VI), pH 7: $(UO_2)_4(OH)_7^+$, $(UO_2)_3(OH)_5^+$ [a]	-	512.8	-	-	7.4 ± 0.3, 23.5 ± 0.9	
Inorganic phosphate						(Panak et al. 2000)
$UO_2(HPO_4)_{aq}$	497	519	543	570	-	
$UO_2PO_4^-$	499	520	544	571	-	
$UO_2(H_2PO_4)^+$/ $UO_2(HPO_4)$	494	517	541	565	-	
Malonate						(Brachmann et al. 2002)
$UO_2[CH_3(CO_2)_2]$	494	515	540	564	1.24 ± 0.02	
Peptidoglycan						(Barkleit et al. 2009)
R-COO-UO_2^+	498	518	539	566	0.7 ± 0.1	
Fructose-6-phosphate						(Koban et al. 2004)
UO_2-F6P	497.1	519.0	543.3	568.9	0.13 ± 0.05	
O-phospho-L-threonine						(Günther et al. 2006)
UO_2HPThr	501.8	523.4	546.8	572.6	0.54 ± 0.10	
Glycerol 1-phosphate						(Koban and Bernhard 2004)
$UO_2(C_3H_7O_3PO_3)$	497.2	518.2	542.9	569.0	0.16 ± 0.03	
Paenibacillus sp. *JG-TB8*						(Reitz 2011)
cell-bound U(VI), pH6	497.2	518.3	541.2	564.9	2.99 ± 0.24, 9.21 ± 1.09, 40.4 ± 3.8	
Paenibacillus sp. (Mont Terri isolate)						this work
cell supernatant, pH 4	488.3	509.7	533.2	-	1.03 ± 0.02,	
	497.1	518.9	542.2	569.4	10.1 ± 0.2	
cell supernatant, pH 7	495.6	516.9	540.9	565.8	-	
cell-bound U(VI), pH 4	495.7	516.9	540.5	565.5	0.66 ± 0.01, 2.69 ± 0.05	
cell-bound U(VI), pH 7	-	520.2	-	-	0.53 ± 0.03, 2.34 ± 0.01	

[a] Assigned species according to determined lifetimes.

The second spectral feature of U(VI) in the cell supernatant at pH 4 is quite similar to the spectrum of U(VI) in the supernatant at pH 7 in terms of the position of the main luminescence emission band, indicating the presence of a similar species at both pH values. This gives evidence for a cellular ligand being released which coordinates strongly to U(VI), otherwise the spectral pattern would show a strong pH dependency due to the increasing

formation of uranyl hydroxides with increasing pH. Considering also the relatively sharp emission bands and the position of the emission maxima of U(VI) in the supernatant at pH 7 the presence of pure U(VI) hydroxide can be excluded. Comparing these band positions to those of model compounds of the literature, especially those of UO_2^{2+} coordinated by $H_2PO_4^-$ and HPO_4^{2-} (Panak et al. 2000), a coordination by inorganic phosphate seems probable. Since inorganic phosphate was already proven to be released into the supernatants in significant amounts by means of ion exchange chromatography, a coordination of UO_2^{2+} by inorganic phosphate seems likely.

Comparing the spectrum of U(VI) bound to the cells at pH 4 to that at pH 7, a red shift of 3.2 nm occurs. This significant red shift is in agreement to what was predicted in the calculated U(VI) species distribution. The U(VI) species distribution had shown the increased formation of UO_2^{2+} complexes with deprotonated phosphoryl sites in the neutral pH range while at low pH around pH 4 uranyl is predominantly coordinated via H-phosphoryl and carboxylic sites. This dependency had also been reported by Barkleit et al. investigating the interaction of LPS with U(VI) (Barkleit et al. 2008). A red shift of the emission maxima occurred when going from UO_2^{2+} complexed by protonated phosphoryl to deprotonated phosphoryl sites.

Besides the position of the luminescence emission maxima, also the luminescence lifetimes can be helpful to identify the present species. At pH 4 for U(VI) bound to the cells two lifetimes could be determined: 0.66 and 2.69 µs. For pH 7 also two lifetimes were found: 0.53 and 2.34 µs. To discriminate here between carboxyl and phosphoryl, and potentially even between deprotonated phosphoryl and H-phosphoryl, a measurement at pH 5 in dependency of $[U(VI)]_{initial}$ was carried out in order to attribute the lifetimes to present U(VI) species. The idea behind was based on the determined stability constants of U(VI) bound to the surface functional groups of *Paenibacillus* sp. cells. In case of a deficit of [U(VI)] compared to the [surface sites] U(VI) should be bound at first via protonated phosphoryl sites. With increasing [U(VI)] an increased amount of R-O-PO_3-UO_2 would be formed. If [U(VI)] is increased further finally the carboxyl groups as weakest ligand according to the determined stability constants and in accordance to many exemplary cases in the literature (Rothstein 1962, Fowle et al. 2000, Barkleit et al. 2008) will be covered by U(VI). According to speciation calculations no 1:2 complex with deprotonated phosphoryl sites is expected to be formed at pH 5. The luminescence spectra measured at pH 5 are given in Figure 4.27. Obviously a significant red-shift of about 5 nm occurs at an increased [U(VI)] of $1 \cdot 10^{-4}$ M compared to the spectrum at the smallest investigated [U(VI)] of $1 \cdot 10^{-5}$ M.

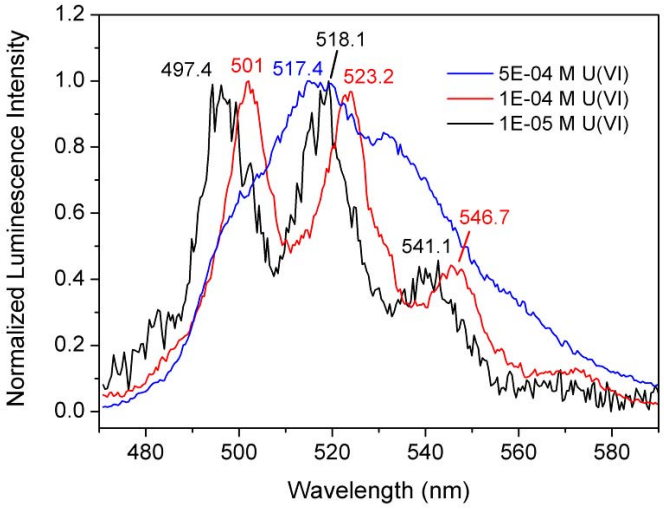

Fig. 4.27 Luminescence spectra of U(VI)-loaded cells with variation of $[U(VI)]_{initial}$ and at pH 5 in 0.1 M $NaClO_4$, $[dry\ biomass]_{initial}$ = 0.2 g/L, U(VI) interaction time = 48 h.

The luminescence emission maxima of the lowest [U(VI] point strongly towards a uranyl phosphoryl interaction. A comparison to the literature reveals that the main emission maxima are almost identical to those found for U(VI) coordinated to O-phospho-*L*-threonine (Günther et al. 2006). The time-resolved measurement at the lowest [U(VI)] indicated biexponential decay revealing lifetimes of 0.54 ± 0.06 µs and 2.55 ± 0.31 µs, whereas at $[U(VI)]_{initial}$ = $1 \cdot 10^{-4}$ M monoexponential decay with a lifetime of 0.56 ± 0.01 µs was found. Thus the spectrum at $[U(VI)]_{initial}$ = $1 \cdot 10^{-4}$ M accompanied by a short lifetime of in average 0.55 µs can clearly be assigned to phosphoryl-bound U(VI), most likely to deprotonated phosphoryl. If the [U(VI)] is increased further the main emission band shifts towards shorter wavelength even below the position of the main emission maximum of the spectrum of the lowest measured [U(VI)]. This finding as well as the spectral pattern observed at this [U(VI)] give indications for a formation of polynuclear U(VI) species. Here monoexponential decay with a lifetime of 2.20 ± 0.22 µs was found.

Considering all these facts, the short lifetime occurring at pH 4 and 7 of about 0.6 µs is most likely attributable to the R-O-PO_3-UO_2 complex. A comparison to the literature undermines the attribution of the short luminescence lifetime to phosphoryl-bound UO_2^{2+} further, since such short luminescence lifetimes have also been reported for UO_2^{2+} coordinated by the phosphate-bearing ligands O-phospho-*L*-threonine (Günther et al. 2006) and fructose-6-phosphate (Koban et al. 2004). A definite assignment of the longer lifetime of about 2.6 µs to a bacterial UO_2^{2+} species is difficult. At pH 4 this lifetime should point to the

R-O-PO_3H-UO_2^+ complex. However, this species is not present at pH 7. It follows that both species, the R-O-PO_3H-UO_2^+ and the (R-O-PO_3)$_2$-UO_2^{2-} complex, have similar lifetimes and longer than that of the R-O-PO_3-UO_2 complex. Similar observations were made by Barkleit et al. for UO_2^{2+}-LPS complexes. Here the R-O-PO_3-UO_2 species had the shortest lifetime with 1.2 µs, followed by 8.3 µs for R-O-PO_3H-UO_2^+ and 13.3 µs for (R-O-PO_3)$_2$-UO_2^{2-} (Barkleit et al. 2008).

EXAFS

X-ray absorption spectroscopy was employed for determining the local structure of U(VI) bound to the surface functional groups of the investigated strains.

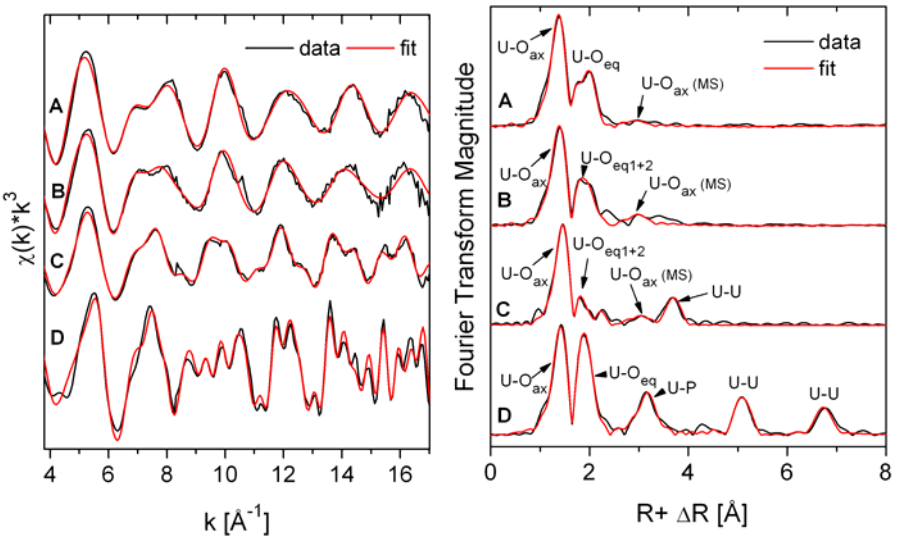

Fig. 4.28 Uranium L_{III}-edge k^3-weighted EXAFS spectra (left) and the corresponding Fourier transformations (right) of the U(VI) complexes formed with *Paenibacillus* sp. MT-2.2 in 0.1 M $NaClO_4$ at pH 4 and 7 (B and C, respectively) compared to the free uranyl ion at pH 2 (A) and the meta-autunite-like structure observed for *P. fluorescens* (D). $[U(VI)]_{initial}$ = 0.1 - 0.2 mM, $[dry\ biomass]_{initial}$ = 0.2 g/L. Black = experimental data, red = fit.

The Mont Terri isolate *Paenibacillus* sp. was investigated regarding its interaction with U(VI) in 0.1 M $NaClO_4$ in dependency on pH. Hence primarily metabolically rather inactive cells were studied. In the following the k^3-weighted $\chi(k)$ spectra and corresponding FTs of U(VI)-loaded *Paenibacillus* sp. cells at pH 4 and 7 are illustrated in comparison to that of the free uranyl ion and the meta-autunite-like structure observed for *P. fluorescens* in contact with U(VI) in SSM with phosphate Figure in 4.28. The corresponding structural parameters of the best fits obtained are summarized in Table 4.10. Investigating the sorption of U(VI) onto *Paenibacillus* sp. cells by EXAFS spectroscopy at both studied pH values a split equatorial

oxygen shell was found indicating the contribution of two different O-donors to UO_2^{2+} coordination.

Table 4.10 EXAFS results on U(VI) interaction with *Paenibacillus* sp.. Coordination numbers N, bond distances R, and Debye-Waller factors σ^2 are given. For comparison the structural parameters of the free uranyl ion and the meta-autunite phase formed with *P. fluorescens* in SSM with phosphate are listed.

Sample composition	**Path**	**N**	**R (Å)**	**σ^2 (Å^2)**	**ΔE_0 (eV)**	**Comments**
A)	U-O_{ax}	2[d]	1.76	0.0013	15.0	T = 298 K
0.05 M U(VI), pH 2	U-O_{eq}	5.2	2.41	0.0068		reduced χ^2 = 161
B)	U-O_{ax}	2[d]	1.78	0.0019	15.1	T = 15 K
Paenibacillus sp. + 0.1 mM	U-O_{eq1}	4.0	2.37	0.0055		reduced χ^2 = 1468
U(VI), pH 4	U-O_{eq2}	0.8	2.50	0.0012		
C)	U-O_{ax}	2[d]	1.81	0.0016	9.3	T = 15 K
Paenibacillus sp. + 0.1 mM	U-O_{eq1}	4[d]	2.34	0.0082		reduced χ^2 = 468
U(VI) , pH 7	U-O_{eq2}	2[d]	2.50	0.0047		
	U-U	1.0	3.85	0.0028		
D)	U-O_{ax}	2[d]	1.79	0.0016	13.0	T = 15 K
P. fluorescens	U-O_{eq}	4[d]	2.29	0.0018		reduced χ^2 = 77
+ 0.2 mM U(VI),	U-P	4[d]	3.63	0.0049		
0.5%-phosphate-SSM,	U-U	4[d]	5.24	0.0032		
pH 7	U-U	4[d]	6.88	0.0016		
	U-O_{ax}	2.0	1.81	0.0016	-8	T = 298 K
(Moll et al. 2000)	U-O_{eq1}	1.9	2.24	0.0030		
	U-O_{eq2}	2.2	2.41	0.0081		
	U-U	2.1	3.87	0.0068	-11	

d) parameter was fixed during fitting procedure

U-O_{eq} bond lengths of 2.34-2.37 Å and 2.50 Å were calculated. For the shorter bond distance a complexation of the uranyl ion by organic phosphate groups is suggested, while the longer bond distance points towards U(VI) interaction with carboxyl groups. Especially in contrast to the highly crystalline m-autunite structure determined in the U(VI) - *P. fluorescens* – 0.5%-P-SSM system (D) the observed features indicate biosorption of U(VI) to the bacterial cell wall functional groups which was also found using TRLFS. The structural parameters (U-O_{ax} and U-U distances) observed for the sample at pH 7 allow the interpretation by two possibilities. First an additional formation of a schoepite-like phase seems possible. However, the structural parameters in terms of N and R deviate from those of a precipitate formed at pH 7 in a bacteria-free system (Moll et al. 2000). Therefore the formation of polynuclear U(VI) surface species might occur. Because of the strong damping of the equatorial oxygen shell due to high structural disorder in this sample the coordination numbers of the equatorial oxygen atoms had to be fixed to fit the equatorial oxygen shell properly.

Reitz et al. also investigated a strain of this genus with EXAFS spectroscopy, *Paenibacillus* sp. JG-TB8 (Reitz 2011). At pH 4.5 as well as at pH 6 also U(VI) biosorption was found at anaerobic conditions. The authors additionally investigated the interaction with U(VI) at aerobic conditions. Interestingly, here it was found that at pH 2 to 3 solely biosorption was observed, but from pH 4.5 on U(VI) was increasingly precipitated as meta-autunite. The authors attributed these findings to a suppression of the bacterial phosphatase at anaerobic conditions. Analogously, for the here investigated Mont Terri isolate also no meta-autunite formation was observed at anoxic conditions, although on the contrary it was proven that inorganic phosphate release takes place at anaerobic conditions.

4.2.2.2 Interaction with Eu(III)/Cm(III)

Potentiometric Titration

The titration curve of Eu(III) and *Paenibacillus* sp. and fit carried out with HYPERQUAD is displayed in Figure 4.29.

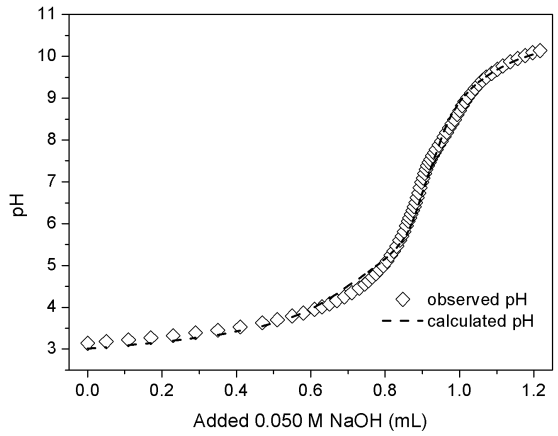

Fig. 4.29 Titration of $1 \cdot 10^{-4}$ M Eu(III) and 0.3 $g_{dry\ weight}$/L *Paenibacillus* sp. cells in 0.1 M NaCl with 0.050 M NaOH and fit with HYPERQUAD.

Comparing the stability constants of the Eu(III) complexes determined in this work with those reported in the literature, it becomes obvious, that for Eu(III) hitherto only complexes having 1:1 stoichiometry based on interaction with bacterial phosphoryl and carboxylic sites were detected (see Table 4.3). The best fit of the titration data was obtained by including the surface species R–COO–Eu^{2+} and R-O-PO_3H-Eu^{2+}.

The here reported stability constant of the R-COO-Eu^{2+} complex formed with *Paenibacillus* sp. surface functional groups coheres with what has been determined with the actinide analog Cm(III) with PG as a model compound of the cell wall of Gram-positive bacteria. The

carboxylic groups of *Paenibacillus* sp. cells evidently display a lower affinity for Eu(III) than for instance *B. subtilis* of a phylogenetically quite similar genus does and also what was determined for the Gram-negative strain *P. fluorescens* in this work. The constant of the R-COO-Eu^{2+} complex formed on the *P. fluorescens* cell surface is quite similar to that of *B. subtilis.*

Regarding the stability constant of the R-O-PO_3H-Eu^{2+} complex formed with the surface functional groups of the investigated strains again the hydrogen phosphoryl sites of *P. fluorescens* cells display a more pronounced affinity towards Eu(III) than that of *Paenibacillus* sp. cells do. Hence overall and taking also the determined surface functional groups densities into account this implies that *P. fluorescens* is more efficient in Eu(III) binding than *Paenibacillus* sp.. Both determined stability constants of the R-O-PO_3H-Eu^{2+} complex agree with what has been determined before on Cm(III) interacting with LPS (Moll et al. 2009).

TRLFS

The Cm(III) aquo ion possesses a characteristic emission maximum at 593.8 nm. From Figure 4.30 it becomes obvious that the luminescence spectrum of Cm(III) in presence of *Paenibacillus* sp. cells is red shifted compared to that of the Cm(III) aquo ion by approximately 5 nm indicating complex formation.

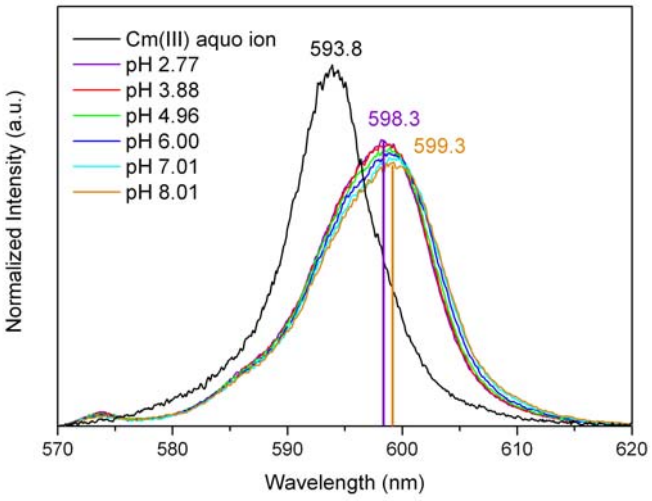

Fig. 4.30 TRLFS spectra in dependency on pH at a [Cm(III)] of $3 \cdot 10^{-7}$ M and [dry biomass] of 0.2 g/L (I = 0.1 M $NaClO_4$). Spectra normalized to surface area.

Obviously in the pH range from 3 to 8 the spectra of Cm(III) in presence of the cells undergo a slight red shift of about 1 nm. A decrease in luminescence intensity occurring in the system

Cm^{3+}-*Paenibacillus* sp. with increasing pH was observed. The pH-dependent spectra were evaluated using SPECFIT to determine the stability constants of the surface complex formed and their single component spectra (see Fig. 4.31). Input parameters for the fit were the previously determined site densities and pK_a values of the surface functional groups of the *Paenibacillus* sp. cells and the stability constants of the relevant Cm^{3+} hydrolytic species (Edelstein et al. 2006). Thereby the complex R-O-PO_3H-Cm^{2+} could be extracted having a stability constant log β of 13.94 ± 0.18.

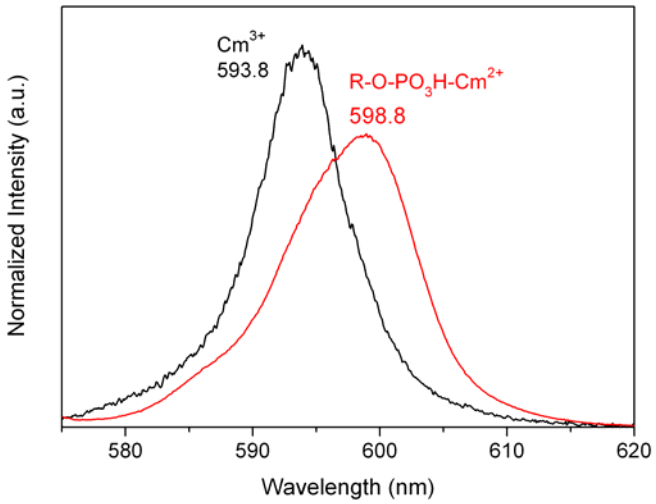

Fig. 4.31 Luminescence emission spectrum of R-O-PO_3H-Cm^{2+} compared to that of Cm^{3+} as derived by peak deconvolution using SPECFIT. The spectra are scaled to the same peak area.

Consequently, the Cm^{3+} speciation in presence of *Paenibacillus* sp. cells was modeled with the program HySS 2009. Two sets of input parameters were used: a) Cm-TRLFS conditions: [Cm(III)] = $3 \cdot 10^{-7}$ M and [dry biomass] = 0.2 g/L, and b) environmental concentrations: [Cm(III)] = $3 \cdot 10^{-7}$ M and [dry biomass] = 0.02 g/L (see Fig. 4.32). The calculated HySS speciation indicates that in the investigated pH range mainly Cm(III) is bound by H-phosphoryl sites. Comparing both speciation diagrams it becomes evident that a decrease of [dry biomass] by factor 10 barely alters the Cm(III) speciation. The R-O-PO_3H-Cm^{2+} complex dominates the speciation up to pH 8 at both conditions, TRLFS and environmental ones. Cm(III) hydrolytic species dominate the speciation at pH greater than 8. Overall this in congruence to what was observed with TRLFS. The calculated speciation vice versa explains why no Cm(III) hydroxides have been detected in the investigated pH range. The determined stability constant of the R-O-PO_3H-Cm^{2+} complex has been compared to relevant literature

data (Table 4.3). Obviously Cm(III) displays high affinity to the phosphoryl sites of the *Paenibacillus* sp. cell surface. No carboxyl interaction could be detected by TRLFS.

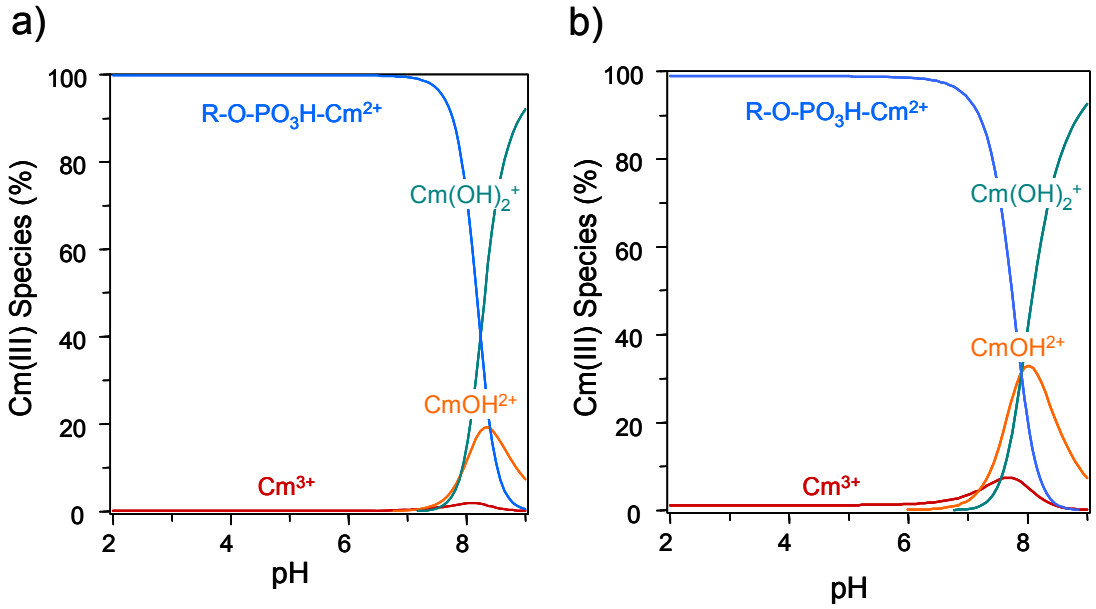

Fig. 4.32 HySS speciation of Cm^{3+} ($3 \cdot 10^{-7}$ M) in presence of *Paenibacillus* sp. cells, **a)** with [dry biomass] relevant for Cm(III) TRLFS measurements (0.2 g/L), and **b)** with environmentally relevant [dry biomass] of 0.02 g/L.

Overall the stability constant of the R–O–PO_3H–Cm^{2+} complex suggests, that Cm(III) is bound with remarkable thermodynamic stability. Compared to the stability of other Cm(III) complexes of environmental relevance, the Cm(III)-*Paenibacillus* complex R–O–PO_3H–Cm^{2+} is more stable than Cm(III) complexes with hydroxide ($Cm(OH)^{2+}$, $Cm(OH)_2^+$ in (Edelstein et al. 2006)), chloride (Fanghänel et al. 1995, Könnecke et al. 1997), and sulfate (Paviet et al. 1996), but significantly less stable than those with phosphate ($CmH_2PO_4^{2+}$, $CmHPO_4^+$ in (Moll et al. 2011)).

Investigating the interaction of *Paenibacillus* sp. cells with Eu(III) using potentiometry a comparatively small stability constant was found for the R–COO–Eu^{2+} complex. Taking this into consideration and additionally that the corresponding Cm(III) complex might possess a low luminescence quantum yield the failure of detecting a Cm(III) carboxyl complex with *Paenibacillus* sp. cells by TRLFS might be explainable. Another effect might be the difference in ratios of [metal] to [dry biomass] in the potentiometry and TRLFS experiments. For TRLFS the ratio was over 300 times lower than for potentiometric titration. With a deficit of [Cm(III)] compared to [surface functional groups] at first favourably the more stable phosphoryl complexes are formed.

Overall there have been indications that besides the R–O–PO_3H–Cm^{2+} complex a second species, most likely R–O–PO_3–Cm^{+}, maybe is present at the *Paenibacillus* sp. cell surface as well. Both previously mentioned characteristics, decrease in luminescence intensity and slight red shift of the pH-dependent spectra, propose that the Cm(III) speciation slightly changes in the investigated pH range. A red shift occurring concomitant to a deprotonation of phosphoryl sites involved in Cm(III) coordination has also been found for Cm(III) interacting ATP (Moll et al. 2005). It seems reasonable to attribute this red shift to a deprotonation rather than to the complex formation with a different surface functional group since the observed red shift is comparatively small and does not point towards increasing interaction with carboxyl moieties (Moll et al. 2009, Moll et al. 2013). Deconvoluting the luminescence sum spectra using SPECFIT with the assumption of two phosphoryl complexes resulted in stability constants (main emission maxima) of the R–O–PO_3H–Cm^{2+} and R–O–PO_3–Cm^{+} complex of 12.73 ± 0.46 (598.5 nm) and 6.62 ± 0.38 (599.5 nm), respectively. As can be seen from the small difference of the calculated main emission maxima, the assignment of these complexes to the spectral observations remains very speculative.

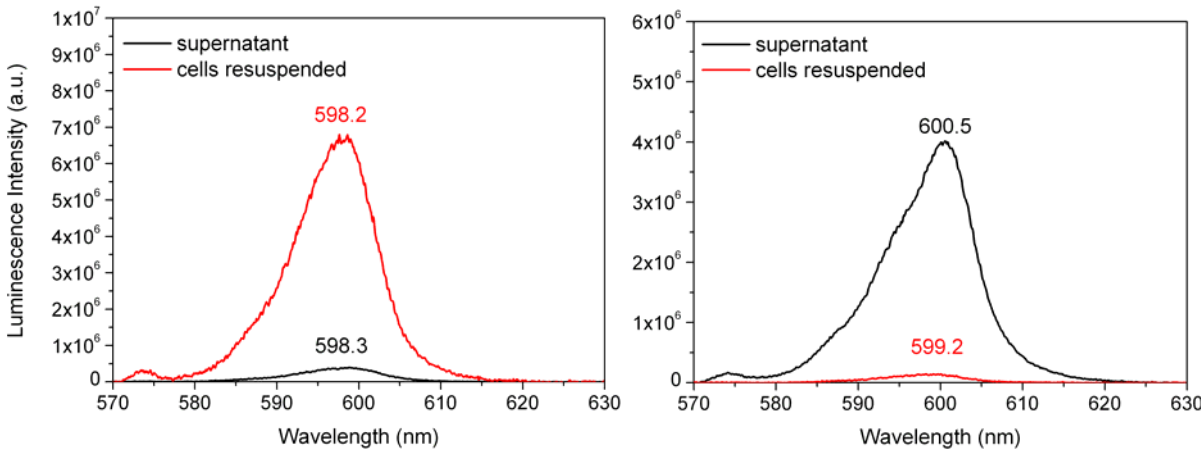

Fig. 4.33 Luminescence spectra of Cm(III) bound to *Paenibacillus* sp. cells and in the corresponding cell supernatants (I = 0.1 M $NaClO_4$) at pH 3 (left) and pH 8 (right).

Over the whole investigated pH region two luminescence lifetimes were detected in the Cm(III)- *Paenibacillus* sp. system: $\tau_1 = 238 \pm 23$ µs and $\tau_2 = 477 \pm 73$ µs. It was found that the longer lifetime decreased from 552 to 424 µs upon increasing the pH from 3 to 8. Subsequently, cells and corresponding supernatants where investigated separately at the pH values 3 and 8 to assign these lifetimes to Cm(III) cell surface or aqueous species. First of all from Figure 4.33 it becomes evident, that after 24 h Cm(III) contact at pH 3 far more Cm(III)

is bound to the cells as at pH 8. Indeed an almost opposite distribution of Cm(III) between the cells and the corresponding cell supernatants can be found. Combined with extraction of the cell-bound Cm(III) with EDTA it could be determined that at pH 3 94.5 % Cm(III) are accumulated by the cells, whereas at pH 8 only 4 % Cm(III) is bound. Using EDTA at both pH values all cell-bound Cm(III) could be removed indicating a reversible binding of Cm(III) exclusively to the cell surface functional groups.

Table 4.11 Luminescence emission maximum and lifetime of Cm-*Paenibacillus* sp. complex in comparison to literature data.

Species/ complex	Emission peak maximum (nm)	Lifetime (µs)	Reference
Cm(III) aquo ion	593.8	65 ± 2	This work
Cm^{3+}-*Paenibacillus* sp. Complex			This work
$R–O–PO_3H–Cm^{2+}$	598.8	477 ± 73	
Cm^{3+}–*Pseudomonas fluorescens* complexes			this work,
$R–COO–Cm^{2+}$	601.9	121 ± 10	(Moll et al. 2013a)
$R–O–PO_3H–Cm^{2+}$	599.6	390 ± 78	
Cm^{3+}–*Desulfovibrio äspöensis* complex	600.1	162 ± 5	(Moll et al. 2004)
Cm^{3+}-PG species (from *B. subtilis*)			(Moll et al. 2009,
$R-COO-Cm^{2+}$	602.0	230	Moll et al. 2013a)
Cm^{3+}-organic phosphoryl complexes			(Moll et al. 2005)
$Cm-ATPH_2^+$	598.6	89	
Cm-ATPH	600.3	92	
$Cm-ATP^-$	601.0	187	
Cm^{3+}-inorganic phosphate complexes			(Moll et al. 2011)
$CmH_2PO_4^{2+}$	599.6	71 ± 3	
$CmHPO_4^+$	600.8	118 ± 18	
Cm(III) phosphate colloids	603.1	220 ± 20	

For Cm(III) bound to the cell surface at both pHs monoexponential decay with a mean lifetime of 477 ± 73 nm was determined (see Table 4.11). Hence from both detected lifetimes in the bacterial Cm(III) suspensions at all investigated pH values the longer lifetime can be clearly assigned to the cell-bound Cm(III). This implies that only one type of functional group is involved in complex formation over the whole investigated pH region. As consequence, the lifetime of in average 238 ± 23 µs belongs to a Cm(III) species in the aqueous phase. At pH 3 hardly any Cm(III) emission decay could be detected due to the low [Cm(III)] remaining in solution after sorption to the biomass. But at pH 8 the time-resolved measurements of the supernatant after 24 h Cm(III) contact revealed two luminescence lifetimes: 183 ± 46 µs and 327 ± 19 µs. The first one might indicate the formation of Cm(III) phosphate while the second one implies complexation by functional groups of organic origin. Possibly the second lifetime

is attributable to Cm(III) being complexed by cell-released matter. A more specified assignment based on the present data is difficult.

To prove the concrete surface functional group involved in complexing Cm^{3+} at the cellular envelope as proposed by SPECFIT analysis, the determined emission maximum and lifetime of the R–O–PO_3H–Cm^{2+} complex have been compared to those of Cm(III) complexes formed with the Gram-negative strains *P. fluorescens* (CCUG 32456A) determined in this work (Moll et al. 2013a) and *D. äspöensis* (Moll et al. 2004), with PG as a model compound of the cell wall of Gram-positive bacteria (Moll et al. 2009), and with soluble organic and inorganic phosphates (Moll et al. 2005, Moll et al. 2011). All data is summarized in Table 4.11.

Generally, it can be found that binding of Cm(III) to carboxylic groups of cell surfaces or model compounds of such display emission maxima at higher wavelength than that of Cm(III) bound to phosphoryl groups. In contrast to the results with *Paenibacillus* sp. with *P. fluorescens* besides the R-O-PO_3H-Cm^{2+} complex also complexation involving carboxylic groups was detected (Moll et al. 2013a). The lifetime of the R-O-PO_3H-Cm^{2+} complex formed with *P. fluorescens* cell surface functional groups is the one in the literature coming closest to the here reported value for the R-O-PO_3H-Cm^{2+} complex. Lifetimes of carboxyl-bound Cm^{3+} are constantly smaller and apparently do not match the here reported lifetimes. Hence the analysis made using SPECFIT can be undermined by the examination of the luminescence emission maxima and lifetimes.

The finding that Cm(III) sorption efficiency underlies such a strong pH dependency gives rise for the assumption that some cellular ligand is released at pH 8 over time (24 h) which desorbs the cell-bound Cm(III) (see Fig. 4.30 an 4.33). The hypothesis that some cellular ligand release occurs at pH 8 is supported by the comparison of the emission spectra of cells + supernatant (day before) with that of the supernatant taken after 24 h. The comparison reveals a) a slight shift of the emission maximum from 599.2 to 600.5 nm, and b) a slight increase in the luminescence intensity, which had been reported previously to occur concomitant to a Cm(III) complexation by inorganic phosphate (Moll et al. 2011). Since the emission maximum of the supernatant at pH 8 located at 600.5 nm coincides also with that of Cm(III) phosphate species ($CmH_2PO_4^{2+}$ and $CmHPO_4^{+}$ at 599.6 and 600.8 nm, respectively) (Moll et al. 2011) most reasonably phosphate has been released by the cells which coordinates Cm(III) in the aqueous phase. This implies a pH-dependent phosphatase activity of *Paenibacillus* sp. in presence of Cm(III), which had also been proven for the interactions of this strain and *P. fluorescens* with U(VI) (chapters 4.2.2.1 and 5.2.1.1, respectively).

In summary and to propose an overall model for Cm(III) interaction with *Paenibacillus* sp. cells affecting the Cm(III) speciation: e.g. at pH 3 Cm(III) initially is present in solution solely as the Cm(III) aquo ion. As such it must adhere well to the cell surfaces since 95 % Cm(III) gets immobilized, although remarkable cell-mediated phosphate release occurs. It was shown that Cm(III) forms primarily the complex R-O-PO_3H-Cm^{2+} at the cell envelope. At pH 3 in minor amounts $CmHPO_4^+$ and $CmH_2PO_4^{2+}$ coexist with the cell-bound Cm^{3+}. At pH 8 compared to pH 3 the amounts of cell-bound Cm(III) and $CmHPO_4^+$/ $CmH_2PO_4^{2+}$ are reversed.

4.3 Summary

The results showed that for U(VI) and Cm(III)/Eu(III) cellular binding is strongly pH-dependent. For U(VI) the maximum binding capacities for *Sporomusa* sp. MT-2.99 and *Paenibacillus* sp. MT-2.2 were found at pH 7. Both strains possess high U(VI) binding capacities, e.g. *Paenibacillus* adsorbs up to 211 mg $U/g_{dry\ weight}$ at an $[U(VI)]_{initial}$ of 48 mg/L at pH 7. U(VI) interaction experiments with both strains showed that mainly phosphoryl and carboxyl moieties of the cell envelope were responsible for U(VI) binding via biosorption. The following bacterial U(VI) surface species were identified by potentiomertric titration: R–COO–UO_2^+, R–O–PO_3–UO_2, R–O–PO_3H–UO_2^+, and (R–O–PO_3)$_2$–UO_2^{2-}. The U(VI) speciation in the both systems could be successfully validated by the direct speciation method TRLFS. We can conclude from the determined bacterial surface stability constants thermodynamically moderate to strong interaction reactions. These stability constants as one important result of this project can be used in modeling programs calculating the speciation of U(VI) for instance in the vicinity of a potential nuclear waste repository.

Also for Cm(III)/Eu(III) and within the investigated pH-range (2-8) carboxyl and phosphoryl moieties of the bacterial cell envelope were responsible for metal binding. The interaction mechanism of Eu(III)/Cm(III) with *Sporomusa* sp. cells is dominated by a major process a reversible biosorption reaction. However we could identify for Eu(III) and Cm(III) a certain amount, ca. 30%, which is irreversibly bound to the cells. This minor process can be described by a immobilization of Eu(III)/Cm(III) within the complex cell envelope structure of *Sporomusa* sp.. TRLFS studies on the interaction of Cm(III) with *Paenibacillus* sp. revealed that Cm(III) is solely bound by the bacterial phosphoryl moieties. SPECFIT analysis indicated the presence of the R-O-PO_3H-Cm^{2+} species over a wide pH range. Although the existence of a Eu(III) species with carboxylic groups at pH 8 was predicted, no such Cm(III) species could be detected at that pH using TRLFS. An explanation might be the difference in

ratios of [metal] to [dry biomass] in the potentiometry and TRLFS experiments. Also the respective Cm(III)-carboxyl complex might have a much lower luminescence quantum yield than Cm(III) complexed by phosphoryl sites. For Cm(III) slightly larger log β values for the bacterial surface complexes were measured compared to Eu(III). However we could also show that Eu(III) can be used as a non-radioactive analogon to mimic bacterial interactions of An(III). Our results suggested that Eu(III)/Cm(III) complexes with the surface functional groups of both strains dominate their respective speciation over a broad pH and biomass concentration range. Overall, with the discussed surface functional groups a moderate to strong interaction with Eu(III) and Cm(III) can be found.

Strong interactions of the Mont Terri Opalinus Clay isolate *Sporomusa* sp. with ^{242}Pu were observed at pH 6 (~ 78 mg Pu/$g_{dry\ weight}$). A higher ^{242}Pu binding capacity of the dead biomass was determined. The ^{242}Pu removal efficiency of *Sporomusa* sp. cells depends on the $[^{242}Pu]_{initial}$. Compared to ^{238}U (> 120 mg U/$g_{dry\ weight}$) the cells are accumulating less plutonium. Approximately 43 % of the initially present Pu(VI) was reduced to Pu(V) due to the activity of the cells during the first 25 h of contact time (99 % after 73 h). We could detect good binding properties of the cell envelope towards Pu(IV)-polymers (immobilization). Especially at long contact times and low initial plutonium concentrations, the cells were able to form relatively high amounts of Pu(IV) and Pu(III). We can postulate a similar interaction mechanism as found for the Äspö strain *D. aespoeensis* (Moll et al. 2006). To sum up, there was a strong influence of *Sporomusa* sp. cells on the Pu oxidation state distribution and hence the speciation.

5 The interaction of the Äspö-strain *P. fluorescens* with selected actinides

Our studies are focused on the determination of direct interaction processes (see also chapter 4 for introduction) between the Äspö-strain *P. fluorescens* and the actinides U(VI), Cm(III) and Pu. Eu(III) was applied in order to validate the TRLFS results obtained with Cm(III) by using an independent technique potentiometric titration. The biomass was supplied as planktonic cells (metabolically active and almost inactive) or fixed in a biofilm. The importance of *Pseudomonads* in for instance environmental waters was also shown by our investigations in Mont Terri pore water (see chapter 2.1.3 and 2.2.2). The goal was to detect differences or similarities of the interaction behavior of the cells towards the used metals.

5.1 Experimental

Preparation of actinide bacteria solutions

U(VI) biosorption by *P. fluorescens* was investigated in dependence on $[U(VI)]_{initial}$, [dry biomass], and pH. The U(VI) binding in dependence on $[U(VI)]_{initial}$ was investigated at pH 4, 6, 7 and 8. For all U(VI) experiments a stock solution of 0.1 M $UO_2(ClO_4)_2$ was used. U(VI) accumulation experiments were carried out in 0.1 M $NaClO_4$. The pH adjustments were made with $HClO_4$ or NaOH. The pH was measured using a glass electrode with a platinum diaphragm (Blueline 16 pH, Schott, Mainz, Germany) calibrated with standard buffers and a pH meter (InoLab720, WTW, Weinheim, Germany). The pH was adjusted with a precision of 0.03 units. To investigate U(VI) sorption in dependence on $[U(VI)]_{initial}$ the dry biomass was set to 0.2 $g_{dry\ weight}$/L, while [U(VI)] was varied from 0.4 to max. 138 mg/L.

To assess also the effect of the $[U(VI)]_{initial}$ on the cell division the samples containing $1 \cdot 10^{-6}$ M and $1 \cdot 10^{-4}$ M uranium at pH 7 and 8 were additionally plated on NB agar and incubated at 30°C. Plates were screened for colony growth and compared to those without uranium contact.

To examine the U(VI) binding in dependence on [dry biomass], [U(VI)] and pH were fixed to $1 \cdot 10^{-4}$ M and 6.0, respectively, and the dry biomass concentration was varied between 0.05 - 0.8 g/L. After 48 h U(VI) contact the cells were centrifuged and supernatants analyzed regarding [U(VI)] with ICP-MS. Furthermore the adsorption of UO_2^{2+} onto the reaction vessel as source of error of this experiment was investigated. Therefore after the U(VI) interaction experiment the reaction tubes were rinsed 3 times with Milli-Q water and then incubated for 2 days with 1 M HNO_3 to desorb U(VI). Solutions where then analysed with ICP-MS regarding [U(VI)]. All experiments were done in duplicate. In addition to the analysis of the

supernatants regarding [U(VI)], selected samples were also analysed regarding the release of inorganic phosphate in dependency on the pH and $[U(VI)]_{initial}$ by means of IEC. To judge to which extent phosphate release occurs without U(VI) added furthermore pure bacterial solutions were analysed.

U(VI) TRLFS samples were prepared as described in section 4.1 and analysed analogously. Furthermore, besides studying the interaction of U(VI) with *P. fluorescens* in 0.1 M $NaClO_4$, also the interaction in 0.5%-phosphate-SSM was investigated to enhance metabolic activity of the cells. For this purpose the cells which were grown in 0.5%-phosphate-SSM, were washed two times in fresh 0.5%-phosphate-SSM and resuspended in the same to yield a final dry biomass concentration of 0.2 g/L. [U(VI)] and pH were set to $1 \cdot 10^{-4}$ M and 7.0, respectively. Interaction time was 48 h.

The Cm(III) experiments were performed in a glove box under a N_2 atmosphere at 25 ºC. As a background electrolyte, analytical grade 0.1 M $NaClO_4$ was used. The curium(III) concentration was fixed at 0.3 µM. In two runs, the biomass concentration was kept constant at 0.2 $g_{dry\ weight}$/L, while varying pH between 8.0-1.4 and 1.5-8.0, respectively. In two runs, the biomass concentration was changed between 0.01 and 1000 $mg_{dry\ weight}$/L at pH 3.05 and 6.08, respectively. In order to obtain information on the binding strength and the reversibility of the biosorption process, the curium(III) on the biomass was extracted with 0.01 M EDTA solution (pH 5) as described by Panak and Nitsche 2001. The data were evaluated in analogy to the Cm(III) measurements with the Mont Terri Opalinus Clay isolates (see chapter 4.1).

The Pu experiments were performed in analogy to the ^{242}Pu–*Sporomusa* sp. system (see chapter 4.1 for detailed information). The Pu–*P. fluorescens* experiments were performed at [dry biomass] of 0.2 $g_{dry\ weight}$/L and pH 6.2 under N_2 atmosphere at 25 °C in 0.1 M $NaClO_4$ solution. $[^{242}Pu]_{initial}$ was varied between 0.2 and 100 mg/L. Detailed investigations of the distribution of the different Pu oxidation states were made at a fixed concentration of Pu, $[^{242}Pu]_{initial}$ of 24 ± 0.8 mg/L. Samples were taken after defined time steps. The separation of cells from the supernatant solution was performed by centrifugation (5000g).

Biofilms: addition of U(VI) and analysis

After a *P. fluorescens* biofilm had formed (see chapter 3), 2.8 mL of 1×10^{-2} M $UO_2(ClO_4)_2$ were added to 400 mL of the nutrient medium to a final U(VI) concentration of 23.8 mg/L (1×10^{-4} M) in the glass plunger. As shown in the literature uranium concentration of 0.238 mg/L (1×10^{-6} M) to 59.51 mg/L (2.5×10^{-4} M) are representing ecologically relevant uranium concentrations, which were encountered in the vicinity of uranium contaminated

sites, e.g. flooded uranium mine in Königstein, Germany (Krawczyk-Bärsch et al. 2011) and uranium-mining rockpile in Schlema, Germany (Geipel et al. 1994). The duration of the uranium sorption experiment was limited to 42 h.

Samples of the nutrient media were taken for analysis before and directly after the addition of uranium. At the end of the experiments samples were centrifuged and the supernatant were taken. They were acidified and analyzed for the determination of cations by means of inductively coupled plasma spectrometry (ICP-MS) using both an ELAN 9000 ICP-MS spectrometer (PerkinElmer, Überlingen, Germany) and an AXIOM ICP-MS spectrometer (VG Thermo Elemental, Winsford, UK). The anions were determined by means of ion chromatography (IC) using the 732/733 IC system (Metrohm, Filderstadt, Germany). The biofilm was taken after the experiments and ultra centrifuged (Ultracentrifuge Optima XL100K, Rotor: SW 32Ti; Beckman Coulter) for 1 h with 187000 × g. The formed pellet was freeze-dried (ALPHA 1-4 LSC, Christ), refined and decomposed for determination of the uranium concentration in the biofilm dry mass by ICP-MS.

Biofilms: microsensor measurements

Concentration profiles of oxygen in 20 μm steps in Z-axis were measured in the biofilm by electrochemical microelectrodes (tip diameter = 8–12 μm) of the micro-Clark design (Unisense, Denmark). The electrodes were fixed in a holder on a motor-driven micromanipulator stage, which was connected to a picoammeter. The motor controller of the micromanipulator communicated with a PC, controlled from the PC with the program PROFIX (Unisense, Denmark). A two-point linear calibration was used as described in Krawczyk-Bärsch et al. 2008. The redox potential was determined by a miniaturized platinum electrode (RD-10; Unisense, Denmark). The function was checked against the defined redox buffers of 470 mV (pH 4 buffer) and 295 mV (pH 7 buffer) using a prepared quinhydrone redox buffer solution (MERCK, Darmstadt, Germany). The values were corrected for the hydrogen electrode potential (+239 mV, after Cammann and Galster, 1997). The pH was measured using a miniaturized conventional pH electrode (PH-10, Unisense, Denmark). The pH electrode was calibrated against commercially available buffers for pH 4.008, 6.86, and 9.18 (WTW GmbH & Co. KG, Weilheim, Germany). The pH and redox potential electrodes were connected via a high-impedance millivoltmeter to a separate reference electrode (REF-50), an open-ended Ag/AgCl electrode with a gel-stabilized electrolyte (Unisense, Denmark).

Potentiometric titration

The titration of *P. fluorescens* and U(VI)/Eu(III) was carried out as described in chapter 3.1.3 and in Moll et al. 2013a. The [dry biomass] and [U(VI)/Eu(III)] were set to 0.3 $g_{dry\ weight}$/L and $1 \cdot 10^{-4}$ M, respectively. As background electrolytes 0.1 M $NaClO_4$ for U(VI) and 0.1 M NaCl for Eu(III) were used. For the calculation of the stability constants of the U(VI)/Eu(III) surface complexes from the titration data the software HYPERQUAD was used.

Experimental setup of the applied spectroscopic techniques

The individual experimental setups for measuring the U(VI)/Cm(III) signal have been described in detail in section 4.1.

5.2 Results and discussion

5.2.1 Planktonic cells

5.2.1.1 Interaction with U(VI)

U(VI) biosorption studies

Regarding the biosorption efficiency, *P. fluorescens* cells display a strong affinity for U(VI) Figure 5.1. Up to 540 mg U/$g_{dry\ weight}$ can be bound at an $[U(VI)]_{initial}$ of 138 mg/L at pH 6.

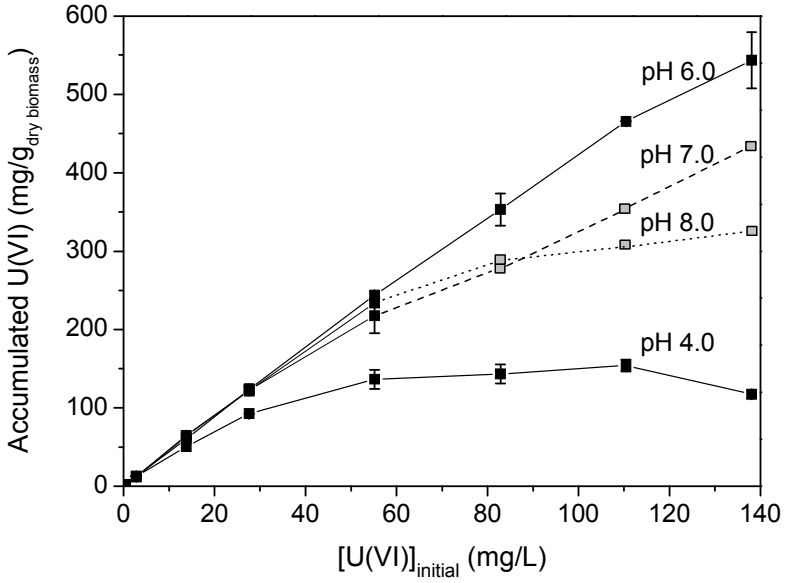

Fig. 5.1 U(VI) binding onto *P. fluorescens* (0.2 $g_{dry\ weight}$/L) in dependence on $[U]_{initial}$ at different pH values in 0.1 M $NaClO_4$. U(VI) interaction time = 48 h.

The high binding potential of this strain becomes even more evident when compared to the biosorption efficiencies reported for other microbial strains concerning U(VI) binding (Bengtsson et al. 1995, Vogel et al. 2011). At pH 6 at maximum sorption the cells bind 5 times as much U(VI) as at pH 4 at $[U(VI)]_{initial}$ of 138 mg/L. At pH 7 and 8 the experimental initial U(VI) concentration is limited to < 60 mg/L because of the precipitation of U(VI) hydroxides. Thus for these two pH values the data is represented as dashed lines. Nevertheless a general trend can be observed: upon increasing pH a maximum sorption can be found at pH 6, afterwards sorption decreases with pH continuously.

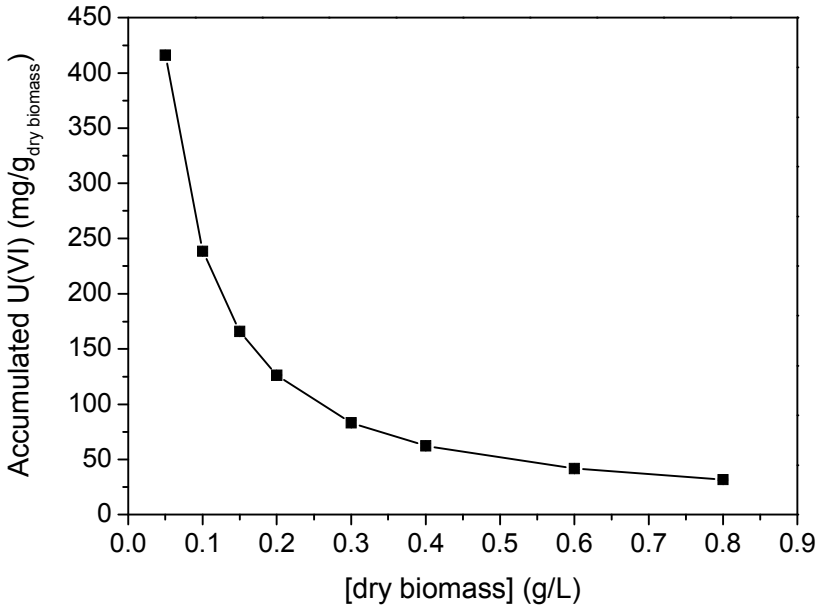

Fig. 5.2 U(VI) binding onto *P. fluorescens* (0.2 $g_{dry\ weight}$/L) in dependence on [dry biomass] at pH 6.0 in 0.1 M $NaClO_4$, $[UO_2^{2+}] = 1 \cdot 10^{-4}$ M.

Considering the initial U(VI) speciation prior to contact with the cells, towards pH 6 increasingly the $(UO_2)_2CO_3(OH)_3^-$ complex is formed having a maximum at approximately pH 6. The appearance of this complex coheres with the observed sorption maximum at pH 6. Hence it seems likely that the $(UO_2)_2CO_3(OH)_3^-$ complex has a high affinity to the bacterial surface. Also an increasing degree of deprotonation of the cell surface functional groups might contribute to a more efficient U(VI) binding with higher pH. At pH > 6 the $UO_2(CO_3)_3^{4-}$ complex increasingly forms which appears to have a lower affinity for the bacterial cell surface since the U(VI) surface load drops from pH 6 on. The other effect that needs to be regarded is the cellular release of inorganic phosphate into the supernatants which alters the U(VI) speciation. This effect has been analyzed with TRLFS.

A source of error of this measurement has been identified to be the adsorption of U(VI) to the reaction tube walls. The incubation of the reaction vessels with HNO_3 after sorption experiments revealed that a systematic loss of U(VI) in dependence on pH due to adsorption of U(VI) at the reaction tube walls occurs, which was pH-dependent and amounted to maximum 11%. This loss was accounted for in the calculation of the amount of U(VI) bound per g dry biomass.

Besides the varied parameters discussed previously, also the number of cells present in the host rock is unknown and thus must be considered as a varying parameter. Thus the effect of the amount of cellular matter given as [dry biomass] has also been studied as a factor influencing the U(VI) sorption efficiency. The results are presented in the following.

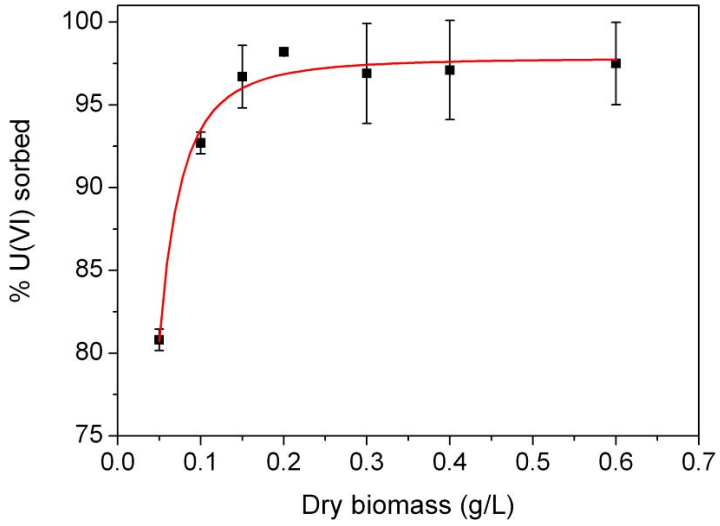

Fig. 5.3 Accumulation of U(VI) in (%) in dependence on the [dry biomass] in 0.1 M $NaClO_4$ at pH 6.

With increasing biomass concentration the relative biosorption efficiency decreases significantly (see Fig. 5.2). This phenomenon is common in literature. It is proposed that the decreased biosorption efficiency is due to increased agglomeration of cells resulting in a decreased availability of surface functional groups (Panak and Nitsche 2001, Chatterjee and Ray 2008, Gad et al. 2010). This explanation seems reasonable, because the dependency of the amount of accumulated U(VI) on the [dry biomass] would ideally reveal a linear relationship. Since this is not the case, the number of effective cellular coordination sites must have been lowered by any effect which most likely is a such agglomeration.

Furthermore it was found that if the sorption is expressed as % sorbed U(VI) in dependence on the dry biomass (Fig. 5.3) an asymptotic sorption curve is gained. The sorption levels off at

about 97 to 98% bound U(VI). Hence regardless of [dry biomass] a small percentage of U(VI) will remain in solution. Consequently, this is an indication for ligand release by *P. fluorescens* leading to UO_2^{2+} mobilization.

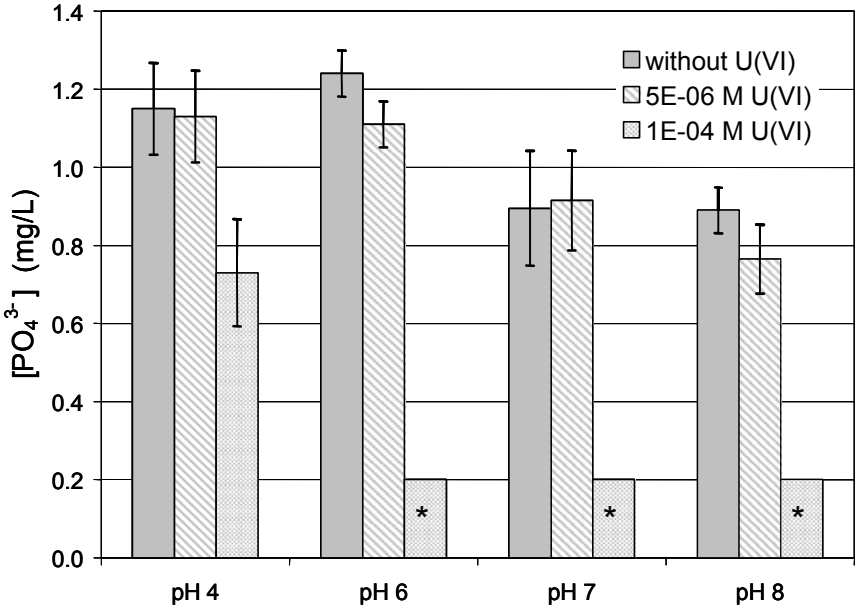

Fig. 5.4 Phosphate liberation in dependence on $[U]_{initial}$ at different pH values in 0.1 M $NaClO_4$. [dry biomass] = 0.2 g/L, U(VI) interaction time = 48 h. * Phosphate content below detection limit of the IEC of 0.2 mg/L.

Because of the indications for ligand release this cellular response was studied in detail. In specific the release of inorganic phosphate and its dependency on [U(VI)] was investigated and the results are discussed in the following. Figure 5.4 illustrates the dependency of the inorganic phosphate release by *P. fluorescens* cells on the initial U(VI) concentration and pH. It can be seen that phosphatase activity is maximum at pH 6. At an [U(VI)] of $5 \cdot 10^{-6}$ M inorganic phosphate liberation is barely altered in comparison to the samples without any U(VI) added. But at an increased [U(VI)] of $1 \cdot 10^{-4}$ M the phosphate liberation decreases drastically below the detection limit of the ion exchange chromatography of 0.2 mg/L for pH values above 4. As an explanation, either U(VI) inhibits phosphatase activity or the cells switch to the phosphorylation of other compounds (e.g. creation of organophosphates like ATP). The ion exchange chromatography could only detect the amount of inorganic phosphate released. The usage of inorganic phosphate for the synthesis of for instance ATP has been proposed to be a response to heavy metal stress (Seufferheld et al. 2008).

Released phosphate affects the U(VI) speciation in the cell supernatants. The release of inorganic phosphate into the cell supernatants should be observable with TRLFS, because U(VI) phosphate complexes give characteristic luminescence spectra.

The metabolic activity of the cells can affect the U(VI) binding efficiency and U(VI) speciation significantly. For instance the cells might respond to U(VI) by immobilizing it as a mineral phase or an enhanced ligand release can occur. Thus the effect of the $[U(VI)]_{initial}$ on the viability of the cells, measured by the active cell division, was also investigated.

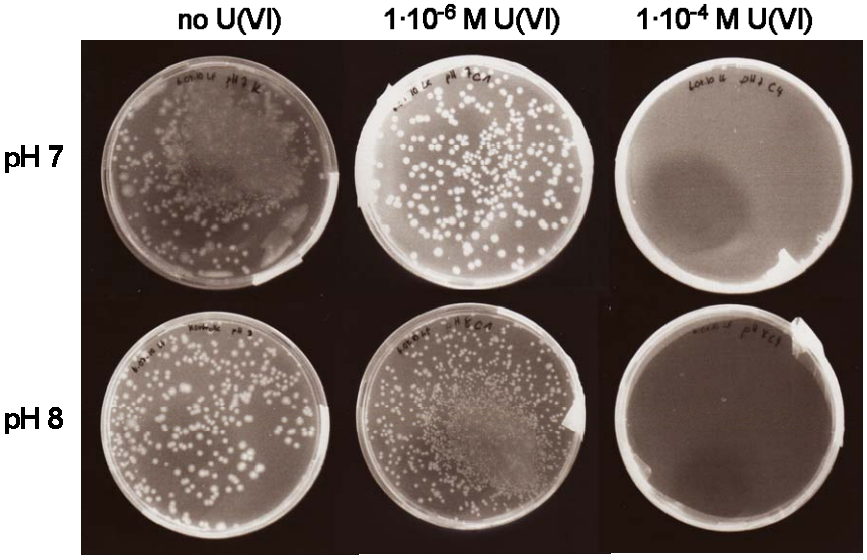

Fig. 5.5 Cell division in dependency on the $[U(VI)]_{initial}$ at pH 7 and 8 in 0.1 M $NaClO_4$ after incubation of plates for 5 days at 30°C.

P. fluorescens was exposed to two different $[U(VI)]_{initial}$: $1 \cdot 10^{-6}$ M and $1 \cdot 10^{-4}$ M. After U(VI) contact for 48 h and dilution the test suspensions were plated on NB agar to allow still vivid bacteria to form colonies. Figure 5.5 illustrates the impact of $[U(VI)]_{initial}$ on the cell division and thus cell viability. It can be seen that while at $[U(VI)]_{initial}$ of $1 \cdot 10^{-6}$ M the cell division is barely altered in comparison to cells without uranium contact, at $[U(VI)]_{initial}$ of $1 \cdot 10^{-4}$ M cell dividing seems to be completely inhibited, which indicates the complete suppression of cell division in potentiometry and TRFLS experiments.

Potentiometric Titration

Figure 5.6 illustrates the titration curve of U(VI) with *P. fluorescens* and the fit with HYPERQUAD using a three-site model. The fit included the pK_a values and site densities of the bacteria (Moll et al. 2013a). In addition the following hydrolytic uranyl species and their stability constants were included in the fit: $(UO_2)_2(OH)_2^{2+}$, $(UO_2)_3(OH)_5^{+}$, $(UO_2)_4(OH)_7^{+}$ (Guillaumont et al. 2003). The titration curve could be modeled with a very good fit result when the complexes R-COO-UO_2^{+}, R-O-PO_3H-UO_2^{+}, R-O-PO_3-UO_2, and (R-O-PO_3)$_2$-UO_2^{2-} were considered, as can be seen from the HYPERQUAD fit result (Fig. 5.6). The respective calculated stability constants are summarized and compared to literature data in Table 5.1.

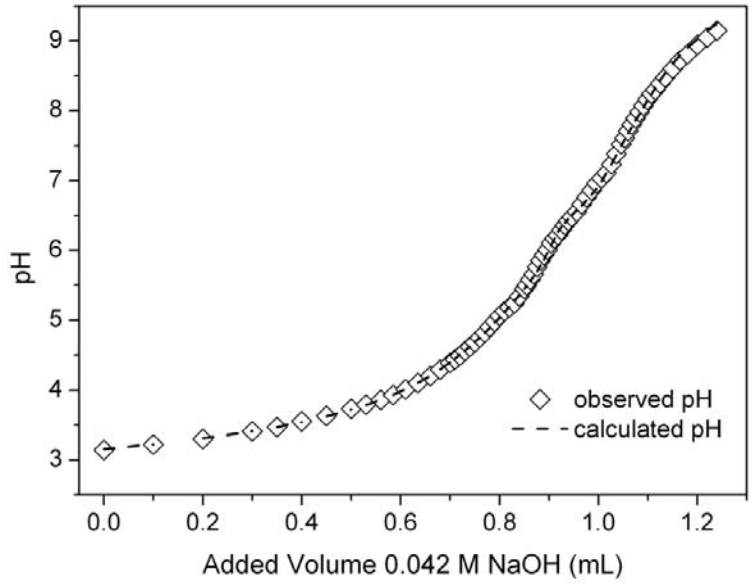

Fig. 5.6 Titration of $1 \cdot 10^{-4}$ M UO_2^{2+} and 0.3 $g_{dry\ weight}$/L cells in 0.1 M $NaClO_4$ with 0.042 M NaOH and fit with HYPERQUAD.

As it can be seen from Table 5.1 a moderate to strong interaction of U(VI) with the surface functional groups of *P. fluorescens* can be found. The affinity of uranyl to phosphoryl groups is much higher than that to carboxylic sites. Since lipopolysaccharide (LPS) is a major and the very outer part of the cell wall of Gram-negative bacteria, the determined complex stability constants have been compared to UO_2^{2+} interacting with LPS (Barkleit et al. 2008). Besides LPS, the results on UO_2^{2+} interacting with peptidoglycan (PG) (Barkleit et al. 2009) are also listed for comparison. PG is the second outer cell wall polymer and hence can not be excluded to interact with U(VI). Further the results are compared to those on *Sporomusa* sp. gained within this work. Again also the results are shown in comparison to U(VI) bound to the surface functional groups of *B. subtilis* (Fowle et al. 2000). A good agreement can be found in comparison to the results on LPS gained by (Barkleit et al. 2008) in terms of the stability constants of U(VI) bound by deprotonated and H-phosphoryl groups. Thus a coordination of U(VI) with *P. fluorescens* with phoshoryl groups of the LPS part of the bacterial membrane is likely. Comparing the results on *P. fluorescens* to those on *Sporomusa* sp. quite some deviation exists especially in view of the determined constants of the 1:1:0-complexes. This makes clear that the stability of U(VI) complexes formed at bacterial cell surfaces can not be generalized based on the Gram behaviour. Some discrepancy to the literature is observed in case of the interaction with carboxylic groups, especially in comparison to the results published by Fowle et al. on the Gram-positive strain *B. subtilis* (Fowle et al. 2000).

Table 5.1 Calculated stability constants of UO_2^{2+} complexes with *P. fluorescens* surface functional groups and comparison to literature.

Species	Complex	xyz [a]	log β_{xyz} (± SD)	Method	Reference
P. fluorescens	R-COO-UO_2^+	110	6.66 ± 0.05	PT	this work,
	R-O-PO_3-UO_2	110	7.54 ± 0.18		published in
	R-O-PO_3H-UO_2^+	111	12.73 ± 0.06		(Lütke et al. 2012)
	$(R\text{-}O\text{-}PO_3)_2$-$UO_2^{2-}$	120	12.97 ± 0.07		
Sporomusa sp.	R-COO-UO_2^+	110	4.75 ± 0.98	PT	This work
	R-O-PO_3-UO_2	110	8.58 ± 0.04		
	R-O-PO_3H-UO_2^+	111	13.07 ± 0.06		
	$(R\text{-}O\text{-}PO_3)_2$-$UO_2^{2-}$	120	13.30 ± 0.09		
Peptidoglycan	R-COO-UO_2^+	110	7.28 ± 0.03 //	PT //	(Barkleit et al. 2009)
			6.90 ± 0.20	TRLFS	
Lipopoly-	R-COO-UO_2^+	110	5.93 ± 0.17	PT	(Barkleit et al. 2008)
saccharide	R-O-PO_3-UO_2	110	7.50 ± 0.30 //	PT //	
			7.53 ± 0.25	TRLFS	
	R-O-PO_3H-UO_2^+	111	11.66 ± 0.30 //	PT //	
			12.01 ± 0.10	TRLFS	
	$(R\text{-}O\text{-}PO_3)_2$-$UO_2^{2-}$	120	13.80 ± 0.37	TRLFS	
B. subtilis	R-COO-UO_2^+	110	5.4 ± 0.2	Adsorption	(Fowle et al. 2000)
	R-O-PO_3H-UO_2^+	111	11.8 ± 0.2	experiment	

[a] metal / ligand / H^+.

Generally the gained result on the carboxylic interaction with U(VI) is closer to the values published by Barkleit et al. (Barkleit et al. 2008, 2009), which were in case of peptidoglycan specially attributed to the interaction of U(VI) with diaminopimelic acid groups.

Impact of P. fluorescens on the U(VI) speciation

Again two different sets of conditions were used for the HySS speciation calculation. On the one hand, a U(VI) species distribution was calculated according to the TRLFS conditions in order to interpret the results gained with this technique (a). On the other hand, to predict the U(VI) speciation in the field of a nuclear waste repository, repository or environmentally relevant U(VI) concentrations were used as input parameters (b). Furthermore the relevant U(VI) hydrolytic species and their stability constants were included in the calculation. In

specific, these were the hydroxyl complexes which could be included in the fit of the titration data: $(UO_2)_2(OH)_2^{2+}$, $(UO_2)_3(OH)_5^{+}$, and $(UO_2)_4(OH)_7^{+}$ (Guillaumont et al. 2003).

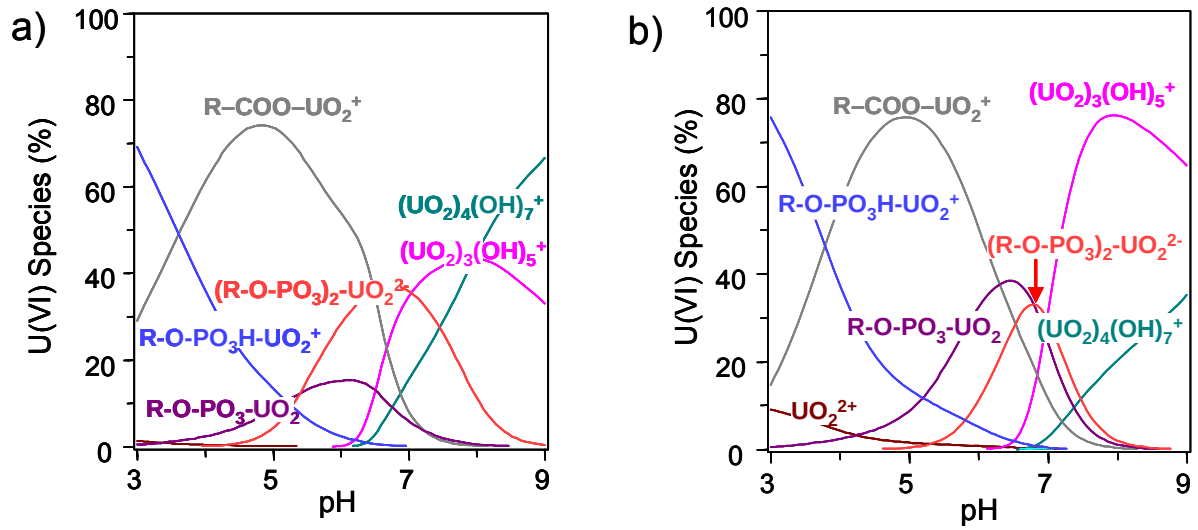

Fig. 5.7 U(VI) species distributions in presence of *P. fluorescens* cells in dependence on pH calculated using HySS 2009 at **a)** TRLFS conditions: [U(VI)] = $1 \cdot 10^{-4}$ M, [dry biomass] = 0.2 g/L, and **b)** environmentally relevant concentrations: [U(VI)] = $1 \cdot 10^{-6}$ M, [dry biomass] = 0.02 g/L. CO_2-free system.

At TRLFS conditions (Fig. 5.7 a) the U(VI) species distribution in presence of *P. fluorescens* reveals that in the acidic pH range below pH 3.5 U(VI) binds to the cell surface mainly via protonated phosphoryl groups. The results gained by (Fowle et al. 2000) on the interaction of U(VI) with *B. subtilis* have demonstrated that the best fit for uranium binding at low pH is the one including adsorption onto protonated phosphoryl sites, thus supports the calculated U(VI) speciation in presence of *P. fluorescens*. From the calculated speciation it can also be seen that U(VI) binding by carboxylic sites plays a dominant role over a wide pH range up to around pH 7. At pH 7 fully deprotonated phosphoryl groups are mainly responsible for U(VI) binding. If the pH is increased further uranyl hydroxides dominate the U(VI) speciation in aqueous solution (in a CO_2-free system). The U(VI) interactions with bacterial surface functionalities suppressed and hence shifted the U(VI) hydrolysis towards higher pH (approximately by two pH units). Calculating a U(VI) species distibution at environmentally relevant concentrations ([U(VI)] = $1 \cdot 10^{-6}$ M, [dry biomass] = 0.02 g/L) almost the same species distribution is gained as that shown in Figure 5.7 a. The only remarkable difference is that at these conditions the R-O-PO_3-UO_2 complex is present in greater amounts. At pH 6.5 15 % more R-O-PO_3-UO_2 complex is present at $1 \cdot 10^{-6}$ M UO_2^{2+} mainly lowering the amount of present carboxyl bound U(VI) accordingly.

In view of an overall comprehesive understanding of the process of U(VI) interaction with the cells affecting the U(VI) speciation, besides the binding of U(VI) to the cell surface functional

groups also the release of phosphate needs to be regarded. Both processes are concurrent to each other and affect the U(VI) sorption efficiency. Based on the results gained with potentiometry and the phosphate analysis in the cell supernatants the following conceptual model is proposed: at the beginning before U(VI) contact with the cells U(VI) is mainly present e.g. at pH 6 as $(UO_2)_2CO_3(OH)_3^-$ or as $(UO_2)_3(OH)_5^+$ at aerobic and anaerobic conditions, respectively. In presence of the cells these complexes readily sorb onto the cell envelope of *P. fluorescens* cells forming the surface complexes R-O-PO_3H-UO_2^+, R-O-PO_3-UO_2, (R-O-PO_3)$_2$-UO_2^{2-} and R-COO-UO_2^+. In the time frame of 2 h no significant amount of phosphate is released by the cells. Within 48 h after U(VI) contact the cells have released significant amounts of phosphate which competes with the cell surface functional groups for U(VI). Increasingly soluable U(VI) phosphoryl species (e.g. $UO_2PO_4^-$ at pH 6) are formed alongside with U(VI) sorbed to the surface functional groups forming the stated complexes.
To validate the U(VI) complexes found with potentiometry, again the direct speciation technique TRLFS was used. The results are presented in the following.

TRLFS

Investigating the interaction of the Äspö isolate *P. fluorescens* with U(VI) by TRLFS the following differentiation was made: on the one hand the U(VI) interaction with metabolically rather inactive cells in $NaClO_4$ solution was studied. On the other hand *P. fluorescens* was contacted with U(VI) in SSM as a minimal medium to allow metabolic activity of the cells. Microorganisms have adapted strategies to endure high concentrations of heavy metals through active microbial processes like for instance biomineralization. Thus the interaction of U(VI) with metabolically active cells was also assessed.

a) Metabolically inactive *P. fluorescens* cells

From both, the cells and the corresponding cell supernatants, U(VI) luminescence spectra were collected. Spectra of the U(VI)-loaded cells at different pHs were compared among each other Figure 5.8 a). The same was done for the spectra of the cell supernatants Figure 5.8 b). While the band positions of the static spectra give insights into possible U(VI) surface species formed, the time-resolved measurements give indications of the number of present luminescent species. According to Figure 5.8 a obviously at pH 4 and 6 U(VI) must have a similar coordination environment at the cell surface because of the similar band positions. For the same reason this is true for pH 7 and 8. Nevertheless, the difference between these two pH pairs reveals a strong pH dependency of the U(VI) speciation at the cell surface, which has

already been shown with potentiometric titration.

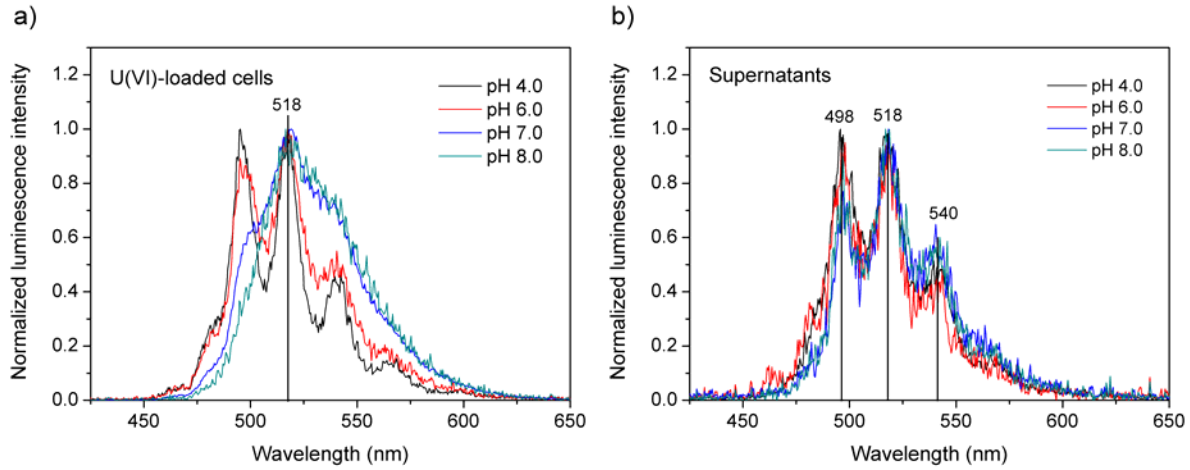

Fig. 5.8 Luminescence spectra of U(VI)-loaded cells (a) and U(VI) in the cell supernatants (b) at different pHs in 0.1 M $NaClO_4$ after 48 h U(VI) contact.

With increasing pH here a slight red shift of the luminescence spectra occurs. This red shift can be the basis of further spectral interpretations, as will be explained in the following. If the luminescence spectra of U(VI) in the cell supernatants are compared (Fig. 5.8 b) it becomes obvious that the positions of the emission maxima at different pH values are quite similar. Thus a similar coordination of U(VI) in the supernatants can be expected. This signifies already that some cellular ligand must have been released which coordinates strongly to U(VI), otherwise the spectra would show a strong pH dependency due to the increasing formation of U(VI) hydroxides with higher pH. The comparison of the luminescence maxima of the samples (498, 518 and 540 nm) coincide with those given for soluble inorganic U(VI) phosphate complexes (Panak et al. 2000), see Table 5.2. Since inorganic phosphate release has already been proven by means of ion exchange chromatography, it seems probable that U(VI) is bound by inorganic phosphate groups in the supernatants after 48 h U(VI) contact. Noticeable is also that the luminescence spectra of the U(VI)-loaded cells at pH 4 and 6 are similar to those of all measured supernatants in terms of the band positions. Thus representative spectra, in specific one spectrum of the 6 mentioned similar ones (U(VI)-loaded cells at pH 4) and the spectrum of the U(VI)-loaded cells at pH 7, have been compared to those of bacteria-free U(VI) solutions for further evaluation (Fig. 5.9). In general, it was found that the spectra of the U(VI)-loaded cells show a significant red shift compared to the respective reference samples which is an indication for complex formation with the cell surface and also proving that no pure U(VI) hydroxide is present. The presence of U(VI) hydroxide can also be excluded because of the short luminescence lifetimes found for U(VI)

attached to the cells of 0.46 µs in average and 1.48/1.69 µs (Table 5.2).

Table 5.2 Position of luminescence emission maxima and luminescence lifetimes in comparison to literature data.

Species/ complex	Emission maxima (nm)				Lifetimes (µs)	Reference
UO_2^{2+} (100%), pH 1	488.9	510.5	533.9	559.4	1.8 ± 0.2	(Geipel et al. 2000)
U(VI), pH 4:	488.0	509.1	532.2	557.0	1.3 ± 0.1,	This work
UO_2^{2+}, $(UO_2)_2(OH)_2^{2+}$ [a]					8.0 ± 0.7	
U(VI), pH 6:	-	513.1	-	-	7.8 ± 0.1,	
$(UO_2)_4(OH)_7^+$, $(UO_2)_3(OH)_5^+$ [a]					24.1 ± 3.8	
U(VI), pH 7:	-	512.8	-	-	7.4 ± 0.3,	
$(UO_2)_4(OH)_7^+$, $(UO_2)_3(OH)_5^+$ [a]					23.5 ± 0.9	
U(VI), pH 8:	-	512.7	-	-	7.5 ± 0.2,	
$(UO_2)_4(OH)_7^+$, $(UO_2)_3(OH)_5^+$ [a]					24.9 ± 0.9	
Inorganic phosphate						(Panak et al. 2000)
$UO_2(HPO_4)_{aq}$	497	519	543	570	-	
$UO_2PO_4^-$	499	520	544	571	-	
$UO_2(H_2PO_4)^+$/ $UO_2(HPO_4)$	494	517	541	565	-	
Malonate						(Panak et al. 2000)
$UO_2[CH_3(CO_2)_2]$	494	515	540	564	1.24 ± 0.02	
$UO_2[CH_3(CO_2)_2]_2^{2-}$	494	517	542	566	6.48 ± 0.02	
Peptidoglycan						(Barkleit et al. 2009)
R-COO-UO_2^+	498	518	539	566	0.7 ± 0.1	
Adenosine triphosphate						(Knopp et al. 2003)
UO_2-ATP	495	517	540	566	-	
Fructose-6-phosphate						(Koban et al. 2004)
UO_2-F6P	497.1	519.0	543.3	568.9	0.13 ± 0.05	
Lipopolysaccharide						(Barkleit et al. 2008)
R-O-PO_3H-UO_2^+	497.2	518.9	542.4	567.3	8.3 ± 0.6	
R-O-PO_3-UO_2	498.1	519.6	542.9	567.5	1.2 ± 0.4	
$(R\text{-}O\text{-}PO_3)_2$-$UO_2^{2-}$	499.7	521.0	544.3	568.9	13.3 ± 1.4	
P. fluorescens						This work
all supernatants [b]	497.5	517.9	539.6	-	0.52 ± 0.06,	(Lütke et al. 2012)
					3.6 to 8.9	
Cell-bound U(VI), pH 4 and 6 [b]	497.0	517.9	539.7	-	0.44 ± 0.02,	
					1.48 ± 0.10	
Cell-bound U(VI), pH 7 and 8 [b]	-	519.1	-	-	0.47 ± 0.04,	
					1.69 ± 0.01	

[a] Assigned species according to determined lifetimes. [b] Average luminescence emission maxima are given.

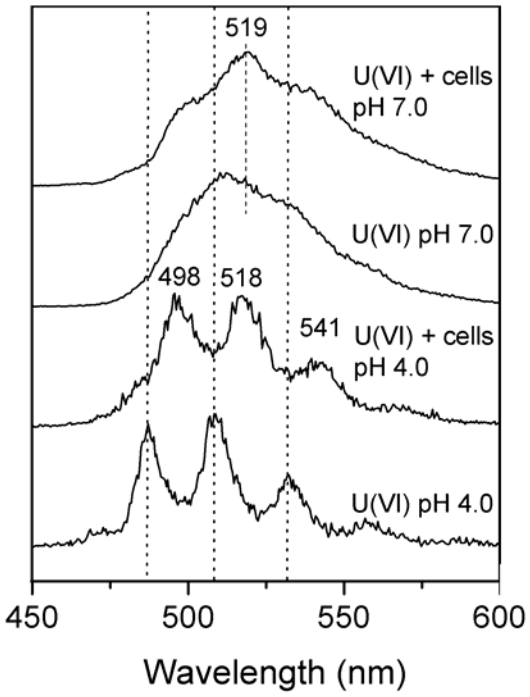

Fig. 5.9 Comparison of representative spectra of U(VI) bound by *P. fluorescens* in 0.1 M $NaClO_4$ with cell-free U(VI) solutions.

From the luminescence band positions and the comparison to the literature it can be concluded that mainly carboxylic and phosphoryl sites are involved in U(VI) coordination at the cell surface, which supports the results from potentiometric titration. By trend, the slight red shift of 1.2 nm observed in the TRLFS spectra upon a pH increase from 4 to 7 goes well with the calculated U(VI) speciation in dependence on the pH. The same trend is observable in the TRLFS data from Barkleit et al., where the luminescence band positions shifted slightly towards higher wavelength, when going from carboxyl- and H-phosphoryl-coordinated U(VI) to U(VI) complexed by deprotonated phosphoryl sites (Barkleit et al. 2008). Thus the observed spectral shift upon increasing pH might be most likely due to the occurrence of the stated complexes.

From the determined luminescence lifetimes, 0.46 µs in average and 1.48/1.69 µs, it can be concluded that two luminescent species are present at all investigated pH values. The determined lifetimes are too short to be attributable to uranyl hydroxides, which have already been excluded based on the luminescence band positions. According to the calculated U(VI) species distribution (Fig. 5.7 a) U(VI) should be coordinated simultaneously by both carboxyl and phosphoryl sites at the relevant TRLFS concentrations. Nevertheless most of the U(VI) carboxyl complexes show no luminescence at room temperature. A few exceptions exist, which caused a smaller bathochromic shift than those observable in the presented data

(Brachmann et al. 2002, Moll et al. 2003, Günther et al. 2006). Thus presumably only the phosphoryl complexes were detected using TRLFS. Because of the occurrence of the short luminescence lifetime of 0.46 µs over the whole investigated pH region, this lifetime is most likely attributable to the R-O-PO_3-UO_2 complex. Such short luminescence lifetimes have also been reported for UO_2^{2+} coordinated by fructose-6-phosphate (Koban et al. 2004) and O-phospho-*L*-threonine (Günther et al. 2006). The second longer lifetime of 1.48 µs observed at pH 4 and 6 then as a consequence is assigned to R-O-PO_3H-UO_2^+. Thus an increase in lifetime upon phosphoryl protonation is observable. The increase of the lifetime upon phosphoryl site protonation has been suggested previously (Günther et al. 2006, Barkleit et al. 2008).

Providing nutrients and thus enhancing cellular metabolism, besides biosorption and ligand release other U(VI) interaction mechanisms might be observable. The impact of metabolically active cells on the U(VI) speciation was assessed with TRLFS in the following chapter.

b) Metabolically active *P. fluorescens* cells

The interaction of U(VI) with metabolically active *P. fluorescens* cells (interaction in 0.5%-phosphate-SSM) displays a completely different interaction scheme as it was the case for metabolically inactive cells.

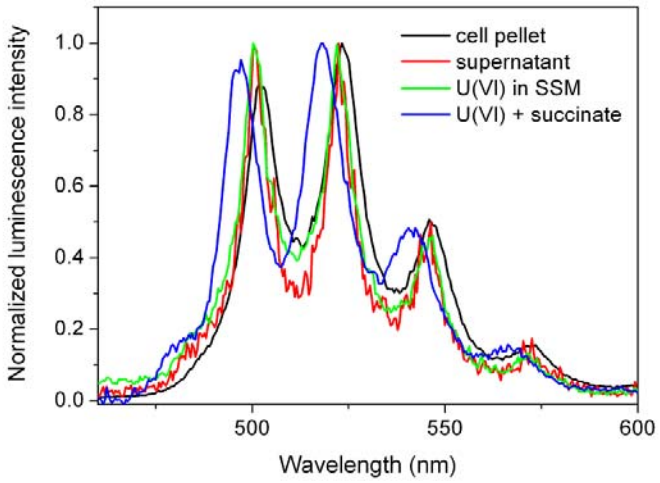

Fig. 5.10 Luminescence spectra of U(VI) at the cell surface of *P. fluorescens* and in the corresponding supernatant after U(VI) contact in 0.5%-phosphate-SSM compared to U(VI) coordinated by the media components and by succinate only. $[U(VI)]_{initial} = 1 \cdot 10^{-4}$ M, [dry biomass] = 0.2 g/L, [$NaClO_4$] = 0.1 M, pH 7.

In Figure 5.10 the luminescence spectra of U(VI) at the *P. fluorescens* cell surface after interaction in the medium are presented. The corresponding supernatant is given in red. For

comparison the spectra of U(VI) in the minimal medium and of U(VI) coordinated to succinate as the major component of the medium are additionally presented. All corresponding emission maxima and lifetimes are summarized in Table 5.3. The spectrum of U(VI) coordinated to the cell surface of *P. fluorescens* reveals a remarkable red shift compared to the spectral emission maxima of uranyl hydroxides and also does not coincide with any of the spectra of U(VI) coordinated to inactive cells because of the greater red shift. From comparison to the literature, in specific U(VI) mineral phases as for instance meta-autunite (Wang et al. 2008), the formation of a meta autunite- or (sodium) uranyl phosphate-like phase is suggested. Thus, if nutrients are available for metabolic activity, obviously the cellular response to U(VI) changes completely from biosorption to biomineralization. To evaluate this further, EXAFS spectroscopy was applied.

Table 5.3 Emission maxima of spectra shown in Figure 5.10 in comparison to selected U(VI) mineral phases stated in the literature.

Sample/ Species	**Emission Maxima (nm)**				**Lifetimes [µs]**	**Reference**
meta-autunite	501.1	522.1	546.8	572.7	66.7 ± 8.0	(Wang et al. 2008)
syn. U(VI) phosphate	498.1	520.2	544.8	571.9	14.5	
syn. Na U(VI) phosphate	501.1	523.0	546.8	573.5	141.7	
U(VI) succinate	497.0	518.0	541.3	567.1	-	This work
U(VI) SSM	500.7	522.4	545.5	571.7	-	
Supernatant	500.7	522.8	545.5	571.7	1.17 ± 0.01	
cell pellet	502.0	523.3	546.3	572.5	0.63 ± 0.01	
					3.59 ± 0.04	

EXAFS

A particular aim was to assess how cell viability of *P. fluorescens* is affecting the U(VI) speciation, to verify the TRLFS results on that matter. So far, TRLFS had indicated that metabolically inactive cells accumulate U(VI) primarily through biosorption, whereas metabolically active cells precipitate U(VI) as a meta-autunite-like mineral phase. Three different conditional cases were distinguished: U(VI) interaction in 1) SSM without any phosphate added, 2) the same supplemented with phosphate (0.5%) (both cases to allow

metabolic activity), and 3) 0.1 M $NaClO_4$ (suppression of metabolic activity). For case 2) [PO_4^{3-}] was chosen so that no prior U(VI) phosphate precipitation occurs.

EXAFS sample preparation already revealed a pronounced ability of metabolically active *P. fluorescens* cells to remediate U(VI) from solution with the aid of phosphate in contrast to a lack of phosphate as illustrated in Figure 5.11.

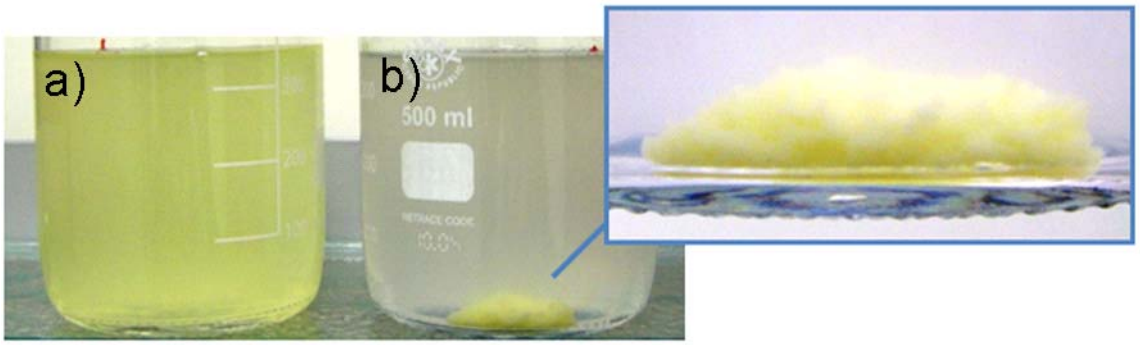

Fig. 5.11 Induced formation of immobile U(VI)-cell agglomerate in case of U(VI) interaction with *P. fluorescens* in SSM supplemented with phosphate **(b)** in contrast to interaction in SSM without any phosphate added **(a)**. [U(VI)] = 0.2 mM, [dry biomass] = 0.2 g/L, pH 7.0.

An immobile U(VI)-cell agglomerate is formed by the aid of phosphate. Evidently, the U(VI) separation efficiency is greatly enhanced in the case of interaction in SSM supplemented with phosphate. ICP-MS measurements showed that 99 % uranium was removed from solution and fixed in the formed cell agglomerate (Fig. 5.11 b). This stable U(VI)-cell agglomerate formed under conditions of stirring (110 rpm). Hence, this procedure is of technical interest for treating U(VI)-contaminated waste effluents. On the identified mechanism a patent application was filed.

XANES analysis showed for all samples that the oxidation state of UO_2^{2+} was not altered by the interaction with the biomasses of both strains (data not shown). In the following the k^3-weighted $\chi(k)$ spectra and corresponding Fourier transformations (FTs) of the different examined cases for *P. fluorescens* are presented (Fig. 5.12). The corresponding structural parameters of the best fits obtained are summarized in Table 5.4.

The EXAFS oscillations and corresponding Fourier transforms of the samples B) to D) display similar features. The radial distance to the axial oxygen atoms increases comparing the free UO_2^{2+} and UO_2^{2+} bound to the biomass by at least 0.02 Å indicating the complexation of U(VI). The radial distance to O_{ax} is slightly higher at pH 7 compared to that at pH 4 pointing towards an increased complexation of the uranyl ion by electron donors with increasing pH.

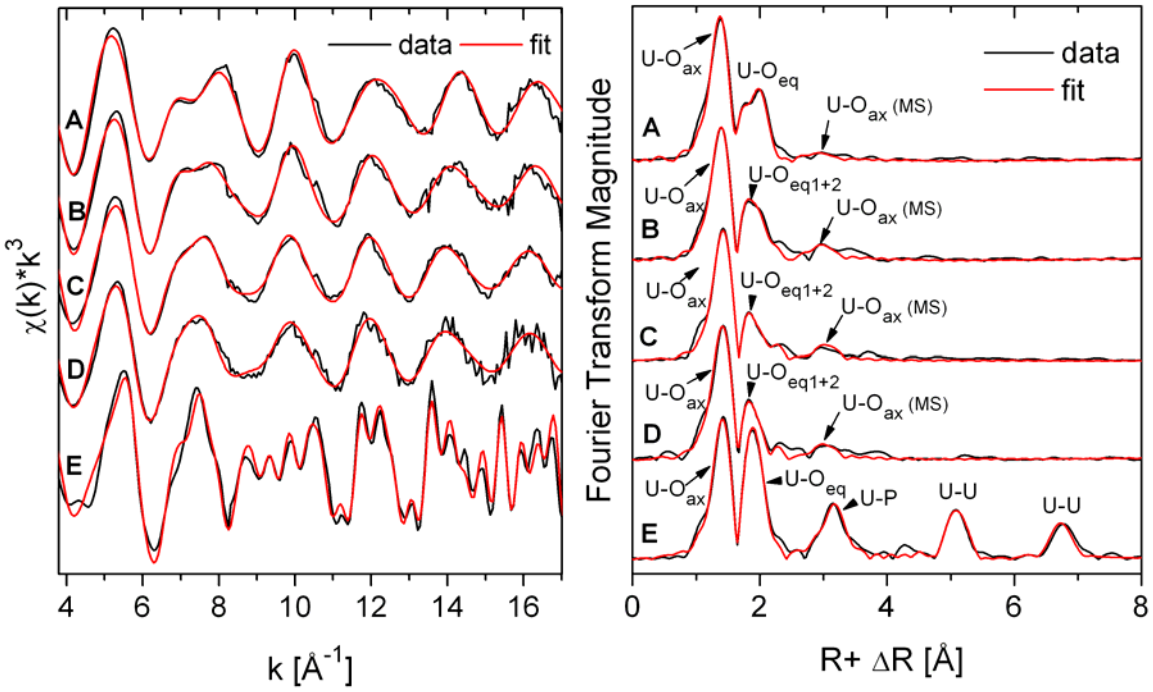

Fig. 5.12 Uranium L_{III}-edge k^3-weighted EXAFS spectra (left) and the corresponding Fourier transformations (right) of the U(VI) complexes formed with *P. fluorescens* in 0.1 M $NaClO_4$ at pH 4 and 7 (B and C, respectively) and in SSM at pH 7 without any phosphate added (D) and supplemented with phosphate (E) compared to the free uranyl ion at pH 2 (A). $[U(VI)]_{initial}$ = 0.1 - 0.2 mM, [dry biomass]$_{initial}$ = 0.2 g/L. Black = experimental data, red = fit.

For the samples B) to D) a split equatorial oxygen shell was found pointing towards simultaneous carboxyl and phosphoryl interaction. U-O_{eq} bond lengths of 2.34-2.37 Å and 2.52-2.54 Å were calculated. The short U–O_{eq1} bond distance suggests a monodentate coordination of the uranyl ion by organic phosphate groups (Hennig et al. 2001, Koban et al. 2004), while the longer bond distance indicates coordination by carboxylate groups (Denecke et al. 1998, Moll et al. 2003). Overall these findings suggest biosorption of U(VI) to the bacterial cell wall functional groups. No indications for biomineralization were found in the spectra. This changes completely when examining the U(VI) interaction with *P. fluorescens* in SSM supplemented with phosphate (E). As can be seen from the small χ^2 value of 77 of the fit a meta-autunite-like structure represents quite a good model for the U(VI) complexes formed in contact with *P. fluorescens* in SSM with phosphate. Four equidistant equatorial O-atoms (R = 2.29 Å) as well as U-P and U-U radial distances point strongly towards the formation of meta-autunite, $Ca(UO_2)_2(PO_4)_2 \cdot 6\ H_2O$ (Makarov and Ivanov 1960).

Table 5.4 EXAFS results on U(VI) interaction with *P. fluorescens*. Coordination numbers N, bond distances R, and Debye-Waller factors σ^2 are given. For comparison the structural parameters of the free uranyl ion are listed.

Sample composition	**Path**	**N** [a]	**R (Å)** [b]	**σ^2 (Å^2)** [c]	**ΔE_0 (eV)**	**Comments**
A)	U-O_{ax}	2[d]	1.76	0.0013	15.0	T = 298 K
0.05 M U(VI), pH 2	U-O_{eq}	5.2	2.41	0.0068		reduced χ^2 = 161
B)	U-O_{ax}	2[d]	1.78	0.0018	15.6	T = 15 K
P. fluorescens + 0.1 mM	U-O_{eq1}	5.0	2.37	0.0077		reduced χ^2 = 90
U(VI), pH 4	U-O_{eq2}	0.7	2.52	0.0010		
C)	U-O_{ax}	2[d]	1.80	0.0018	17.9	T = 15 K
P. fluorescens + 0.1 mM	U-O_{eq1}	4.6	2.36	0.0094		reduced χ^2 = 2249
U(VI) , pH 7	U-O_{eq2}	1.0	2.53	0.0028		
D)	U-O_{ax}	2[d]	1.79	0.0018	14.9	T = 15 K
P. fluorescens	U-O_{eq1}	5.5	2.34	0.0097		reduced χ^2 = 239
+ 0.2 mM U(VI),	U-O_{eq2}	0.5	2.54	0.0010		
0%-phosphate-SSM, pH 7						
E)	U-O_{ax}	2[d]	1.79	0.0016	13.0	T = 15 K
P. fluorescens	U-O_{eq}	4[d]	2.29	0.0018		reduced χ^2 = 77
+ 0.2 mM U(VI),	U-P	4[d]	3.63	0.0049		
0.5%-phosphate-SSM,	U-U	4[d]	5.24	0.0032		
pH 7	U-U	4[d]	6.88	0.0016		

a) errors in coordination numbers are ± 25%; *b)* errors in bond distances are ± 0.02 Å; *c)* Debye-Waller factor; *d)* parameter was fixed during fit

Exceptional is the high order of the bacteria-mediated structure formed. It exceeds even what has been reported for EXAFS studies on pure meta-autunite minerals so far. Using light microscopy a high cell density was found in this EXAFS sample. TRLFS also had shown that a meta-autunite-like structure most likely is present. Overall this suggests that in dependence on the metabolic activity of the cells and the availability of phosphate a highly crystalline meta-autunite based structure is formed. For *P. fluorescens* is could be shown that not only the metabolic activity of the cells is responsible for biomineralization, since for sample D, where the cells were incubated with U(VI) in SSM without phosphate no meta-autunite was observed. In the past it was shown that microorganisms are capable of using also organic phosphoryl compounds, e.g. glycerol 3-phosphate (Beazley et al. 2007), to generate meta-

autunite. Also some strains are able to form meta-autunite although no additional phosphate source is available (Reitz 2011). The here investigated strain required inorganic phosphate but formed an exceptionally highly ordered meta-autunite-like phase.

5.2.1.2 Interaction with Cm(III)/Eu(III)

The P. fluorescens Cm(III) system: TRLFS

A strong decrease in the emission band of the free Cm^{3+} at 593.7 nm could be detected already at pH 1.43 and a biomass concentration of 0.2 $g_{dry\ weight}$/L. A new red-shifted emission band at 599.6 nm occurred simultaneously showing the influence of a first Cm^{3+}– *P. fluorescens* species (Fig. 5.13 A). This observation demonstrates that *P. fluorescens* interacts with curium(III) from acidic solutions. This is in agreement with earlier results based on large log K_d values for curium(III) observed at pH 3 and 4 by Ozaki et al. 2004.

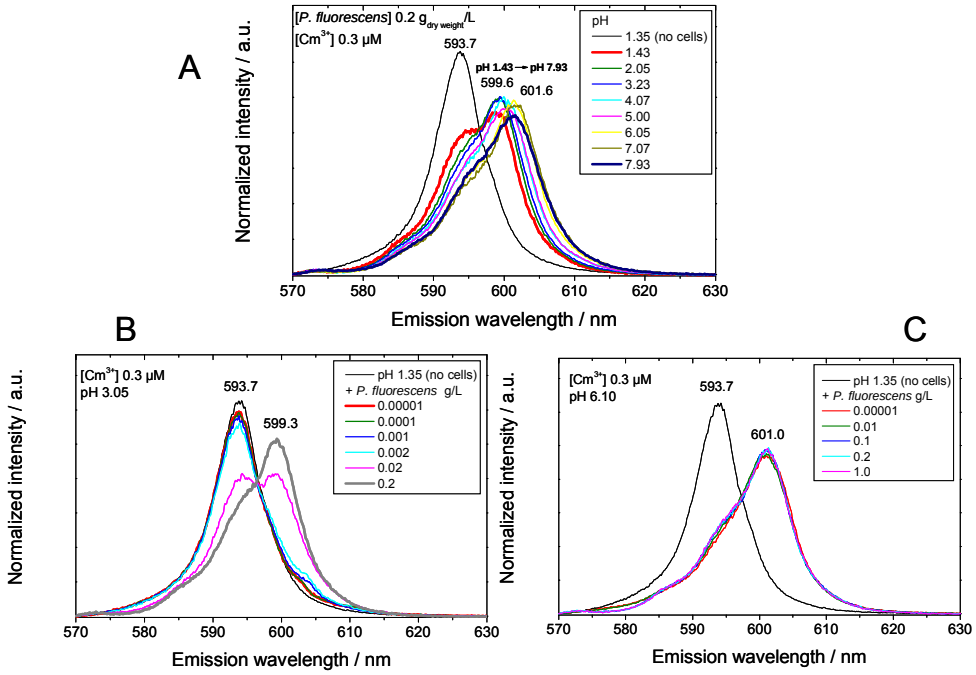

Fig. 5.13 Luminescence emission spectra of 0.3 µM curium(III) in 0.1 M $NaClO_4$ measured: A) as a function of pH at a fixed biomass concentration of 0.2 $g_{dry\ weight}$/L; B) and C) as a function of the biomass concentration at pH 3.05 and 6.10. The spectra are scaled to the same peak area.

The dependencies found in the TRLFS spectra (Fig. 5.13 A) suggested the occurrence of two individual Cm^{3+}– *P. fluorescens* species between pH 1.4 and 8 having emission maxima at ca. 599.6 (*Cm^{3+} – P. fluorescens species 1*), and 601.6 nm (*Cm^{3+} – P. fluorescens species 2*). Figure 5.13 B presents the changes observed in the emission spectra at pH 3.05 and 0.3 µM

curium(III) as a function of the biomass concentration. The presence of the emission band at 599.3 nm at biomass concentrations greater than 2 $mg_{dry\ weight}/L$ indicates the formation of *Cm^{3+} – P. fluorescens species 1*. By contrast, all curium(III) already exists as *Cm^{3+} – P. fluorescens species 2* at a very low biomass concentration of 0.01 $mg_{dry\ weight}/L$ at pH 6.1 indicated by the emission maximum at 601 nm (Fig. 5.13 C). The pH-dependent change of the emission data of the Cm^{3+}– *P. fluorescens* system implies the involvement of two functional groups located at the cell envelope structure.

Table 5.5 Spectroscopic properties of the identified curium(III) species.

	Cm^{3+} (aq)	**R–O–PO_3H–Cm^{2+}** [a]	**R–COO–Cm^{2+}** [b]
Excitation		353.3 (12.0)	353.7 (10.1)
(nm)	374.4 (3.3)[c]	375.3 (5.4)	376.0 (6.2)
	380.1 (2.9)	381.8 (6.2)	382.4 (5.6)
	395.7 (2.4)	397.8 (3.5)	398.3 (3.7)
Emission	**593.7 (8.2)** [d]	587.2 [d]	586.6 [d]
(nm)		594.2 [d]	595.0 [d]
		599.6 (7.0)	**601.9** (8.0)
Lifetime	67 ± 2	125 ± 3	111 ± 4
(µs)		364 ± 88	421 ± 15

[a] In 0.2 $g_{dry\ weight}/L$ *P. fluorescens* at pH 3.04 (85% R–O–PO_3H–Cm^{2+} = Cm^{3+}–*P. fluorescens* species 1).
[b] In 0.2 $g_{dry\ weight}/L$ *P. fluorescens* at pH 6.02 (80% R–COO–Cm^{2+} = Cm^{3+}–*P. fluorescens* species 2).
[c] Values in parentheses are full width at half- maximum.
[d] Shoulder.

TRLFS of the supernatants and the curium(III) loaded biomass after washing with 0.1 M $NaClO_4$ (0.2 $g_{dry\ weight}/L$) showed that only ≤ 10% of the total curium(III) luminescence intensity remained in solution independent of pH. Hence ≥ 90 % of the curium(III) was always associated with the biomass. To obtain information on the reversibility and the binding strength of bacterial Cm(III) surface complexes, we extracted the cell-bound curium(III) with 0.01 M EDTA solution (pH 5). For all biomass concentrations and independent of pH, between 90 and 100% of the curium(III) was released from the cells. Hence the process is reversible and confirms the formation of surface complexes with functional groups of the cell envelope. The bacterial complexes are less stable than the curium(III)–EDTA complex (see Table 4.3).

In all bacterial samples a bi-exponential luminescence decay behavior was measured. The occurrence of two lifetimes suggests that two distinct chemical environments contribute to the

speciation of the accumulated curium(III) by the biomass. The averaged value of the shorter lifetime was calculated to be 121 ± 10 µs, whereas the component with the longer lifetime was calculated to be 390 ± 78 µs. These lifetimes correspond to 4.5 and 1, respectively, remaining water molecule in the curium(III) first coordination sphere.

Due to the results of time dependent measurements with the 1200 line mm^{-1} grating of a sample at pH 6 (0.3 µM Cm and 0.2 $g_{dry\ weight}$/L) and the biomass-dependent experiments at pH 3.05, the longer lifetime can be assigned to *Cm^{3+} – P. fluorescens species 1*, whereas the shorter lifetime corresponds to *Cm^{3+} – P. fluorescens species 2*.

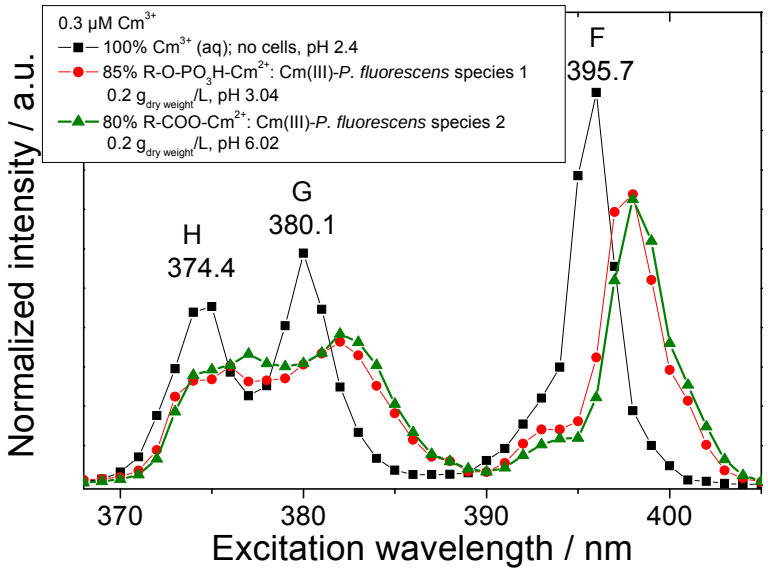

Fig. 5.14 Excitation spectra of curium(III) measured in the *P. fluorescens* (CCUG 32456) system.

The excitation spectra measured in the curium(III)–*P. fluorescens* system were characterized by sharp, well-resolved absorption bands coming from intense transitions to the H-, G-, and F-states (see Fig. 5.14). Depending on the pH and hence on the speciation different excitation spectra were detected, with representative examples presented in Fig. 5.14. Compared to the spectrum of the Cm^{3+} aquo ion a strong red shift of about 2 nm was detected for the cell-bound curium(III). The red shift of the absorption bands was combined with an increase in luminescence line widths of the H, G, and F absorption bands, e.g. F band: 397.8 (3.5) nm for *Cm^{3+} – P. fluorescens species 1* and 398.3 (3.7) nm for *Cm^{3+} – P. fluorescens species 2* compared with 395.7 (2.4) nm for Cm^{3+} (see Table 5.5). The excitation spectra clearly support our conclusions drawn from the luminescence emission measurements concerning the speciation of aqueous curium(III) in the *P. fluorescens* system.

The program SPECFIT was used to extract the bacterial curium(III) surface complexation constants (Tab. 4.3) and the single component spectra (Fig. 5.15). The variations observed in the emission data (see Fig. 5.13) could be described by the formation of two curium(III) surface complexes. Within the investigated pH range, most likely bacterial carboxyl and phosphoryl groups were responsible for curium(III) coordination on the cell envelope. Because of the strong interactions detected in the acidic pH region, a protonated curium(III) phosphoryl complex likely occurred followed by a carboxyl complex at higher pH. The best fits were obtained with two 1 : 1 complexes, R–O–PO_3H–Cm^{2+} and R–COO–Cm^{2+}. The surface complexation constants were calculated to be log $ß_{111}$ = 12.7 ± 0.6 for the protonated phosphoryl complex, and log $ß_{110}$ = 6.1 ± 0.5 for the carboxyl coordination (see Table 4.3 and Moll et al. 2013a). The presented single component spectra were averaged from the individual spectra calculated for every run (see Fig. 5.15).

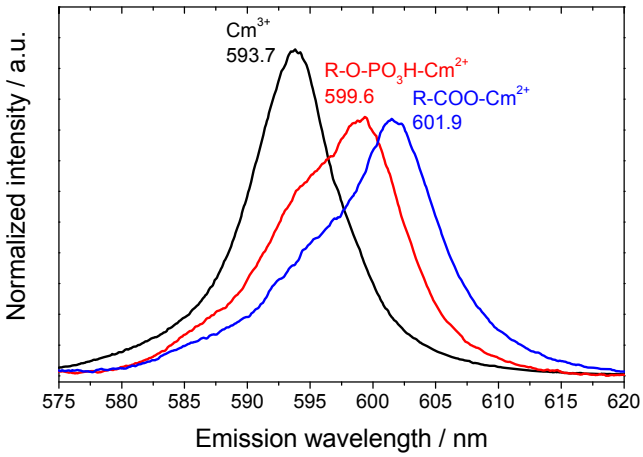

Fig. 5.15 Luminescence emission spectra of the single components in the Cm^{3+}– *P. fluorescens* (CCUG 32456) system, as derived by peak deconvolution using SPECFIT. The spectra are scaled to the same peak area.

The emission peak maximum is shifted from 593.7 nm for the Cm^{3+} aquo ion to 599.6, and 601.9 nm when curium(III) occurs in the two identified 1 : 1 *P. fluorescens* complexes. The spectroscopic properties of the identified Cm^{3+}–*P. fluorescens* species are summarized in Table 5.5.

The assignment of the emission maxima of Cm^{3+}–*P. fluorescens* species to curium(III) coordinated to hydrated phosphoryl– (599.6 nm) and carboxyl–groups (601.9 nm) can be explained as follows. It is well known that bacterial cell surfaces provide carboxyl, phosphoryl, and hydroxyl/amine groups for metal coordination (e.g., Markai et al. 2003, Yoshida et al. 2004). This was also confirmed by our titration experiments. When curium(III) interacts with deprotonated carboxyl groups of polyelectrolytes (e.g., humic acid), and

biomacromolecules (e.g., lipopolysaccharide, peptidoglycan) this results in an red-shifted emission maximum between 601 and 602.3 nm (see Table 4.6). The interaction with hydrated phosphoryl groups is characterized by a less red-shifted emission maximum around 600 nm.

The interaction mechanism of Cm(III) with *P. fluorescens* cells is dominated by a reversible biosorption reaction. A consideration of Cm^{3+}–*P. fluorescens* surface complexation constants takes into account the values presented in Table 4.3 for M:L:H species of 1 : 1 : 1 and 1 : 1 : 0 stoichiometry. It can be seen that curium(III) forms strong complexes with phosphoryl and carboxyl groups of the bacterial cell envelope. Log β values describing curium(III) carboxyl interactions range from 5.2 to 7.0 (Moll et al. 2009, Kim et al. 1993), whereas organic protonated phosphoryl species are characterized by stability constants around 13 (Moll et al. 2005, 2009). We have to admit that the amount of available data for biomacromolecules that can serve as a comparison for validating the bacterial data is limited. However, the determined values for the two Cm^{3+}–*P. fluorescens* surface complexes fit into these ranges of biomacromolecules having carboxyl and phosphoryl groups and are therefore reasonable.
A detailed characterization of aqueous Cm^{3+}–*P. fluorescens* species based on the changes of the intrinsic luminescence of Cm^{3+} has not been reported before. Moreover curium(III) surface complexation constants of bacterial cells are unknown.

The P. fluorescens Eu(III) system: potentiometric titration

Figure 5.16 illustrates the titration curve of europium(III) with *P. fluorescens* and the fit with HYPERQUAD.

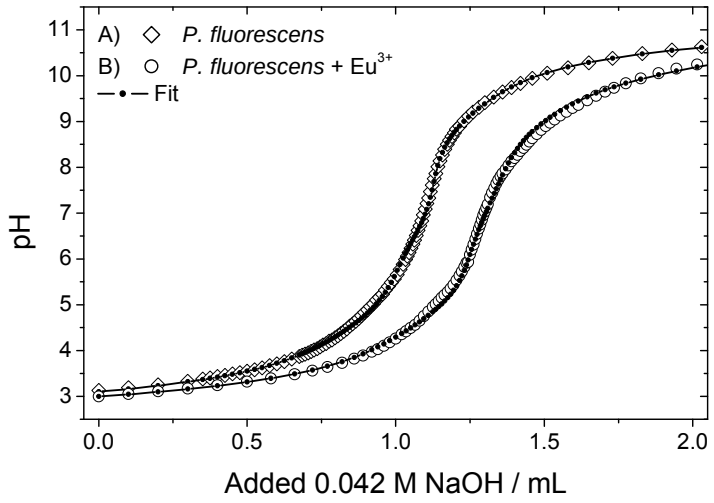

Fig. 5.16 pH curve of a *P. fluorescens* suspension with 0.3 $g_{dry\ weight}$/L titrated with 0.042 M NaOH: A) no europium(III) added; and B) + 0.1 mM europium(III).

The fit included the pK_a values and site densities of the bacteria. In evaluation of the curium(III) speciation results, the description of the bacterial cell wall with two major global binding sites (carboxyl and phoshoryl) was applied which is also a common approach (Markai et al. 2003). In addition the following hydrolytic europium(III) species and their stability constants were included in the fit: $Eu(OH)^{2+}$ and $Eu(OH)_2^{+}$. The titration curve could be modeled best when the complexes $R–COO–Eu^{2+}$ and $R–O–PO_3H–Eu^{2+}$ were considered, as can be seen from the HYPERQUAD fit result (Fig. 5.16). The respective calculated stability constants are summarized and compared to literature data in Table 4.3. The curium(III) speciation in the *P. fluorescens* system was successfully validated by potentiometric titrations using europium(III) as an analogue for curium(III).

Impact of P. fluorescens on the Cm(III) speciation

The luminescence and excitation data of the Cm^{3+}–*P. fluorescens* system can be described by the formation of two main species where two different functional groups of the cell envelope interact with the metal ion. These groups, phosphoryl and carboxyl moieties, bind curium(III) as a function of pH (see Fig. 5.17 A).

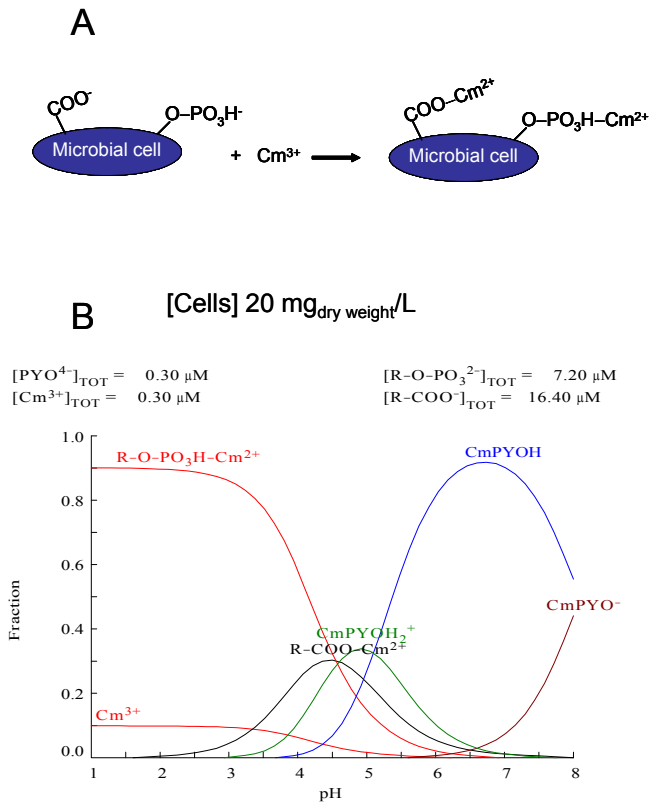

Fig. 5.17 A) Schematic illustration of the proposed bonding of curium(III) on functional groups of the *P. fluorescens* cell envelope and B) Speciation of curium(III), 0.3 µM, in aqueous solutions with equimolar concentration of PYO as a function of pH providing 80-fold (20 $mg_{dry\ weight}/L$) excess of functional groups from the *P. fluorescens* cell envelope.

To determine whether direct interactions with *P. fluorescens* cells and/or the pyoverdin complexation is important to the aqueous behavior of curium(III), the speciation in the following scenario was investigated. As average concentrations of *P. fluorescens* cells in groundwater, 20 $mg_{dry\ weight}$/L (24 µM of active functional groups), respectively, were used, low curium(III) and pyoverdin concentrations of 0.3 µM, respectively, can be expected (see Fig. 5.17 B). The influence of Cm^{3+}–*P. fluorescens* species on curium(III) speciation was already evident under low biomass conditions especially in the acidic pH range. One can conclude that bacterial curium(III) species dominate between pH 2 and 4.5 (direct interactions). On the other hand, the influence of Cm^{3+}–PYO species on curium(III) speciation was already evident under equimolar conditions (indirect interactions). Hence, strong Cm^{3+} species were formed, indicating the great potential of pyoverdin-type bioligands to bind curium(III) over a broad pH range (5-8). This underlines the significant Cm^{3+}-binding properties of hydroxamate- and catecholate containing pyoverdin-type siderophores compared to phosphoryl and carboxyl groups of the cell envelope. However, it demonstrates also that both interaction processes, direct and indirect, influence the curium(III) behavior in geochemical environments with resident bacteria at pH values between 2 and 8. If *P. fluorescens* cells produced pyoverdin-type siderophores and the curium(III)–pyoverdin species were transported to the cells like the corresponding iron(III)–pyoverdin species, the sorption capacity of the cells for curium(III) would increase.

5.2.1.3 Interaction with Pu

The P. fluorescens Pu system – Accumulation experiments

The amount of Pu decreased with time due to accumulation by *P. fluorescens* cells as shown in Fig. 5.18. Steady state conditions were reached after approximately 8 days (200 h). The kinetic data (see Fig. 5.18) again could be successfully fitted to a bi-exponential law ($y = y_0 + A\ 1\ e^{-(x/t1)} + A\ 2\ e^{-(x/t2)}$). The kinetic fits showed that the overall process consists of at least two parts: a fast process having a time frame of ~ 1 h (e.g., biosorption) and a much slower process with a time frame of ~ 700 h (e.g., bioreduction). We observed still decreasing amounts of Pu in solution (supernatants) at contact times > 200 h. This can be interpreted by a larger Pu binding capacity of the dead biomass (see also Fig. 5.19 left). It could be demonstrated that the $[^{242}Pu]_{initial}$ influences the amount of Pu associated with cells of *P. fluorescens*. At an intial Pu concentration of 0.2 mg/L, we observed a removal efficiency of

67 %. Whereas at $[^{242}Pu]_{initial}$ of 100 mg/L, the removal efficiency decreased to a level of 26 % (see Fig. 5.19 left).

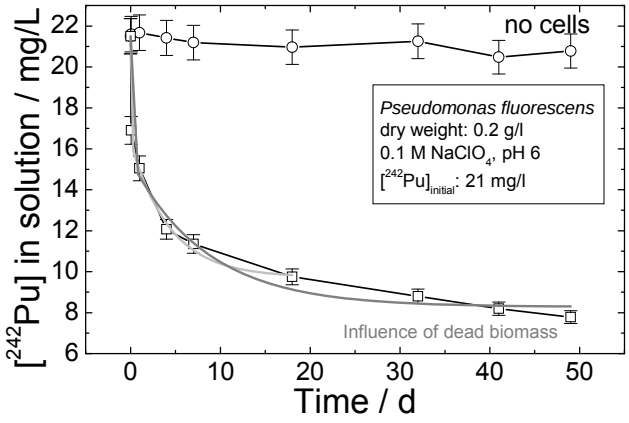

Fig. 5.18 Decrease of the ^{242}Pu concentration in solution due to interaction with cells of *P. fluorescens*.

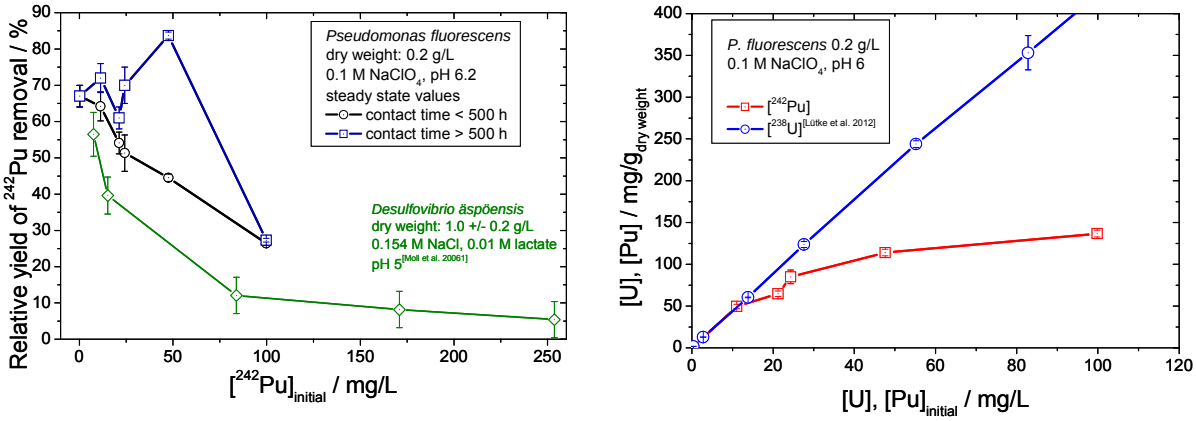

Fig. 5.19 Removed uranium and plutonium from the test solutions by cells of *P. fluorescens* as a function of the initial actinide concentration at pH 6.2.

Besides the bacterial Pu interactions explored in the project, similar observations were made in our earlier study with *D. aespoensis* (Moll et al. 2006). As depicted in Fig. 5.19 (left) also *P. fluorescens* cells are more effective in binding Pu at pH 6.1 compared to *D. aespoeensis*. Comparing the plutonium results with uranium (see Fig. 5.19 right), the measurements indicate that the cells of *Sporomusa* sp. accumulating less plutonium especially at $[^{242}Pu]_{initial}$ > 10 mg/L. As explained earlier one explanation could be a higher stress to the cells caused by the higher toxicity/radiotoxicity of ^{242}Pu compared to ^{238}U. The maximum concentration of accumulated Pu by the biomass was 125 ± 16 $mg/g_{dry\ weight}$.

The Pu–P. fluorescens system – Pu oxidation state distribution

First insights in the Pu oxidation state distribution were obtained by absorption spectroscopy (data not shown). The absorption spectra of the blank solutions (e.g. 100 mg/L Pu) are dominated by the contribution of Pu(VI), 820-890 nm, and absorption bands coming from the Pu(IV)-polymers at wavelength < 500 nm as shown for the Pu–*Sporomusa* sp. system (see Fig. 4.17). The Pu(VI) speciation is dominated by the Pu(VI)–hydroxo species: $(PuO_2)_2(OH)_2^{2+}$/$(PuO_2)_2(OH)_4^0$ (aq) at 849 nm and $PuO_2(OH)_3^-$ at 863 nm according to Reilly and Neu 2006. In the supernatants after separation of the cells we found a relatively fast decrease of the Pu(VI) absorption bands. After 96 h less than 36 % of Pu(VI) remained compared to 90 % in the blank solution. Similar to the Pu–*Sporomusa* sp. system we found in increase of the Pu(V) absorption band at 568 nm with the contact time. This suggests an enrichment of Pu(V) in the supernatants. This Pu(V) might be the result of a biotic Pu(VI) reduction by *P. fluorescens* cells.

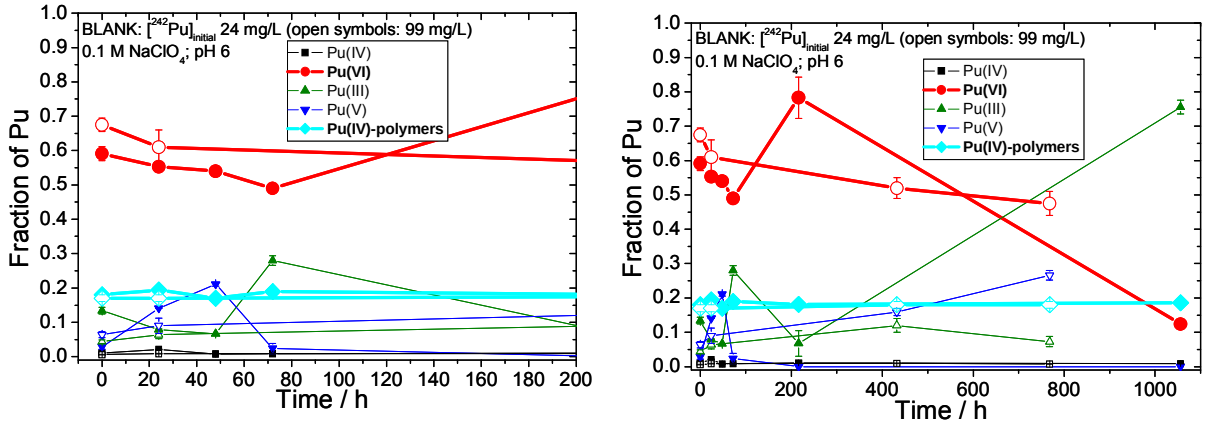

Fig. 5.20 ^{242}Pu oxidation state distributions in the blank samples determined by solvent extraction as a function of time ([^{242}Pu]: 24 mg/L, open symbols: 99 mg/L, 0.1 M $NaClO_4$, pH 6).

To describe the interaction mechanism of Pu with *P. fluorescens*, the time dependent Pu oxidation state distribution was determined in detail by solvent extraction in the blanks where no cells were added, in the supernatants after separating the cells and finally in the acidic biomass suspension.

Within the first 200 h of the experiments it can be seen in Figure 5.20 (left) that the dominating Pu species in the blanks are Pu(VI), 61 ± 9 %, and Pu(IV)-polymers, 18 ± 1 %. At longer contact times (see Fig. 5.20 right) we observed again an instability of Pu(VI) due to abiotic reduction processes (e.g., α-radiation) forming Pu(V). The strong decrease of Pu(VI) and the increase of Pu(III) in one experimental run (filled symbols in Fig. 5.20 right) was not

reproducible and is difficult to explain. In average 97 % of all Pu could be recovered by the solvent extractions.

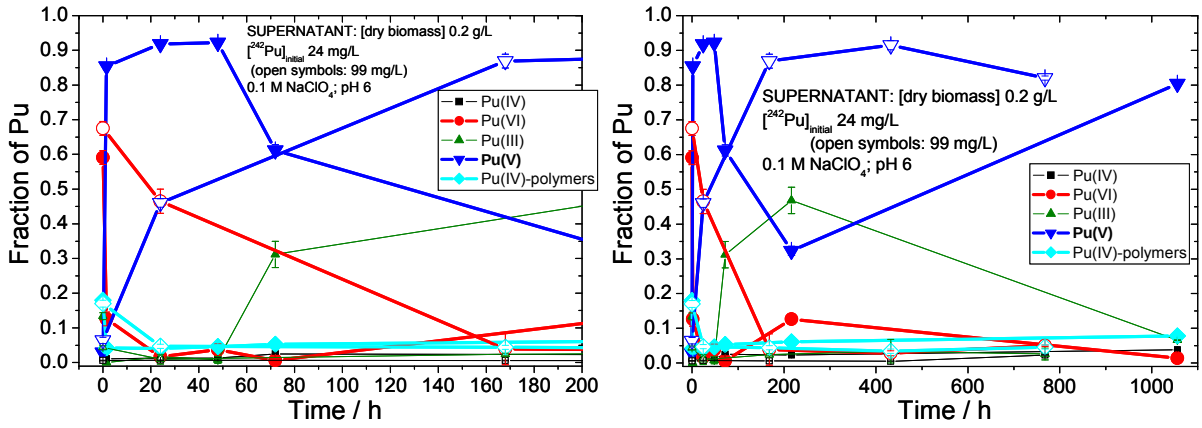

Fig. 5.21 ^{242}Pu oxidation state distributions in the supernatants after separation of the cells determined by solvent extraction as a function of time ([^{242}Pu]: 24 mg/L, open symbols: 99 mg/L, [dry biomass] 0.3 g/L, 0.1 M $NaClO_4$, pH 6).

A significant change of the Pu oxidation state distribution was observed in the supernatant after interaction with the cells as shown in Fig. 5.21. Pu(V) dominates the Pu oxidation state distribution with an average amount of 75 ± 22 %. The decrease of Pu(VI) and the increase of Pu(V) seems to correlate with $[^{242}Pu]_{initial}$. At $[^{242}Pu]_{initial}$ 24 mg/L already after a contact time of 24 h, the amount of Pu(VI) decreased from 59 to 2 %, whereas the Pu(V) content increased from 3 to 92 %. The bioreduction process was slower at $[^{242}Pu]_{initial}$ 99 mg/L. After 24 h the amount of Pu(VI) decreased from 67 to 46 %, whereas the Pu(V) content increased from 6 to 46 %. After 168 h, the Pu(VI) and Pu(V) concentrations reached steady state conditions with average values of 3.0 ± 1.0 % and 87 ± 4 %, respectively. This indicates a relatively fast reduction of Pu(VI) to Pu(V) due to the activity of the cells. The bioreduction process of Pu(VI) to Pu(V) by cells of *P. fluorescens* is not understood at the moment, it could take place via an enzymatic reduction where the dead part of the bacterial culture provides electron donors to the actively reducing part. After the interaction the majority of the Pu(V) was detected in solution. We assume that this happens due to the comparable weak complexing properties of the PuO_2^+ ion which is related with a release from the cell envelope. Similar observations were made in the past (Panak and Nitsche 2001, Moll et al. 2006). The amount of Pu(IV)-polymers decreased from 18 to 5 % after 24 h and is then independent from the contact time. This suggests good binding properties of the cell envelope towards Pu(IV)-polymers (biosorption).

After separating the supernatant from the cells, the bacteria were washed twice with 0.1 M $NaClO_4$. The washed biomass was acidified to pH 0 by adding 1 M $HClO_4$. ^{242}Pu

concentration measurements by LSC in the supernatant acidic solution after separating the cells showed that always a certain amount of the accumulated ^{242}Pu remains with the biomass after a contact time of 1 h.

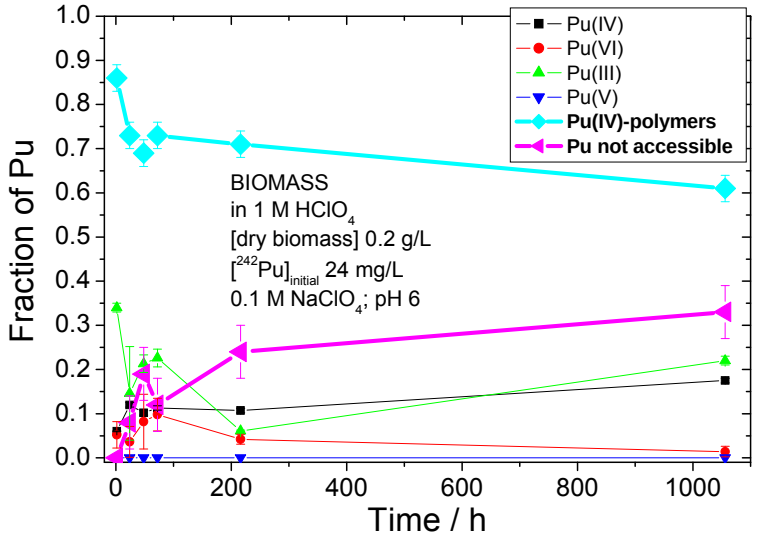

Fig. 5.22 ^{242}Pu oxidation state distributions in the biomass by solvent extraction over the time ([^{242}Pu]: 24 mg/L, [dry biomass] 0.2 g/L, 0.1 M $NaClO_4$, pH 6).

Within $[^{242}Pu]_{initial}$ 24 to 100 mg/L, this amount of strongly bound plutonium increased from 36 % up to 66 % (after contact times of 1100 h). Hence the solvent extractions were performed with the acidified biomass suspensions. The increase of the strongly bound Pu correlates with the amount of inaccessible Pu in the extraction experiments (see Fig. 5.22).

In the following, the results of the oxidation state distribution measurements of the cell bound plutonium are described. After a contact time of 1.5 h, the amount of Pu(VI) associated with the biomass reached steady state value of 5 ± 3 % ($[^{242}Pu]_{initial}$ 24 mg/L). This shows both a fast biosorption and bioreduction of Pu(VI) to Pu(V) under the assumption that Pu(VI) is the origin of Pu(V). The formed Pu(V) gets very fast dissolved from the cell envelope because the amount of Pu(V) associated with the cells was below the detection limit. The Pu(IV)-polymers are clearly dominating the Pu oxidation state distribution, 72 ± 8 %. The increased amount of Pu which is not accessible in the solvent extractions possibly indicates an accumulation inside the bacterial cells. Especially at higher contact times, we could detect Pu(III) and Pu(IV), 18 ± 8 % and 12 ± 3 %, respectively on the biomass.

5.2.2 Biofilms

5.2.2.1 Interaction with U(VI)

Analysis

Analysis show, that the uranium concentration declined from the initial concentration of 23.8 mg/L (1.0×10^{-4} M) to 12.9 mg/L (5.4×10^{-5} M) at the end of the experiments (Table 5.6) with the consequence that uranium had been removed from solution and immobilized.

Table 5.6 Mean concentration of cations and anions in the nutrient media.

	before the addition of U [in mg/L]	**after the addition of U [in mg/L]**	**after the experiment [in mg/L]**
Na	173 ± 10	174 ± 10	178 ± 10
Mg	0,66 ± 0.05	0,83 ± 0.05	1,73 ± 0.1
Al	< 0,01	< 0,01	< 0,01
Si	1,82 ± 0.1	2,09 ± 0.1	3,07 ± 0.1
K	92,3 ± 5	97,2 ± 5	105 ± 5
Ca	7,79 ± 0.5	5,37 ± 0.5	7,01 ± 0.5
Fe	< 0,01	< 0,01	< 0,01
U	**0,001**	**23,8 ± 0.2**	**12,9 ± 0.2**
Cl^-	150 ± 5	157 ± 5	168 ± 5
NO^{3-}	< 0,5	< 0,5	< 0,5
PO_4^{3-}	12,7 ± 0.6	14,8 ± 0.7	**99,8 ± 1**
SO_4^{2-}	13,8 ± 0.6	14,3 ± 0.7	15,2 ± 0.7
CO_3^{2-}	1310 ± 0.6	1245 ± 0.6	1130 ± 0.5

The analysis of the biofilm showed an amount of 4.53 mg uranium per gram biofilm dry mass, which indicates that approximately 10 % of the initial uranium concentration was immobilized in the biofilm. As shown in Table 5.6, phosphate in the nutrient medium increased from 12.7 mg/L to 99.8 mg/L after the end of the experiment. This corresponds to a release of 34.8 mg of phosphate from the biofilm to the 400 mL of the nutrient medium. We assume that inorganic phosphate ($H_2PO_4^-$) was released from the cellular polyphosphate as a cells' response to the heavy metal stress. The released phosphate was available for the formation of uranyl species. Excessive amounts of phosphate were transported into the nutrient media with the consequence that the amount of phosphate increased strongly.

Microsensor measurements

Microsensor measurements of oxygen concentrations were performed over the total thickness of the biofilm, which could be estimated to be 150-200 µm. The highest average oxygen

concentration (220 µmol/L) was determined at the top of the biofilm and decreased to 25 µmol/L at the biofilm/nutrient medium interface (Fig. 5.23).

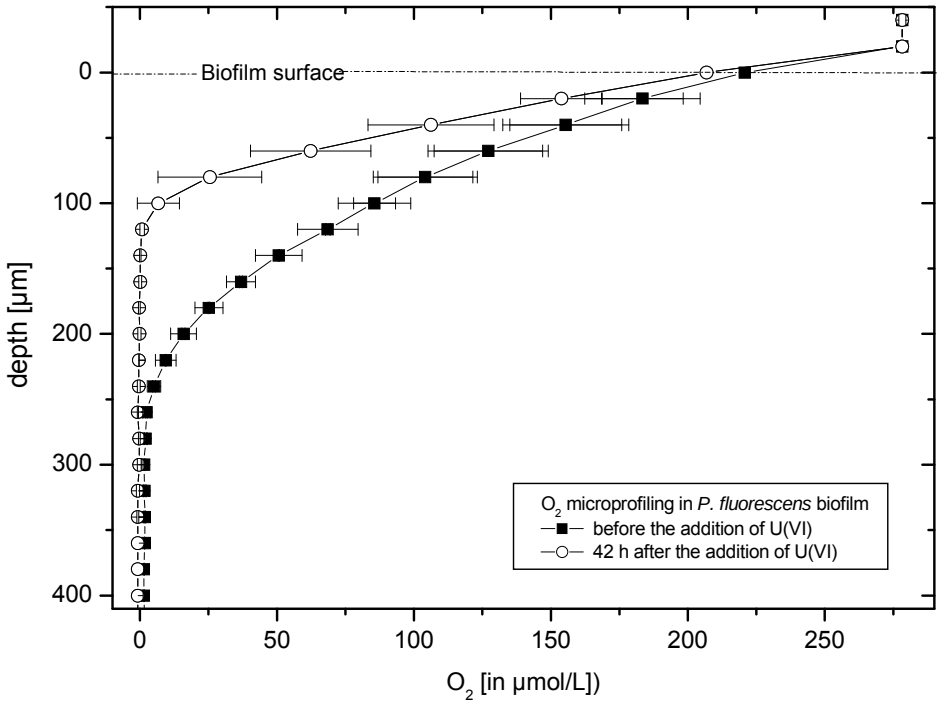

Fig. 5.23 Oxygen concentration profiles in the *P. fluorescens* biofilm before and 42 h after the addition of uranium to the nutrient medium to a final uranium concentration of 1×10^{-4} M.

No oxygen was measured in the nutrient medium, below the biofilm. After adding uranium to the nutrient medium for 42 h, the oxygen concentration decreased faster from the biofilm surface to the biofilm/nutrient medium interface. The curve progression is relatively flat, so that already at a depth of approximately 120 µm the oxygen concentration dropped below the detection limit. The addition of uranium(VI) in ecologically relevant concentrations to the biofilm induced a fast decrease of the oxygen concentration with increasing biofilm depth. The microbial response to the addition of uranium is a stress response of the microbes which is already clearly detectable only two hours after the addition of uranium as described in (Krawczyk-Bärsch et al. 2008). The results indicate that uranium(VI) has a strong effect on the stimulation of the metabolism of the *P. fluorescens* microbes and, consequently, on their respiratory activity and oxygen consumption.

The measured pH of the nutrient medium was in the pH range of 8.5 ± 0.1 before and after the addition of uranium, respectively. In contrast, within the biofilm the pH decreased from 8.0 to 7.5 in the presence of uranium. Similarly, the redox potential measured in the biofilm, was reduced from 388 ± 20 mV to 290 ± 20 mV.

EXAFS analysis

Analyzable uranium EXAFS oscillations were achieved in the biofilm sample based on the XAS data obtained at the uranium L_{III}-edge. Fig. 5.24 shows the raw uranium k^3-weighted EXAFS spectra and their corresponding Fourier transforms. It includes the fits of the experimental data of the biofilm sample, which was contacted with 0.05 mM U(VI) at pH 7. In addition, the fits of the meta-autunite reference are shown for comparison.

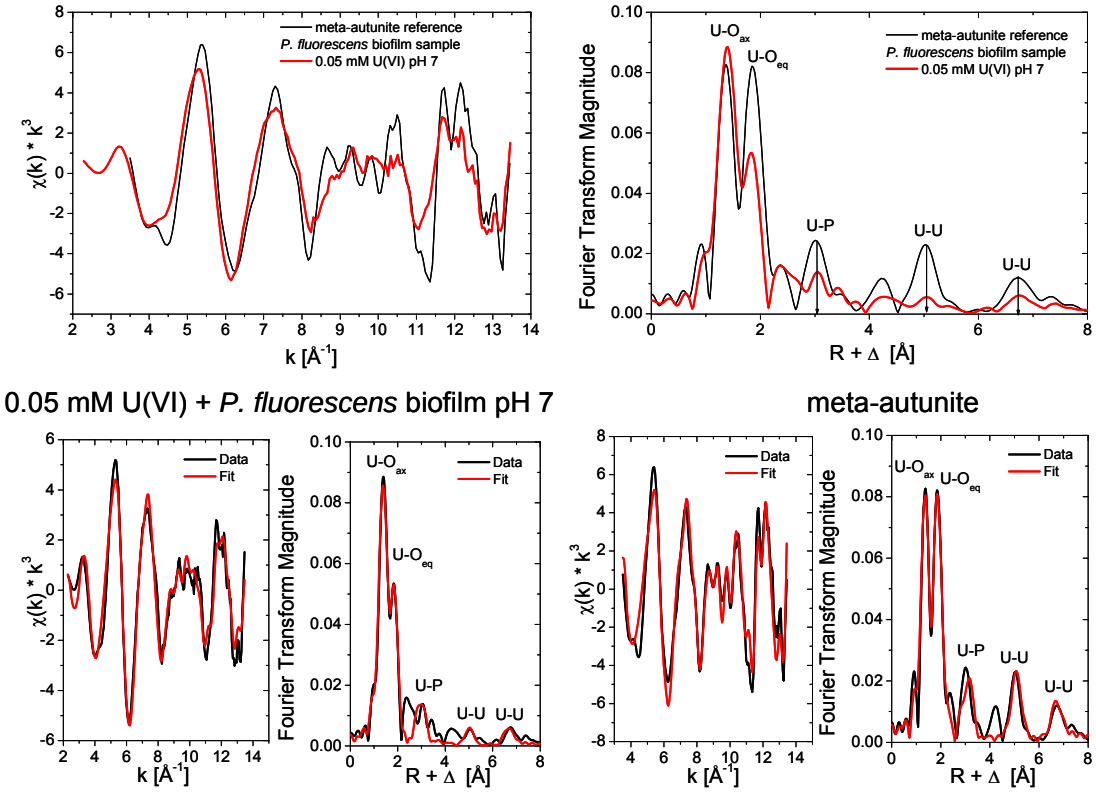

Fig. 5.24 Top: Summary of U L_{III}-edge k^3-weighted EXAFS spectra (left) and the corresponding Fourier transforms (right). Bottom: EXAFS spectra (left) and corresponding Fourier transforms (right) and the best theoretical fits (red line) of the 0.05 mM U(VI) biofilm sample at pH 7 and of the meta-autunite reference.

In Table 5.7 the results of the fits to the experimental data are listed**.** The coordination number (N) of the axial oxygen of the linear uranyl(VI) unit was held constant at two during the fitting procedure. The mean U-O_{ax} distance (R) was measured at 1.78 ± 0.01 Å. The Debye-Waller factor (σ^2) of the U-O_{ax} shell of the biofilm sample contacted with 0.05 mM U(VI) is similar to the value of the crystalline meta-autunite sample. Compared to the meta-autunite reference, there is a tendency of larger Debye-Waller factors measured in the biofilm sample for the higher shells probably due to higher disorder of the respective shells.

Table 5.7 Summary of selected structural parameter based on shell fit analysis of the EXAFS data.

Sample	Shell	N [a]	R (Å) [b]	σ^2 (Å^2) [c]	ΔE_0 (eV) [d]
meta-autunite	U=O	2[f]	1.78 (1.78)[e]	0.0027	8.6
	U-O_{eq}	3.6	2.28 (2.32)[e]	0.0010	
	U-P	4[f]	3.62 (3.59)[e]	0.0085	
	U-U	4[f]	5.24 (5.23)[e]	0.0032	
	U-U	4[f]	6.87 (6.96)[e]	0.0014	
P. fluorescens biofilm + 0.05 mM U(VI) pH 7	U=O	2[f]	1.79	0.0024	6.2
	U-O_{eq}	4.3	2.29	0.0053	
	U-P	2[f]	3.61	0.0148	
	U-U	2[f]	5.21	0.0068	
	U-U	2[f]	6.86	0.0020	

[a] Errors in coordination numbers (N) are ± 25 %; [b] Errors in radial distance (R) are ± 0.02 Å; [c] Debye-Waller factor (σ^2); [d] Shift in threshold energy (ΔE_0); [e] bond distances based on the XRD analysis from meta-Autunite published by Makarov et al. (1960); [f] fixed parameter (for bacterial samples based on the XRD analysis from meta-Autunite published by Makarov et al. (1960).

The similarities of the EXAFS oscillation features especially in k-space between 8 and 12 Å^{-1} observed in the biofilm sample and in the meta-autunite reference points to the beginning formation of meta-autunite like U(VI) structure in the biofilm sample. This could be seen also in the corresponding Fourier Transforms depicted in Fig. 5.24. There are strong indications especially for heavier backscatterer like U(VI) at distance values above 4 Å (see Fig. 5.24). The structural parameters are in agreement with the corresponding meta-autunite values (Table 5.7).

Thermodynamic calculation

The speciation diagram was constructed using the geochemical speciation code Geochemist's Workbench, version 9.0.2/React. For the thermodynamical calculation of the predominance fields of various uranium species at 25°C the analytical data for the nutrient medium after uranium addition were used. The database used was the thermo.dat accompanying the code, supplemented by the most recent NEA database for aqueous uranium species and by solubility data for uranium minerals (Guillaumont et al. 2003) and in addition for the calcium carbonate uranium(VI) species (Bernhard et al. 2001). In the distribution diagram of uranium(VI)

species of the aqueous phase as a function of pH at 25°C (Fig. 5.25) two uranium(VI) species, $UO_2(CO_3)_3^{4-}$ and $Ca_2UO_2(CO_3)_3$, were calculated in the pH range from 6 to 12.5.

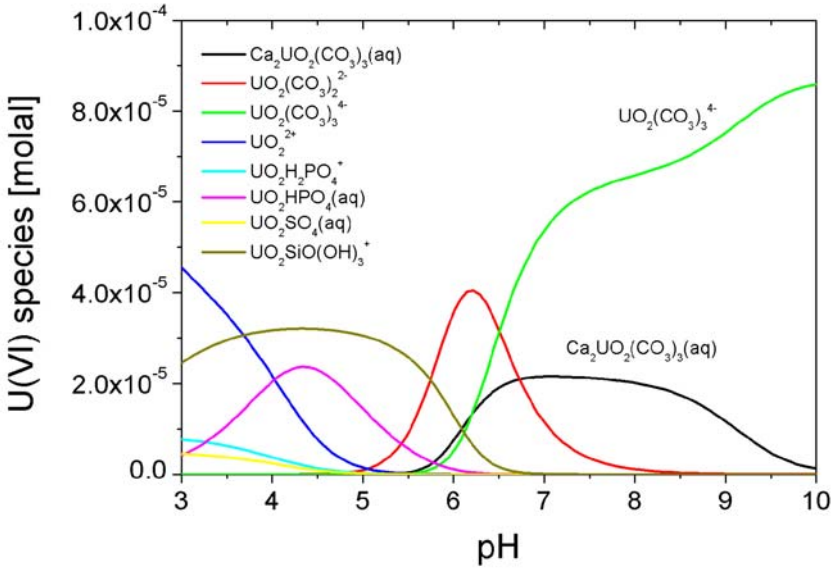

Fig. 5.25 Distribution diagram of uranium(VI) species of the aqueous phase of the uranium(VI) contaminated nutrient medium as a function of pH at 25°C, using the geochemical speciation code Geochemist´s Workbench Version 9.0.2/React.

Although the complex formation constant of calcium uranyl carbonate species is higher than the complex formation constant of the binary uranyl carbonate species, the formation of $Ca_2UO_2(CO_3)_3$ species is limited by the low calcium concentration. In the neutral to the medium acid pH range the formation of the uranyl carbonate species UO_2CO_3 and $UO_2(CO_3)_2^{2-}$ was predicted. In the pH range < 5 the dominant species $UO_2SiO(OH)^{3+}$, UO_2HPO_4 and UO_2^{2+} were calculated.

U(VI) speciation in the nutrient medium investigated by TRLFS

Laser-induced fluorescence spectroscopy at 153 K was used to spectroscopically identify the uranyl species formed in the U(VI) contaminated nutrient medium of the *P. fluorescence* biofilm. The measured emission spectrum is characterized by four emission bands, as shown in the luminescence spectrum (Fig. 5.26). In addition, the spectra of the aqueous uranyl carbonate species $Ca_2UO_2(CO_3)_3$ and $UO_2(CO_3)_3^{4-}$ were obtained for comparison. The results were compared with the luminescence properties of the aqueous uranyl carbonate complexes, described in Krawczyk-Bärsch et al. 2012 and Steudtner et al. 2011, respectively.

The band positions of the obtained luminescence spectra of the $Ca_2UO_2(CO_3)_3$ and $UO_2(CO_3)_3^{4-}$ species are similar to those found in our studied uranium contaminated nutrient medium as described in Fig. 5.26. Hence, it can be assumed that the aqueous $Ca_2UO_2(CO_3)_3$

and $UO_2(CO_3)_3^{4-}$ species were formed under the given experimental conditions in the nutrient medium of the *P. fluorescence* biofilm.

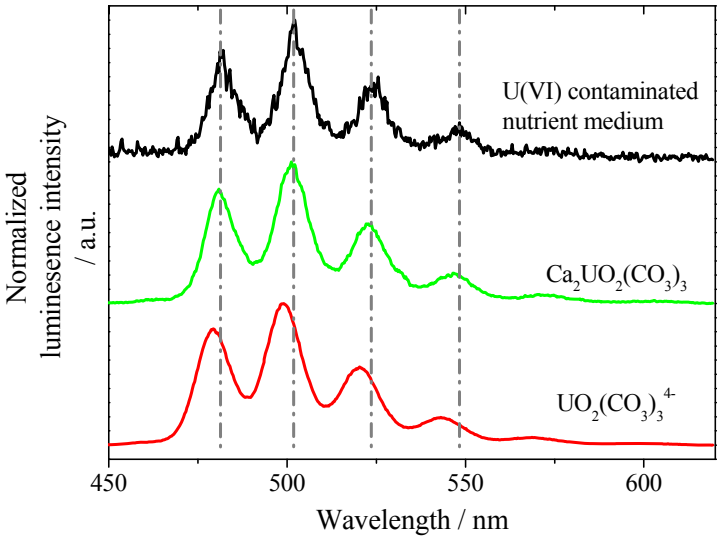

Samples	**Luminescence emission bands / ± 0.5 nm**				**Ref.**
Nutrient medium	482.2	502.2	524.0	546.9	This work
$Ca_2UO_2(CO_3)_3$	481.4	501.3	522.7	545.9	This work
$UO_2(CO_3)_3^{4-}$	479.4	499.9	520.1	542.9	This work
Literature					
$Ca_2UO_2(CO_3)_3$	483.6	502.3	523.2	547.4	Krawczyk-Bärsch et al. 2012
$UO_2(CO_3)_3^{4-}$	480.7	499.9	520.3	542.5	Steudtner et al. 2011

Fig. 5.26 Luminescence spectra of the uranium contaminated nutrient medium at 153 K in comparison to the spectra of uranyl carbonate species $Ca_2UO_2(CO_3)_3$ and $UO_2(CO_3)_3^{4-}$, which were described in the literature. For clarity, the spectra were normalized to the same maximum intensities.

Summary of P. fluorescens biofilm experiments

In our studies, 10 % of the initially present uranium was removed from solution and immobilized exclusively in biofilm cells of *P. fluorescens*. EXAFS analysis indicated that the biofilm immobilized uranium occurred as U-phosphate minerals autunite or meta-autunite. By thermodynamic calculations and laser-induced fluorescence spectroscopy it could be shown, that calcium uranyl carbonates species ($Ca_2UO_2(CO_3)_3$ and $UO_2(CO_3)_3^{4-}$) were formed in the nutrient medium of the *P. fluorescence* biofilm. These species are characterized by larger stability constants than the ones of the U(VI) species with functional groups of the bacterial surface. This explains why 80 % of the initially present uranium remains in the aqueous solution. Hence these species can contribute to the migration of U(VI) and consequently to environmental hazard.

5.3 Summary

As already shown for the Mont Terri isolates U(VI) and Cm(III)/Eu(III) cellular binding is strongly pH-dependent. For U(VI) the maximum binding capacities for the Äspö strain *P. fluorescens* were found at pH 6. *P. fluorescens* possess the highest U(VI) binding capacities, 244 mg $U/g_{dry\ weight}$ at an $[U(VI)]_{initial}$ of 55 mg/L, found in this study. U(VI) interaction experiments demonstrated that mainly phosphoryl and carboxyl moieties of the cell envelope were responsible for U(VI) binding via biosorption. The following bacterial U(VI) surface species were identified by potentiomertric titration: $R–COO–UO_2^+$, $R–O–PO_3–UO_2$, $R–O–PO_3H–UO_2^+$, and $(R–O–PO_3)_2–UO_2^{2-}$. The U(VI) speciation could be successfully validated by the direct speciation method TRLFS. We can conclude from the determined bacterial surface stability constants thermodynamically moderate to strong interaction reactions. It was found that the U(VI) binding efficiency of *P. fluorescens* can be enhanced by allowing metabolic activity of the cells and by providing phosphate. Here a remarkable interaction mechanism could be identified: combined TRLFS, EXAFS and microscopic studies revealed that a highly ordered meta-autunite-like structure is formed which quite effectively removes and immobilizes uranium (99% uranium is removed from solution). Different strategies of coping with U(VI) were observed comparing *P. fluorescens* planktonic cells and biofilms under the chosen experimental conditions. An enhanced capability of the biofilm to form meta-autunite in comparison to the planktonic cells was proven. Conclusively, the *P. fluorescens* biofilm is more efficient in U(VI) detoxification than the planktonic cells.

The experiments in the Cm^{3+}– *P. fluorescens* system can be described by the formation of two main species where two phopshoryl and carboxyl moieties of the cell envelope interact with the metal ion as a function of pH. The interaction mechanism of Eu(III)/Cm(III) with the cells is dominated by a reversible biosorption reaction. SPECFIT analysis indicated the presence of the $R\text{-}O\text{-}PO_3H\text{-}Cm^{2+}$ and $R\text{-}COO\text{-}Cm^{2+}$ species as a function of pH. The spectroscopic speciation could be successfully validated by potentiometric titration using Eu(III) as a non-radioactive analogon to mimic bacterial interactions of An(III). Speciation calculations were performed whether direct Cm(III) interactions with *P. fluorescens* cells and/or the pyoverdin complexation is important to the aqueous behavior of curium(III). The influence of Cm^{3+}–*P. fluorescens* species on curium(III) speciation was already evident under low biomass conditions especially in the acidic pH range. One can conclude that bacterial curium(III) species dominate between pH 2 and 4.5 (direct interactions). On the other hand, the influence of Cm^{3+}–PYO species on curium(III) speciation was already evident under equimolar conditions (indirect interactions). It could be demonstrated that both interaction processes,

direct and indirect, influence the curium(III) behavior in geochemical environments with resident bacteria at pH values between 2 and 8. If *P. fluorescens* cells produced pyoverdin-type siderophores and the curium(III)–pyoverdin species were transported to the cells like the corresponding iron(III)–pyoverdin species, the sorption capacity of the cells for curium(III) would increase.

Strong interactions of ^{242}Pu with planktonic cells of the Äspö strain *P. fluorescens* at pH 6 could be detected (~ 120 mg Pu/$g_{dry\ weight}$). The results showed a higher ^{242}Pu binding capacity of dead biomass. The relative yield of ^{242}Pu removal depends on $[^{242}Pu]_{initial}$. Also for *P. fluorescens* less ^{242}Pu was accumulated compared to ^{238}U (466 mg U/$g_{dry\ weight}$). 85 ± 17 % of the initially present Pu(VI) was reduced to Pu(V) most likely due to the activity of the cells within the first 24 h of contact time. This reduction process was much faster than in the abiotic controls. Good binding properties of Pu(IV)-polymers on functional groups of the cell envelope were observed. In general, a strong impact of the Äspö strain *P. fluorescens* on the Pu speciation was found. The overall interaction mechanism seems similar to the one detected for the Äspö strain *D. äspöensis* (Moll et al. 2006).

6 Summary and outlook

The aim of this project was to determine the microbial diversity in Mont Terri Opalinus Clay by direct molecular culture-independent retrievals and by cultivation/enrichment experiments, the cultivation and characterization of Mont Terri Opalinus Clay specific bacteria and to assess An/Ln binding onto bacteria with a focus on the thermodynamics and the elucidation of interaction mechanisms. We have compared An/Ln interactions of the Äspö-strain *P. fluorescens* CCUG 32456A obtained with planktonic cells and with biofilms.

For the first time microbial tDNA could be isolated from 50 g unperturbed Mont Terri Opalinus Clay. We could show that the core surface sample is occupied by bacteria not or barely presented in the parallel sample from the inner part of the core. Hence, clay from the inner part of the core should be analyzed to avoid contaminants which might penetrate into the core during the sampling. Based on the analysis of the tDNA the bacterial diversity of the unperturbed inner core sample is dominated by representatives of *Firmicutes*, *Betaproteobacteria*, and *Bacteriodetes*. *Firmicutes* also dominate after treatment of the clay with R2A medium. Bacteria isolated from Mont Terri Opalinus Clay on R2A medium were related to *Sporomusa* spp., *Paenibacillus* spp., and *Clostridium* spp.. All further investigations are concentrated on the unique isolates *Sporomusa* sp. MT-2 and *Paenibacillus* sp. MT-2. Cells of these types were comprehensively analyzed in terms of growing, morphology, functional groups of the cell envelope, and cell membrane structure.

The strains *P. fluorescens* (CCUG 32456A) (granite: Äspö HRL, Sweden), *Paenibacillus* sp. MT-2.2, and *Sporomusa* MT-2.99 (both Opalinus Clay: Mont Terri URL, Switzerland) were studied concerning their behaviour towards the actinides uranium, curium and plutonium. Additionally Eu(III) has been investigated as inactive analog to Cm(III). Besides the structural and thermodynamic characteristics of the actinide surface complexes formed also the overall interaction mechanisms and binding capacities of the strains were of interest.
The results showed that for the actinides U(VI) and Cm(III) cellular binding is strongly pH-dependent. For U(VI) the maximum binding capacities for *Sporomusa* sp. MT-2.99, *Paenibacillus* sp. MT-2.2 and *P. fluorescens* were found at pH 6 and 7. All strains possess high U(VI) binding capacities, e.g. *P. fluorescens* adsorbs up to 244 mg $U/g_{dry\ weight}$ at an $[U(VI)]_{initial}$ of 55 mg/L at pH 6. It was found that the U(VI) binding efficiency of *P. fluorescens* can be enhanced by allowing metabolic activity of the cells and by providing phosphate. Here a remarkable interaction mechanism could be identified: combined TRLFS,

EXAFS and microscopic studies revealed that a highly ordered meta-autunite-like structure is formed which quite effectively removes and immobilizes uranium (99% uranium is removed from solution). The advantage is that the mechanism proceeds fast and the compact agglomerate formed can be removed without any further partitioning step. Overall this implies an effective remediation strategy for treating contaminated soils and waste water effluents.

In view of the versatile possible interaction mechanisms between bacteria and actinides, it was found that all investigated strains display indirect interaction in the form of a pronounced pH-dependent phosphatase activity and concomitant phosphate release, which was highest at pH 6 for *P. fluorescens* and *Paenibacillus* sp.. Enzyme activity was drastically decreased in presence of U(VI). The inhibition threshold was much lower for *Paenibacillus* sp. than for *P. fluorescens*. Phosphatase activity of *Paenibacillus* sp. was drastically reduced at an initial [U(VI)] of $1 \cdot 10^{-6}$ M. This [U(VI)] barely had any effect on phosphate release by *P. fluorescens* cells. Using TRLFS it was proven that phosphate was released into the medium and binds dissolved U(VI). Luminescence emission maxima of the obtained spectra indicated that soluble inorganic U(VI) phosphate complexes are formed. In presence of Cm(III) *Paenibacillus* sp. cells also displayed a pronounced phosphatase activity which was strongly pH-dependent. At pH 3 95% Cm(III) were bound while in the neutral pH range only 4% Cm(III) were accumulated due to phosphate release. Extraction studies with EDTA showed that binding was completely reversible indicating a pure biosorption process to the cell envelope. This was also observed for *P. fluorescence*. For *Sporomusa* sp. the interaction mechanism with Eu(III)/Cm(III) is dominated by a major process a reversible biosorption reaction. However we could identify a certain amount, ca. 30%, which is irreversibly bound to the cells. This minor process can be described by a immobilization of Eu(III)/Cm(III) within the complex cell envelope structure of *Sporomusa* sp.

Investigating the structures of the U(VI) complexes formed at the cell surfaces of all strains using TRLFS and EXAFS it could be demonstrated that in case of metabolically inactive planktonic cells also a pure biosorption process dominates. This differs to what was found for *P. fluorescens* biofilms. Here it could be shown that after U(VI) interaction in $NaClO_4$ the strain was capable of forming meta-autunite (Krawczyk-Bärsch et al. 2013). Hence different strategies of coping with U(VI) were observed comparing *P. fluorescens* planktonic cells and biofilms under the chosen experimental conditions. An enhanced capability of the biofilm to form meta-autunite in comparison to the planktonic cells was proven. Conclusively, the *P. fluorescens* biofilm is more efficient in U(VI) detoxification.

To assess the biosorption processes occurring with metabolically inactive cells in detail to finally provide thermodynamic data on the binding of U(VI), Cm(III) and Eu(III) to the cell surface functional groups, the cell surfaces were characterized using a combined approach of microbiological methods and potentiometry. Gram staining, amino peptidase test and KOH test gave insights into the general structure of the outer cell wall. The Äspö isolate *P. fluorescens* (CCUG 32456A), as it is true for all strains of the genus *Pseudomonas*, was proven to be Gram-negative indicating LPS to be the very outer part of the cell membrane. The new Mont Terri isolate *Sporomusa* sp. MT-2.99 was also characterized to be Gram-negative. The new Mont Terri isolate *Paenibacillus* sp. MT-2.2 was characterized to be Gram-positive which signifies that PG makes up the very outer part of the cells, as it is the case for other strains of this genus.

For all bacterial strains a three-site model (carboxyl, phosphoryl and amine moieties) was used to successfully fit the titration data. To obtain thermodynamic data on the U(VI), Cm(III) and Eu(III) binding to the cell surface functional groups and for the purpose of validating the stoichiometries of the complexes formed, potentiometry and TRLFS were employed. For the characterization of the U(VI) and Eu(III) complexes formed potentiometry was combined with an evaluation using HYPERQUAD. The usage of HYPERQUAD for fitting titration data involving bacterial metal interactions is also a novel approach. Using potentiometry for all bacterial species the following U(VI) surface complexes and their stability constants were determined: $R{-}COO{-}UO_2^{+}$, $R{-}O{-}PO_3H{-}UO_2^{+}$, $R{-}O{-}PO_3{-}UO_2$, and $(R{-}O{-}PO_3)_2{-}UO_2^{2-}$. Using TRLFS measurements it could be shown that the $R{-}O{-}PO_3{-}UO_2$ complex for all investigated strains possesses a very short luminescence lifetime for U(VI) species (average: 0.52 µs) in comparison to those of the $R{-}O{-}PO_3H{-}UO_2^{+}$ and $(R{-}O{-}PO_3)_2{-}UO_2^{2-}$ complexes. For example the U(VI) species distribution in presence of *P. fluorescens* ([U(VI)] = $1{\cdot}10^{-6}$ M, [dry biomass] = 0.02 g/L) reveals that in the acidic pH range below pH 3.5 U(VI) binds to the cell surface mainly via protonated phosphoryl groups. U(VI) binding by carboxylic sites plays a role over a wide pH range up to around pH 7. At pH 7 fully deprotonated phosphoryl groups are mainly responsible for U(VI) binding. Comparing the impact of all strains at environmentally relevant conditions it becomes evident that for *P. fluorescens* the coordination to carboxyl groups plays a much greater role than for the Mont Terri isolates. For *Paenibacillus* sp. the complexation of U(VI) by carboxylic sites is almost suppressed under environmentally relevant U(VI) concentrations. On the first view this finding seems to be contradictory since Gram-negative strains generally are supposed to have a higher number of phosphoryl sites than Gram-positive strains. If the surface site densities are compared it

becomes evident that both strains possess exactly the same ratio of carboxylic groups to phosphoryl sites: 2.3. Thus a different contribution of surface sites to U(VI) binding can not be attributed to the respective site densities but must be correlated to the stability of the complexes formed. Obviously, U(VI) is bound much more stable by the carboxylic sites of *P. fluorescens* than by those of *Paenibacillus* sp. and *Sporomusa* sp. .

Overall, for all strains the following order of stability can be established for the U(VI) complexes formed at the bacterial cell surfaces:

$(R\text{-}O\text{-}PO_3)_2\text{-}UO_2^{2-} > R\text{-}O\text{-}PO_3H\text{-}UO_2^{+} > R\text{-}O\text{-}PO_3\text{-}UO_2 > R\text{-}COO\text{-}UO_2^{+}$.

Also for Cm(III)/Eu(III) and within the investigated pH-range (2-8) carboxyl and phosphoryl moieties of the bacterial cell envelope were responsible for metal binding. For Eu(III) with the bacterial isolates the surface species $R\text{-}COO\text{-}Eu^{2+}$ and $R\text{-}O\text{-}PO_3H\text{-}Eu^{2+}$ were identified and characterized thermodynamically. In addition for *Sporomusa* sp. the surface species $R\text{-}O\text{-}PO_3\text{-}Eu^{+}$ was found. Evidently the surface functional groups of *Sporomusa* sp. have a higher affinity to Eu(III) than those of *Paenibacillus* sp. and *P. fluorescens*. Here it is also valid that phosphoryl interaction results in higher thermodynamic stability than carboxyl interaction.

TRLFS studies on the interaction of Cm(III) with *Paenibacillus* sp. revealed that Cm(III) is solely bound by the bacterial phosphoryl moieties. SPECFIT analysis indicated the presence of the $R\text{-}O\text{-}PO_3H\text{-}Cm^{2+}$ species over a wide pH range. Although the existence of a Eu(III) species with carboxylic groups at pH 8 was predicted, no such Cm(III) species could be detected at that pH using TRLFS. An explanation might be the difference in ratios of [metal] to [dry biomass] in the potentiometry and TRLFS experiments. Also the respective Cm(III)–carboxyl complex might have a much lower luminescence quantum yield than Cm(III) complexed by phosphoryl sites.

For Cm(III) slightly larger log β values for the bacterial surface complexes were measured compared to Eu(III). However we could also show that Eu(III) can be used as a non-radioactive analogon to mimic bacterial interactions of An(III). Our results suggested that Eu(III)/Cm(III) complexes with the surface functional groups of all strains dominate their respective speciation over a broad pH and biomass concentration range.

The calculated stability constants of the U(VI) and Cm(III) complexes with the bacterial surface functional groups suggest a moderate to strong interaction of the bacterial surfaces with the investigated actinides (lanthanide).

To summarize, the following simplified overall schemes of the impact of the bacterial strains on the U(VI) and Cm(III) speciation are proposed:

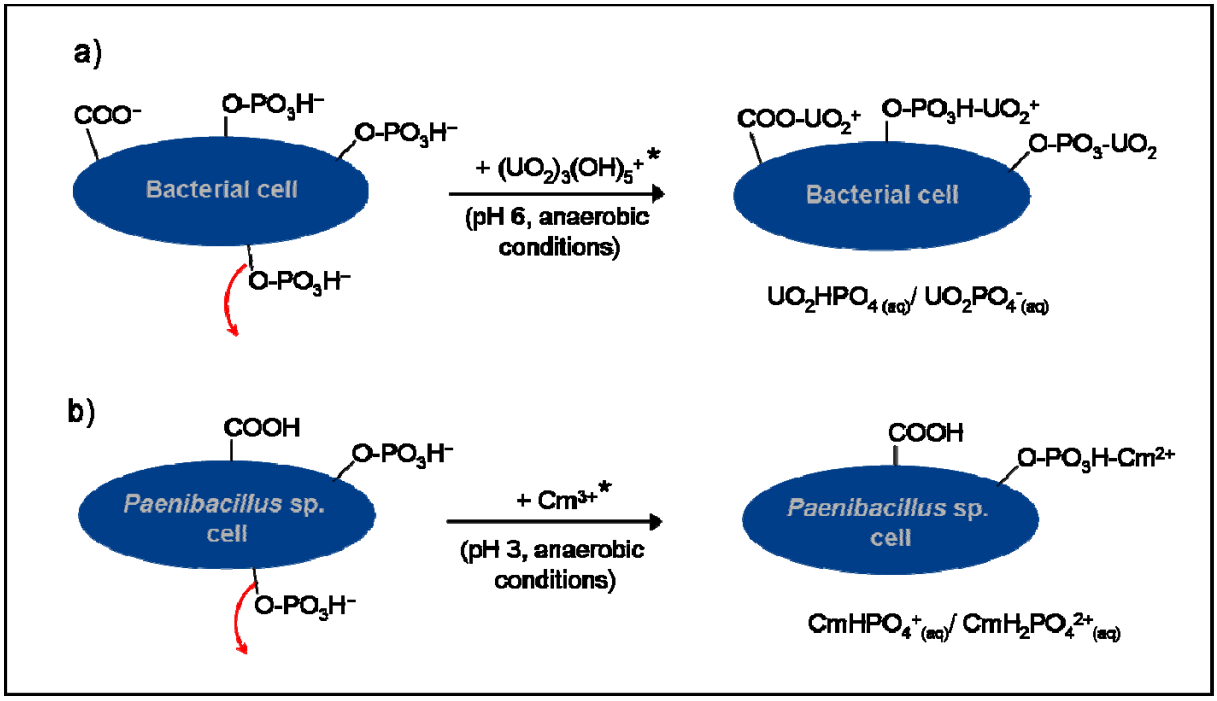

Fig. 6.1 Simplified schemes of impact of bacterial cells on U(VI) and Cm(III) speciation at anaerobic conditions. **a)** U(VI) interaction with either *P. fluorescens*, *Sporomusa* sp. or *Paenibacillus* sp. at pH 6, **b)** Cm(III) interaction with *Paenibacillus* sp. at pH 3, * dominant species at stated pH.

It could be demonstrated that even at low bacterial mass the effect on actinide mobilization can not be disregarded comparing the determined stability constants to those of other complexes of environmental relevance, such as that formed with e.g. citrate, CO_3^{2-}, and SO_4^{2-}. Strong interactions of the Mont Terri Opalinus Clay isolate *Sporomusa* sp. and the Äspö-strain *P. fluorescens* with ^{242}Pu were observed at pH 6 (~ 78 mg Pu/$g_{dry\ weight}$ and ~ 120 mg Pu/$g_{dry\ weight}$, respectively). A higher ^{242}Pu binding capacity of the dead biomass was determined. The ^{242}Pu removal efficiency of *Sporomusa* sp. and *P. fluorescens* cells depends on the $[^{242}Pu]_{initial}$. Compared to ^{238}U (> 120 mg U/$g_{dry\ weight}$) the *Sporomusa* cells are accumulating less plutonium. For *Sporomusa* sp. approximately 43 % of the initially present Pu(VI) was fastly reduced to Pu(V) most likely due to the activity of the cells during the first 25 h of contact time (99 % after 73 h). This reduction process was much slower in all abiotic controls. We could detect good binding properties of the cell envelope towards Pu(IV)-polymers (immobilization). Especially at long contact times and low initial plutonium concentrations, *Sporomusa* sp. cells were able to form relatively high amounts of Pu(IV) and

Pu(III). For *P. fluorescens* 85 ± 17 % of the initially present Pu(VI) was reduced to Pu(V) in the presence of the cells within the first 24 h of contact time. In general, we can postulate a similar interaction mechanism as found for the Äspö strain *D. aespoeensis* (Moll et al. 2006). To sum up, there was a strong influence of *Sporomusa* sp. and *P. fluorescens* cells on the Pu oxidation state distribution and hence the speciation.

In conclusion, Mont Terri Opalinus Clay contains bacterial communities. The capability of the identified representatives of *Bacilli*, *Negativicutes* and *Clostridia* to form spores gives them a potential to survive in unfavourable conditions as present in the clay. The isolated Mont Terri Opalinus Clay isolates may influence the speciation and hence the migration behaviour of selected An/Ln under environmental conditions. The stability constants calculated in this project are valuable for modelling the U(VI) and Cm(III) speciation and distribution in the environment. Hence the results contribute to better estimating the safety of a planned nuclear waste deposition site.

Further studies should focus on the determination of the microbial diversity and actinide/lanthanide interactions with indigenous microbes in other potential host rock formations suitable for a nuclear waste repository. Such studies are planned for salt formations. One important task to investigate further are studies of the metabolic activity of indigenous microbes in such formations. The metabolic activity can affect the physical and geochemical conditions of a geologic repository and hence the speciation of accidentally released An. The quantification of the total microbial DNA in terms of cell numbers in pore waters and cores for instance as a function of depth should be addressed further. The performed laboratory experiments in this study could be extended to more environmental conditions (e.g., ternary systems containing the host rock – microbial cells – metals). All this would complete our knowledge of microbial processes influencing the fate of accidentally released actinides and fission products in the environment.

7 References

Albrecht-Gary, A.-M., Blanc, S., Rochel, N., Ocaktan, A. Z., and Abdallah, M. A. 1994, Bacterial iron transport: coordination properties of pyoverdin PaA, a peptidic siderophore of *Pseudomonas aeruginosa*, Inorg. Chem., 33, 6391-6402.

Alderighi, L., Gans, P., Ienco, A., Peters, D., Sabatini, A., and Vacca, A. 1999, Hyperquad simulation and speciation (HySS): a utility program for the investigation of equilibria involving soluble and partially soluble species, Coord. Chem. Rev., 184, 311-318.

Anderson C., Johnsson A., Moll H., Pedersen K. 2011. Radionuclide Geomicrobiology of the Deep Biosphere. Geomicrobiol. J., 28, 540-561.

Ankudinov, A. L., Ravel, B., Rehr, J. J., and Conradson, S. D. 1998, Real-space multiple-scattering calculation and interpretation of X-ray absorption near-edge spectra, Phys. Rev. B: Condens. Matter, 58, 7565-7575.

Barkleit, A., Moll, H., and Bernhard, G. 2008, Interaction of uranium(VI) with lipopolysaccharide, Dalton Trans., 2879-2886.

Barkleit, A., Moll, H., and Bernhard, G. 2009, Complexation of uranium(VI) with peptidoglycan, Dalton Trans., 5379–5385.

Barkleit A., Acker M., Bernhard G. 2013. Europium(III) complexation with salicylic acid at elevated temperatures. Inorg. Chim. Acta, 394, 535-541.

Beazley, M. J., Martinez, R. J., Sobecky, P. A., Webb, S. M., and Taillefert, M. 2007, Uranium biomineralization as a result of bacterial phosphatase activity: insights from bacterial isolates from a contaminated subsurface, Environ. Sci. Technol., 41, 5701-5707.

Bencheikh-Latmani, R., Leckie, J. O., and Bargar, J. R. 2003, Fate of uranyl in a quaternary system composed of uranyl, citrate, goethite, and *Pseudomonas fluorescens*, Environ. Sci. Technol., 37, 3555-3559.

Bengtsson, L., Johansson, B., Hackett, T. J., McHale, L., and McHale, A. P. 1995, Studies on the biosorption of uranium by *Talaromyces emersonii* CBS 814.70 biomass, Appl. Microbiol. Biotechnol., 42, 807-811.

Bernhard, G., Geipel, G., Reich, T., Brendler, V., Amayri, S. and Nitsche, H. 2001. Uranyl(VI) carbonate complex formation: Validation of the $Ca_2UO_2(CO_3)_{3\ (aq.)}$ species. Radiochim. Acta, 89, 511–518.

Beveridge, T. J., and Doyle, R. J. 1989, Metal ions and bacteria, New York: John Wiley & Sons Inc.

Binstead, R. A., Zuberbühler, A. D., Jung, B. 2004. SPECFIT Global Analysis System Version 3.0.35.

Boivin-Jahns, V., Ruimy, R., Bianchi, A., Daumas, S, Christen, R. 1996, Bacterial diversity in a deep-subsurface clay environment. Appl. Environ. Microbiol., 62(9), 3405-3412.

Brachmann, A., Geipel, G., Bernhard, G., and Nitsche, H. 2002, Study of uranyl(VI) malonate complexation by time resolved laser-induced fluorescence spectroscopy (TRLFS) Radiochim. Acta, 90, 147-153.

Brookshaw, D. R., Pattrick, R. A. D., Lloyd, J. R., Vaughan, D. J. 2012, Microbial effects on mineral-radionuclide interactions and radionuclide solid-phase capture processes. Mineralog. Mag., 76, 777-806.

Chatterjee, A., and Ray, L. 2008, Biosorption of Cu(II) by immobilized biomass of Bacillus cereus M116 from aqueous solution, J. Sci. Ind. Res., 67, 629-634.

Choppin, G.R., Thakur, P., Mathur, J. N. 2006, Complexation thermodynamics and structural aspects of actinide–aminopolycarboxylates. Coord. Chem. Rev., 250, 936-947.

Cox, J. S., Smith, D. S., Warren, L. A., and Ferris, F. G. 1999, Characterizing heterogeneous bacterial surface functional groups using discrete affinity spectra for proton binding Environ. Sci. Technol., 33, 4514-4521.

Denecke, M. A., Reich, T., Bubner, M., Pompe, S., Heise, K. H., Nitsche, H., Allen, P. G., Bucher, J. J., Edelstein, N. M., Shuh, D. K. 1998, Determination of structural parameters of uranyl ions complexed with organic acids using EXAFS, J. Alloys Compd., 271-273, 123-127.

Dittrich M., Sibler S. 2005, Cell surface groups of two picocyanobacteria strains studied by zeta potential investigations, potentiometric titration, and infrared spectroscopy. J. Colloid. Interface Sci., 286, 487-495.

Edelstein, N. M., Klenze, R., Fanghänel, T., and Hubert, S. 2006, Optical properties of Cm(III) in crystals and solutions and their application to Cm(III) speciation, Coord. Chem. Rev., 250, 948-973.

Fang, L., Cai, P., Chen, W., Liang, W., Hong, Z., and Huang, Q. 2009, Impact of cell wall structure on the behaviour of bacterial cells in the binding of copper and cadmium, Colloids Surf., A, 347, 50-55.

Fanghänel, T., Kim, J. I., Klenze, R., and Kato, Y. 1995, Formation of Cm(III) chloride complexes in $CaCl_2$ solutions, J. Alloys Compd., 225, 308-311.

Fein, J. B., Daughney, C. J., Yee, N., and Davis, T. A. 1997, A chemical equilibrium model for metal adsorption onto bacterial surfaces, Geochim. Cosmochim. Acta, 61, 3319-3328.

Fowle, D. A., Fein, J. B., and Martin, A. M. 2000, Experimental study of uranyl adsorption onto *Bacillus subtilis*, Environ. Sci. Technol., 34, 3737-3741.

Gad, A. S., Attia, M., and Ahmed, H. A. 2010, Heavy metals bio-remediation by immobilized *Saccharomyces cerevisiae* and *Opuntia ficus* in indica waste, J. Am. Sci., 6, 79-87.

Gans, P., Sabatini, A., and Vacca, A. 1996, Investigation of equilibria in solution. Determination of equilibrium constants with the HYPERQUAD suite of programs, Talanta, 43, 1739-1753.

Geipel, G., Thieme, M., Bernhard, G., Nitsche, H. 1994, Distribution of uranium and radionuclides in a uranium-mining rockpile in Schlema, Saxony, Germany. Radiochim. Acta, 66/67, 305.

Geipel, G., Brachmann, A., Brendler, V., Bernhard, G., and Nitsche, H. 1996, Uranium(VI) sulfate complexation studies by time-resolved laser-induced fluorescence spectroscopy (TRLFS), Radiochim. Acta, 75, 199-204.

Geipel, G., Bernhard, G., Rutsch, M., Brendler, V., and Nitsche, H. 2000, Spectroscopic properties of uranium(VI) minerals studied by time-resolved laser-induced fluorescence spectroscopy (TRLFS), Radiochim. Acta, 88, 757-762.

Glorius M., Moll H., Bernhard G. 2008, Complexation of curium(III) with hydroxamic acids investigated by time-resolved laser-induced fluorescence spectroscopy. Polyhedron, 27, 2113-2118.

Günther, A., Geipel, G., and Bernhard, G. 2006, Complex formation of U(VI) with the amino acid L-threonine and the corresponding phosphate ester O-phospho-L-threonine, Radiochim. Acta, 94, 845–851.

Guillaumont, R., Fanghänel, Th., Fuger, J., Grenthe, I., Neck, V., Palmer, D. A., Rand, M. H. 2003, Update on the chemical thermodynamics of uranium, neptunium, plutonium, americium and technetium, OECD/NEA, Paris.

Hansel, C. M., Fendorf, S., Jardine, P. M., Francis, C. A. 2008, Changes in bacterial and archaeal community structure and functional diversity along geochemically variable soil profile. Appl. Environ. Microbiol., 74, 1620-1633.

Heller, A., Barkleit, A., Bernhard, G., Ackermann J. U. 2009, Complexation of europium(III) and curium(III) with urea in aqueous solution investigated by time-resolved laser-induced fluorescence spectroscopy. Inorg. Chim. Acta., 362, 1215-1222.

Heller, A., Barkleit, A., Foerstendorf, H., Tsushima, S., Heim, K., Bernhard, G. 2012, Curium(III) citrate speciation in biological systems: An europium(III) assisted spectroscopic and quantum chemical study. Dalton Trans, 41, 13969-13983.

Hennig, C., Panak, P. J., Reich, T., Rossberg, A., Raff, J., and Selenska-Pobell, S. 2001, EXAFS investigation of uranium(VI) complexes formed at *Bacillus cereus* and *Bacillus sphaericus* surfaces, Radiochim. Acta, 89, 625-631.

Heylen, K., Vanparys, B., Wittebolle, L., Verstraete, W., Boon, N., De Vos, P. 2006, Cultivation of denitrifying bacteria: optimization of isolation conditions and diversity study. Appl. Environ. Microbiol., 72, 2637-2643.

Horrocks, W. D., Sudnick, D. R. 1979, Lanthanide ion probes of structure in biology - Laser-induced luminescence decay constants provide a direct measure of the number of metal-coordinated water-molecules. J. Am. Chem. Soc., 101(2), 334-340.

Hudson, E. A., Allen, P. G., Terminello, L. J., Denecke, M. A., and Reich, T. 1996, Polarized x-ray-absorption spectroscopy of the uranyl ion: Comparison of experiment and theory, Phys. Rev. B: Condens. Matter, 54, 156-165.

Kalinowski, B.E., Oskarsson, A., Albinsson, Y., Arlinger, J., Ödegaard-Jensen, A., Pedersen, K. 2004, Microbial leaching of trace elements from Ranstad mine tailings. Geoderma, 122, 177-194.

Keller, C.: The Chemistry of the Transuranium Elements, Volume 3, Verlag Chemie GmbH, Weinheim, Germany (1971).

Kim, J. I., Rhee, D. S., Wimmer, H., Buckau, G., Klenze, K. 1993, Complexation of trivalent actinide ions (Am^{3+}, Cm^{3+}) with humic acid: a comparison of different experimental methods. Radiochim. Acta, 62, 35-43.

Kim, J. I., Klenze, R., Wimmer, H., Runde, W., Hauser, W. 1994, A study of the carbonate complexation of Cm-III and Eu-III by time-resolved laser fluorescence spectroscopy. J. Alloys Compd., 213–214, 333-340.

Kimura, T., Choppin G. R. 1994, Luminescence study on determination of the hydration number of Cm(III). J. Alloys Compd., 213/214, 313-317.

Kimura, T., Choppin, G. R., Kato, Y., Yoshida, Z. 1996, Determination of the hydration number of Cm(III) in various aqueous solutions. Radiochim. Acta, 72, 61-64.

Kimura, T., Kato, Y. 1998, Luminescence study on hydration states of lanthanide(III)–polyaminopolycarboxylate complexes in aqueous solution. J. Alloys Compd., 277, 806-810.

Knopp, R., Panak, P. J., Wray, L. A., Renninger, N. S., Keasling, J. D., and Nitsche, H. 2003, Laser spectroscopic studies of interactions of UVI with bacterial phosphate species, Chem. Eur. J., 9, 2812-2818.

Koban, A., and Bernhard, G. 2004, Complexation of uranium(VI) with glycerol 1-phosphate, Polyhedron, 23, 1793-1797.

Koban, A., Geipel, G., Roßberg, A., and Bernhard, G. 2004, Uranium(VI) complexes with sugar phosphates in aqueous solution, Radiochim. Acta, 92, 903-908.

Könnecke, T., Fanghänel, T., and Kim, J. I. 1997, Thermodynamics of trivalent actinides in concentrated electrolyte solutions: modelling the chloride complexation of Cm(III), Radiochim. Acta, 76, 131-135.

Krawczyk-Bärsch, E., Grossmann, K., Arnold, T., Hofmann, S., Wobus, A. 2008, Influence of uranium (VI) on the metabolic activity of stable multispecies biofilms studied by oxygen microsensors and fluorescence microscopy. Geochim. Cosmochim. Acta, 72, 5251-5265.

Krawczyk-Bärsch, E., Lünsdorf, H., Arnold, T., Brendler, V., Eisbein, E., Jenk, U., Zimmermann, U. 2011, The influence of biofilms on the migration of uranium in acid mine drainage (AMD) waters. Science of the Total Environment, 409, 3059-3065.

Krawczyk-Bärsch, E., Lünsdorf, H., Pedersen, K., Arnold, T., Bok, F., Steudtner, R., Lehtinen, A., Brendler, V. 2012, Immobilization of uranium in biofilm microorganisms exposed to groundwater seeps over granitic rock tunnel walls in Olkiluoto, Finland. Geochim. Cosmochim. Acta, 96, 94-104.

Krawczyk-Bärsch, E., Lütke, L., Moll, H., Bok, F., Steudtner, R., Roßberg, A., and Brendler, V. 2013, Spectroscopic and microscopic evidence for U(VI) immobilization in cultivated Pseudomonas fluorescens biofilms, Water Res., in preparation.

Kuhner, C. H., Frank, C., Grießhammer, A., Schmittroth, M., Acker, G., Gößner, A., Drake, H. L. 1997, *Sporomusa silvacetica* sp. nov., an acetogenic bacterium isolated from aggregated forest soil. Int. J. Syst. Bacteriol., 47, 352-358.

Lane, D. J. 1991, 16S/23S rRNA gene sequencing. In: Nucleic acid techniques in bacterial systematics. Stackebrandt E, Goodfellow M (Eds). John Wiley & Sons Ltd p. 115-175.

Lloyd, J. R., Gadd, G. M. 2011, The Geomicrobiology of Radionuclides. Geomicrobiol. J., 28, 383–386.

Locock, A. J., and Burns, P. C. 2003, The crystal structure of synthetic autunite, $Ca[(UO_2)(PO_4)]_2(H_2O)11$, Am. Mineral., 88, 240–244.

Lovley, D. R., Philips, E. J. P., Gorby, Y. A., Landa, E. R. 1991, Microbial reduction of uranium. Nature, 350, 413-416.

Lütke, L., Moll, H., Bernhard, G. 2012, Insights on the Uranium(VI) Speciation with *Pseudomonas fluorescen*s on a Molecular Level. Dalton Trans., 41, 13370-13378.

Lütke, L. 2013a, Interaction of selected Actinides (U, Cm) with Bacteria relevant to Nuclear Waste Disposal. Doctoral thesis TU Dresden, Germany.

Lütke, L., Moll, H., Bernhard, G. 2013b, The U(VI) Speciation Influenced by a Novel *Paenibacillus* Isolate from Mont Terri Clay. Dalton Trans., 42, 6979-6988.

Makarov, E. S., and Ivanov, V. I. 1960, Crystal structure of meta-autunite, $Ca(UO_2)_2(PO_4)_2*6H_2O$, Doklady Akad. Nauk SSSR, 132, 673-676.

Makarova, K. S., Aravind, L., Wolf, Y. I., Tatusov, R. L., Minton, K. W., Koonin, E. V., and Daly, M. J. 2001, Genome of the extremely radiation-resistant bacterium Deinococcus radiodurans viewed from the perspective of comparative genomics, Microbiol. Mol. Biol. Rev., 65, 44-79.

Markai, S., Andres, Y., Montavon, G., Grambow, B. 2003, Study of the interaction between europium(III) and *Bacillus subtilis*: fixation sites, biosorption and reversibility. J. Colloid. Interf. Sci., 262, 351-361.

Matz, W., Schell, N., and Bernhard, G. 1999, ROBL – a CRG beamline for radiochemistry and material research at the ESRF, J. Synchrotron Radiat., 6, 1076-1085.

Merroun, M. L., Selenska-Pobell, S. 2008, Bacterial interactions with uranium: An environmental prespective. J. Contam. Hydrol., 102, 285-295.

Moll, H., Reich, T. and Szabó, Z. 2000, The hydrolysis of dioxouranium(VI) investigated using EXAFS and ^{17}O-NMR. Radiochim. Acta, 88, 411-415.

Moll, H., Geipel, G., Reich, T., Bernhard, G., Fanghänel, T., and Grenthe, I. 2003, Uranyl(VI) complexes with alpha-substituted carboxylic acids in aqueous solution, Radiochim. Acta, 91, 11-20.

Moll, H., Stumpf, Th., Merroun, M., Rossberg, A., Selenska-Pobell, S., Bernhard, G. 2004, Time-resolved Laser Fluorescence Spectroscopy Study on the Interaction of Cm(III) with *Desulfovibrio äspöensis* DSM 10631^T. Environ, Sci, Technol, 38, 1455-1459.

Moll, H., Geipel, G., Bernhard, G. 2005, Complexation of Curium(III) by Adenosine 5'-triphosphate (ATP): A Time-resolved Laser-induced Fluorescence Spectroscopy (TRLFS) Study. Inorg. Chim. Acta, 358, 2275-2282.

Moll, H., Merroun, M.L., Hennig, Ch., Rossberg, A., Selenska-Pobell, S., Bernhard, G. 2006, The interaction of *Desulfovibrio äspöensis* DSM 10631^T with plutonium, Radiochim. Acta 94, 815-824.

Moll, H., Johnsson, A., Schäfer, M., Pedersen, K., Budzikiewicz, H., Bernhard, G. 2008a, Curium(III) complexation with pyoverdins secreted by a groundwater strain of *Pseudomonas fluorescens*. Biometals, 21, 219-228.

Moll, H., Glorius, M., Bernhard, G., Johnsson, A., Pedersen, K., Schäfer, M., and Budzikiewicz, H. 2008b, Characterization of pyoverdins secreted by a subsurface strain of Pseudomonas fluorescens and their interaction with uranium(VI), Geomicrobiol. J., 25, 157-166.

Moll, H., Glorius, M., Johnsson, A., Schäfer, M., Budzikiewicz, H., Pedersen, K., Bernhard, G. 2010, Neptunium(V) complexation by naturalpyoverdins and related model compounds, Radiochim. Acta, 98, 517-576.

Moll, H., Glorius, M., Barkleit, A., Roßberg, A., Bernhard, G. 2009, The Mobilization of Actinides by Microbial Ligands Taking into Consideration the Final Storage of Nuclear Waste – Interactions of Selected Actinides U(VI), Cm(III), and Np(V) with Pyoverdins Secreted by *Pseudomonas fluorescens* and Related Model Compounds. Wissenschaftlich-Technische Berichte, FZD-522, Forschungszentrum Dresden-Rossendorf, Dresden and references therein.

Moll, H., Brendler, V., and Bernhard, G. 2011, Aqueous curium(III) phosphate species characterized by time-resolved laser-induced fluorescence spectroscopy, Radiochim. Acta, 99, 775-782.

Moll, H., Bernhard, G. 2012, A TRLFS study of curium(III) naphthalene and hydroxyquinoline complexes in aqueous solution. Polyhedron, 31, 759-766.

Moll, H., Lütke, L., Barkleit, A., Bernhard, G. 2013a, Curium(III) speciation studies with cells of a groundwater strain of *Pseudomonas fluorescens*. Geomicrobiol. J., 30, 337-346.

Moll, H., Lütke, L., Bachvarova, V., Geissler, A., Selenska-Pobell, S., and Bernhard, G. 2013b, Interactions of the Mont Terri Opalinus Clay isolate *Sporomusa* sp. MT-2.99 with curium(III) and europium(III). Geomicrobiol, J, submitted.

Moulin, C., Wei, J., Van Iseghem, P., Laszak, I., Plancque, G., Moulin, V. 1999, Europium complexes investigations in natural waters by time-resolved laser-induced fluorescence. Anal. Chim. Acta, 296, 253-261.

Nyman, J. L., Marsh, T. L., Ginder-Vogel, M. A., Gentile, M., Fendorf, S., Criddle, C. 2006, Heterogeneous response to biostimulation for U(VI) reduction in replicated sediment microcosms. Biodegrad., 17, 303-316.

Ockenden, D. W., Welch, G. A. 1956, J. Chem. Soc., 3358.

Ohnuki, T., Yoshida, T., Ozaki, T., Samadfam, M., Kozai, N., Yubuta, K., Mitsugashira, T., Kasama, T., and Francis, A. J. 2005, Interaction of uranium with bacteria and kaolinite clay, Chem. Geol., 220, 237-243.

Oren, A. 2002, Molecular ecology of extremely halophilic archaea and bacteria, FEMS Microbiol. Ecol., 39, 1-7.

Ozaki, T., Arisaka, M., Kimura, T., Francis, A. J., Yoshida, Z. 2002, Empirical method for prediction of the coordination environment of Eu(III) by time-resolved laser-induced fluorescence spectroscopy. Anal. Bioanal. Chem., 374, 1101-1104.

Ozaki, T., Gillow, J. B., Kimura, T., Ohnuki, T., Yoshida, Z., Francis, A. J. 2004, Sorption behavior of europium(III) and curium(III) on the cell surface of microorganisms. Radiochim. Acta, 92, 741-748.

Panak, P. J., Raff, J., Selenska-Pobell, S., Geipel, G., Bernhard, G., and Nitsche, H. 2000, Complex formation of U(VI) with *Bacillus*-isolates from a uranium mining waste pile, Radiochim. Acta, 88, 71-76.

Panak, P. J., Nitsche, H. 2001, Interaction of aerobic soil bacteria with plutonium(VI). Radiochim. Acta, 89, 499-504.

Panak, P. J., Knopp, R., Booth, C. H., and Nitsche, H. 2002, Spectroscopic studies on the interaction of U(VI) with Bacillus sphaericus, Radiochim. Acta, 90, 779-783.

Paviet, P., Fanghänel, T., Klenze, R., and Kim, J. I. 1996, Thermodynamics of curium(III) in concentrated electrolyte solutions: formation of sulfate complexes in NaCl/ Na_2SO_4 solutions, Radiochim. Acta, 74, 99-103.

Pedersen, K., and Albinsson, Y. 1992, Possible effects of bacteria on trace-element migration in crystalline bed-rock, Radiochim. Acta, 58/59, 365-369.

Pedersen, K. 1997, Microbial life in deep granitic rock, FEMS Microbiol. Rev., 20, 399-414.

Péquignot, C., Larroche, C., and Gros, J. B. 1998, A spectrophotometric method for determination of bacterial biomass in the presence of a polymer, Biotechnol. Tech., 12, 899-903.

Plancque, G, Moulin, V., Toulhoat, P., Moulin, C. 2003, Europium speciation by time-resolved laser-induced fluorescence. Anal. Chim. Acta, 478, 11-22.

Poulain, S., Sergeant, C., Simonoff, M., Le Marrec, C., Altmann, S. 2008, Microbial investigations in Opalinus Clay, an argillaceous formation under evaluation as a potential host rock for a radioactive waste repository. Geomicrobiol. J., 25, 240-249.

Puigdomenech, I. MEDUSA Windows interface to the MS-DOS versions of INPUT, SED and PREDOM: Computer Programs Drawing Equilibrium Diagrams. Trita-OOK-3010, RIT, Stockholm Sweden (1983), Version 29, 2002.

Reilly, S. D., Neu, M. P. 2006, Pu(VI) Hydrolysis: Further Evidence for a Dimeric Plutonyl Hydroxide and Contrasts with U(VI) Chemistry. Inorg. Chem., 45, 1839-1846.

Reitz, T. 2011, U(VI) bioaccumulation by *Paenibacillus* sp. JG-TB8 and *Sulfolobus acidocaldarius*; Au(0) nanoclusters formation on the S-layer of *S. acidocaldarius*, Ph.D. thesis, TU Bergakademie Freiberg.

Renninger, N. S., Knopp, R., Nitsche, H., Clark, D. S., and Keasling, J. D. 2004, Uranyl precipitation by Pseudomonas aeruginosa via controlled polyphosphate metabolism, Appl. Environ. Microbiol., 70, 7404-7412.

Ressler, T. 1998, WinXAS: a program for x-ray absorption spectroscopy data analysis under MS-Windows, J. Synchrotron Radiat., 5, 118-122.

Rodriguez-Diaz, M., Lebbe, L., Rodelas, B., Heyrman, J., De Vos, P., and Logan, N. A. 2005, *Paenibacillus wynnii* sp. nov., a novel species harbouring the nifH gene, isolated from Alexander Island, Antarctica, Int. J. Syst. Evol. Microbiol., 55, 2093-2099.

Rossberg, A., Reich, T., Bernhard, G. 2003, Anal. Bioanal. Chem., 376, 631.

Rothstein, A. 1962, Functional implications of interactions of extracellular ions with ligands of the cell membrane, Circulation, 26, 1189-1200.

Selenska-Pobell, S., Kampf, G., Flemming, K., Radeva, G., Satchanska, G. 2001. Bacterial diversity in soil samples from two uranium waste piles as determined by rep-APD, RISA and 16S rDNA retrieval. Antonie Van Leeuwenhoek, 79, 149-161.

Seufferheld, M. J., Alvarez, H. M., and Farias, M. E. 2008, Role of polyphosphate in microbial adaption to extreme environments, Appl. Environ. Microbiol., 74, 5867-5874.

Shapiro, J. 1967, Induced rapid release and uptake of phosphate by microorganism, *Science*, 155, 1269-1271.

Sheng, L., Szymanowski, J. E. S., and Fein, J. B. 2011, The effects of uranium speciation on the rate of U(VI) reduction by Shewanella oneidensis MR-1, Geochim. Cosmochim. Acta, 75, 3558-3567.

Singer, D. M., Farges, F., Brown Jr., G. E. 2009, Biogenic nanoparticulate UO_2: Synthesis, characterization, and factors affecting surface reactivity, Geochim. Cosmochim. Acta, 73, 3593-3611.

Spring, S., Merkhoffer, B., Weiss, N., Kroppenstedt, R. M., Hippe, H., Stackebrandt, E. 2003, Characterization of novel psychrophilic *clostridia* from an Antarctic microbial mat: description of *Clostridium frigoris* sp. nov., *Clostridium lacusfryxellense* sp. nov., *Clostridium bowmanii* sp. nov. and *Clostridium psychrophilum* sp. nov. and reclassification of *Clostridium laramiense* as *Clostridium estertheticum* subsp. *laramiense* subsp. nov, Int. J. Syst. Evol. Microbiol., 53, 1019-1029.

Steudtner, R., Großmann, K., Götz, C., Geipel, G., Brendler, V. 2013, Luminescence spectra of the $UO_2(CO_3)_3^{4-}$ complex at room temperature, Analyst (submitted).

Steudtner, R., Sachs, S., Schmeide, K., Brendler, V., Bernhard, G. 2011, Ternary uranium(VI) carbonato humate complex studied by cryo-TRLFS, Radiochim. Acta, 99, 687-692.

Stroes-Gascoyne, S., Schippers, A., Schwyn, B., Poulain, S., Sergeant, C., Simonoff, M., Le Marrec, C., Altmann, S., Nagaoka, T., Mauclaire, L., McKenzie, J., Daumas, S., Vinsot, A., Beaucaire, C., Matray, J.-M. 2007, Microbial community analysis of Opalinus clay drill core samples from the Mont Terri underground research laboratory, Switzerland. Geomicrobiol. J., 24, 1-17.

Szabó, Z., Furó, I., and Csöregh, I. 2005, Combinatorial multinuclear NMR and x-ray diffraction studies of uranium(VI)-nucleotide complexes, J. Am. Chem. Soc., 127, 15236-15247.

Takai, K., et al. 2008, Cell proliferation at 122°C and isotopically heavy CH_4 production by a hyperthermophilic methanogen under high-pressure cultivation, Proc. Natl. Acad. Sci. USA, 105, 10949-10954.

Texier, A.-C., Andres, Y., Illemassene, M., Le Cloirec, P. 2000, Characterization of Lanthanide Ions Binding Sites in the Cell Wall of *Pseudomonas aeruginosa*, Environ. Sci. Technol., 34, 610-615.

Thakur, P., Conca, J. L., Van de Burg, L. J., Choppin, G. R. 2009, Complexation and laser luminescence studies of Eu(III), Am(III), and Cm(III) with EDTA, CDTA, and PDTA and their ternary complexation with dicarboxylates, J. Coord. Chem., 62(23), 3719-3737.

Thury, M., Bossart, P. 1999, The Mont Terri Rock Laboratory, a new international research project in a Mesozoic shale formation, in Switzerland, Eng. Geol., 52, 347-359.

Turner, B. F., and Fein, J. B. 2006, ProtoFit: a program for determining surface protonation constants from titration data, Comp. Geosci., 32, 1344-1356.

Vogel, M., Günther, A., Gube, M., Raff, J., Kothe, E., and Bernhard, G. 2011, Interaction of Chlorella vulgaris and *Schizophyllum commune* with U(VI), in The New Uranium Mining Boom (Proceedings of UMH VI), Berlin: Springer, pp. 185-192.

Voet, D., Voet, J. G., and Pratt, C. W. 2002, Lehrbuch der Biochemie, Weinheim, Germany: Wiley.

Wang, Z., Zachara, J. M., Liu, C., Gassman, P. L., Felmy, A. R., and Clark, S. B. 2008, A cryogenic fluorescence spectroscopic study of uranyl carbonate, phosphate and oxyhydroxide minerals, Radiochim. Acta, 96, 591-598.

Webb, S. M. 2005, SIXPACK: a graphical user interface for XAS analysis using IFEFFIT, Phys. Scr., T115, 1011-1014.

Westall, J. C. 1982, FITEQL. A computer program for determination of chemical equilibrium constants from experimental data, Corvallis, OR: Oregon State University.

Wilson, R. E., Hu, Y.-J., Nitsche, H. 2005, Detection and quantification of Pu(III, IV, V, and VI) using a 1.0-meter liquid core wave guide, Radiochim. Acta, 93, 203-206.

Yankson, K.K., Steck, T.R. 2009, Strategy for extracting DNA from clay soil and detecting a specific target sequence via selective enrichment and real-time (quantitative) PCR amplification, Appl. Environ. Microbiol., 75, 6017-6021.

Yee, N., Benning, L. G., Phoenix, V. R., Ferris, F. G. 2004, Characterization of metal-cyanobacteria sorption reactions: A combined macroscopic and infrared spectroscopic investigation, Environ. Sci. Technol., 38, 775-782.

Yoshida, T., Ozaki, T., Ohnuki, T., Francis, A. J. 2004, Interactions of trivalent and tetravalent heavy metal-siderophore complexes with *Pseudomonas fluorescens*, Radiochim. Acta, 92, 749-753.

8 Acknowledgement

The authors are indebted for the use of the Cm-248 to the U.S. Department of Energy, Office of Basic Energy Sciences, through the transplutonium element production facilities at Oak Ridge National Laboratory which was made available as part of a collaboration between HZDR and the Lawrence Berkeley National Laboratory (LBNL).

We thank the BGR for providing the Mont Terri Opalinus Clay samples.

The authors thank Dr. S. Sachs and Dr. K. Schmeide for providing the Pu-242 stock solution.

We thank Dr. F. Bok for the thermodynamic calculations using the geochemical speciation code Geochemist's Workbench.

For supporting measurements and aid indispensable for this project thanks is addressed to: Prof. Mohamed L. Merroun, Ursula Schaefer, Aline Ritter, Katrin Flemming, Monika Dudek, and Frank Hille.

The XAS measurements were performed at BM20 (ROBL) at the European Synchrotron Radiation Facility (ESRF) in Grenoble (France). In particular, thanks are given to Dr. A. Scheinost, Dr. A. Rossberg, and Dr. C. Hennig for their support during the XAS measurements and their help in evaluating the data.

At this place we would like to take the opportunity to thank all colleagues who contributed to the success of this work.

HZDR
HELMHOLTZ ZENTRUM DRESDEN ROSSENDORF

Bautzner Landstr. 400
01328 Dresden, Germany
Tel. +49 351 260-2433
Fax +49 351 260-12433
h.moll@hzdr.de
http://www.hzdr.de